Technical Report Documentation Page

1. Report No. ABC-UTC-2013-C3-UNR05-Final	2. Government Accession No.	3. Recipient's Catalog No.	
4. Title and Subtitle **Analytical Investigations and Design Implications of Seismic Response of a Two-Span ABC Bridge System**		5. Report Date April 2019 6. Performing Organization Code	
7. Author(s) Elmira Shoushtari (0000-0002-0044-2314), M. Saiid Saiidi, Ahmad Itani (0000-0002-9813-6314), Mohamed A. Moustafa (0000-0002-1006-7685)		8. Performing Organization Report No.	
9. Performing Organization Name and Address Department of Civil and Environmental Engineering Florida International University 10555 West Flagler Street, EC 3680 Miami, FL 33174		10. Work Unit No. (TRAIS) 11. Contract or Grant No. DTRT14-G-UTC41	
12. Sponsoring Organization Name and Address Accelerated Bridge Construction University Transportation Center Florida International University 10555 W. Flagler Street, EC 3680 Miami, FL 33174		13. Type of Report and Period Covered Final Report (July 2016 to May 2019) 14. Sponsoring Agency Code	
15. Supplementary Notes Visit www.abc-utc.fiu.edu for other ABC reports.			
16. Abstract Despite the numerous advantages that accelerated bridge construction (ABC) offers, it has not been embraced in moderate and high seismic areas. This is due to insufficient research data investigating the effect of interaction between ABC connections and prefabricated components, guidelines for their seismic design, as well as the reliable analytical modeling methods for ABC bridges. The current study covers the analytical investigations of a two-span bridge system with six ABC connections tested on shake tables at the University of Nevada, Reno to address these issues. The analytical framework of the study comprised two phases: Pre-test analysis helped in estimating the design forces for preliminary design of components and determining input ground motions and the test loading protocol. As part of the post-test analysis, response of the OpenSees computational model with actual material properties and shake table motions was compared with measured response of the bridge model. This computational model was adequate in capturing the overall seismic response of the bridge model. The effects of the vertical ground motions and bi-axial excitations on the seismic response of bridge elements and ABC connections were investigated and found that some of the response parameters can be significantly affected by near-fault earthquakes. Design implications were developed based on the results of the shake table test, previous studies on the connections, and the parametric studies. The report also presents design guidelines for the rebar hinge pocket connection and hybrid grouted duct connection.			
17. Key Words Accelerated bridge construction, shake table test, OpenSees, Vertical excitation, steel girder, hybrid cap beam, grouted duct, rebar hinge pocket (socket) connection, simple for dead continuous for live		18. Distribution Statement No restrictions.	
19. Security Classification (of this report) Unclassified.	20. Security Classification (of this page) Unclassified.	21. No. of Pages 106	22. Price

Form DOT F 1700.7 (8-72) Reproduction of completed page authorized

(this page is intentionally left blank)

Analytical Investigations and design Implications of Seismic Response of a Two-Span ABC Bridge System

Final Report

April 2019

Principal Investigator: M. Saiidi and A. Itani

Department of Civil and Environmental Engineering

Florida International University

Authors

Elmira Shoushtari

M. Saiid Saiidi

Ahmad M. Itani

Mohamed Moustafa

Sponsored by

Accelerated Bridge Construction University Transportation Center

A report from

University of Nevada, Reno

Department of Civil and Environmental Engineering, MS 258

1664 N. Virginia St.

Reno, NV 89557

www.unr.edu/cee

DISCLAIMER

The contents of this report reflect the views of the authors, who are responsible for the facts and the accuracy of the information presented herein. This document is disseminated in the interest of information exchange. The report is funded, partially or entirely, by a grant from the U.S. Department of Transportation's University Transportation Program. However, the U.S. Government assumes no liability for the contents or use thereof.

ABSTRACT

Despite the numerous advantages that accelerated bridge construction (ABC) offers, it has not been embraced in moderate and high seismic areas. This is due to insufficient research data investigating the effect of interaction between ABC connections and prefabricated components, guidelines for their seismic design, as well as the reliable analytical modeling methods for ABC bridges. The current study covers the analytical investigations of a two-span bridge system with six ABC connections tested on shake tables at the University of Nevada, Reno to address these issues. The analytical framework of the study comprised two phases: Pre-test analysis helped in estimating the design forces for preliminary design of components and determining input ground motions and the test loading protocol. As part of the post-test analysis, response of the OpenSees computational model with actual material properties and shake table motions was compared with measured response of the bridge model. This computational model was adequate in capturing the overall seismic response of the bridge model. The effects of the vertical ground motions and bi-axial excitations on the seismic response of bridge elements and ABC connections were investigated and found that some of the response parameters can be significantly affected by near-fault earthquakes. Design implications were developed based on the results of the shake table test, previous studies on the connections, and the parametric studies. The report also presents design guidelines for the rebar hinge pocket connection and hybrid grouted duct connection.

ACKNOWLEDGMENTS

This project was supported by the Accelerated Bridge Construction University Transportation Center (ABC-UTC at www.abc-utc.fiu.edu) at Florida International University (FIU), as lead institution, and Iowa State University (ISU) and the University of Nevada-Reno (UNR) as partner institutions. The authors would like to acknowledge the ABC-UTC support.

The author would like to extend special appreciation to the ABC-UTC and the U.S. Department of Transportation Office of the Assistant Secretary for Research and Technology for funding this project.

The authors would like to thank the Research Advisory Panel members: Bijan Khaleghi, Washington State DOT; Elmer Marx, Alaska DOT&PF; Tom Ostrom, Caltrans.

Several companies and organizations are thanked for various contributions to the project: Lafarge North America Inc. for donating UHPC material, C&K Johnson Industries for donating corrugated metal ducts, Reno Iron Works for fabrication of steel girders at a reduced cost, Utah Pacific Steel and NSBA for donating the steel girders, cross frames, and other steel accessories. Mr. Don Newman is thanked for his diligent efforts and meticulous attention to construction of the test model.

Thanks are due the UNR Earthquake Engineering Laboratory staff Dr. Patrick Laplace, Chad Lyttle, Todd Lyttle, and Mark Lattin for their unfailing support and assistance. The support and advice of ABC-UTC director, Dr. Atorod Azizinamini, is greatly appreciated. Thanks are due to Mojtaba Alian, Jose Benjumea Royero, Jared Jones, Amir Sadeghnezhad, Dr. Alireza Mohebbi, Dr. Ali Mehrsoroush, and Azin Ghaffari for their dedicated assistance along the course of this study. Amir Sadeghnezhad is especially thanked for development of the design guideline for SDCL connections, which is included in Appendix D.

CONTENTS

LIST OF FIGURES

LIST OF TABLES

CHAPTER 1: INTRODUCTION

1.1. Project Motivation

Bridge cast-in-place construction may lead to traffic delays, subject highway workers and the traveling public to increased probability of accidents, and affect the regional economy because of prolonged construction. By utilizing prefabricated bridge elements, accelerated bridge construction (ABC) shortens onsite construction time. Accordingly, ABC saves time and money for the traveling public and enhances the work-zone safety. Due to the fact that prefabricated components are built offsite and under controlled environmental conditions, ABC provides the opportunity to use novel materials and to increase the quality and durability of the components. ABC can also reduce the total duration of projects as prefabrication of bridge components can be performed simultaneously.

Connections between prefabricated elements (hereby referred to as ABC connections) play a crucial role in adequate performance of ABC bridges under moderate and strong earthquakes. ABC connections have to be practical and efficiently constructible and at the same time provide clear load path under vertical and lateral loading. When used for connecting columns to the adjoining members, ABC connections must allow for the energy dissipation in the column while maintaining the capacity and the integrity of the structural system.

Researchers (Matsumoto et al. 2001; Restrepo et al. 2011; Tazarv and Saiidi 2014; Motaref et al. 2011; Mehrsoroush, et al. 2016; Mehraein and Saiidi 2016) have developed and investigated a variety of ABC connections and prefabricated elements in the past decade. These connections include but are not limited to grouted duct connections, pocket and socket connections, mechanical bar splices, simple for dead continuous for live (SDCL) connections of various configurations, and connections for partial or full precast deck panels. The primary intent of these studies was to assess the local behavior of ABC connections, formulate preliminary design guidelines, and build a certain level of confidence in utilizing ABC techniques. As such, experimental studies have been limited either to the component level or bridge subassemblies. Another typical limitation of these studies has been that they focus on connection behavior under uni-directional loading. For example, column cap-beam connections were studied in two-column pier models that were subjected only to in-plane loading.

While providing invaluable information on the local behavior of ABC connections, component tests do not provide confidence in the performance of the bridge systems when subjected to bi-directional loading. Therefore, to understand the holistic seismic behavior of ABC bridges ABC connections along with prefabricated elements should be integrated into a bridge system and studied under realistic bi-axial seismic loading. Bridge system studies need to include experimental and analytical component. The focus of the present report is on analytical studies.

1.2. Research, Objectives, and Tasks

Comprehensive analytical and experimental investigations of a large-scale two-span steel girder bridge model incorporating six ABC connection types subjected to bi-directional horizontal earthquake motions were conducted. The aforementioned ABC connections were: (1) column-to-footing rebar hinge pocket connection; (2) column-to-hybrid cap beam grouted duct connection; (3) simple for dead continuous for live (SDCL); (4) panel-to-girder grouted pocket connection; (5) spliced deck panel rebars in the transverse panel-to-panel joints filled with ultra-high

performance concrete (UHPC); and (6) spliced deck panel rebars in UHPC-filled panel-to-panel joint over the pier.

The primary objectives of this research project were to:

1. Investigate the system level seismic performance of six ABC connections under horizontal bi-directional seismic excitations at different limit states;
2. Determine the adequacy of the available design methods for ABC components and connections;
3. Evaluate the feasibility of the construction methods and identify construction issues in handling and connecting various prefabricated elements;
4. Evaluate the adequacy of current finite element modeling methods for ABC bridge systems.
5. Conduct analytical studies of the effect of key parameters that were not investigated in the experimental program.

A mix of experimental and computational efforts was undertaken to meet the aforementioned objectives. These efforts can be summarized as:

- *Task 1 – Literature review:* A literature search was conducted to identify past studies on select ABC connections, as well as the most recent analytical modeling methods and results on dynamic load studies of prefabricated bridge elements and their connections.
- *Task 2 – Identify critical macroscopic and microscopic bridge model response parameters and extract measured data for use in analytical studies:* The accuracy and acceptability of analytical modeling methods was assessed at two levels: global response simulation and local response simulation. The global seismic response consist of forces and displacements and relationship between these parameters that define stiffness and its variation as inelastic deformation in steel and concrete develop. Local responses of importance are curvature and rotations in addition to strains in superstructure steel girders, steel reinforcement, and concrete at various critical sections of elements and connections.
  The curvature and rotation data indicated the extent of section nonlinearity, while the strain data helped explaining some of the visible damage that was documented in the shake table tests. Although SDCL, the cap beam, the superstructure, and the footing are designed to be capacity protected, the measured data were streamlined for correlation studies with the analytical model and an assessment was made if these elements were indeed capacity protected. This task was completed based on the extensive evaluation of the test results that confirmed that only the column top plastic hinges and the two-way hinges at column bases need to be modeled as nonlinear elements.
- *Task 3 – Conduct analytical studies of the bridge model:* The analytical framework of this study comprised two broad phases: 1) Pre-test analysis helped in estimating the design forces for preliminary design of components, determining input ground motion and the loading protocol, and identifying the critical locations to be instrumented; 2) As part of the post-test analysis, response of the analytical model with actual material properties and shake table motions was compared with measured response of the bridge model.

  To fulfill the objectives of the analytical phase, two and three-dimensional finite element models of the two-column bent and the bridge system were developed in OpenSees and

SAP2000 software packages. Linear analysis under service dead and live loads, nonlinear static analysis, and nonlinear response history analysis were conducted on the models.

- *Task 4 – Refine the analytical model and conduct parametric studies:* Refinement of the analytical model was completed and reasonable correlation between the analytical and experimental results was achieved. After the acceptable correlation was obtained, there was sufficient confidence in the analytical modeling techniques, and the analytical model was used for parametric studies. The parameters were carefully selected to address issues that could be affected by a system response rather than component response. The ultimate target of the parameters was to generate information that could be incorporated in ABC seismic design guidelines. One of the parameters was the effect of biaxial earthquake motions. Past experimental studies on bridge piers have focused on the in-plane response of the piers, and conclusions have been reached. Motion was applied to the bridge model in one direction at a time and results were compared with those from biaxial motion studies. Another parameter that is being studied is the effect of vertical motions. Due to limitations, only the horizontal components of the ground motions were applied in the shake table test. The ground motions were selected to induce the maximum possible vertical ground motion effects on the bridge.
- *Task 5 - Summarize the investigation and the results in final report:* The current document is the final report prepared meeting the RITA requirements for UTC funded projects. The content of the report contains a detailed summary of the results from the preceding tasks.

1.3. Research Advisory Panel (RAP)

The project work was done in collaboration with the Research Advisory Panel (RAP). The following people participated in the RAP:

- Tom Ostrom (California Department of Transportation)
- Bijan Khaleghi (Washington state DOT)
- Elmer Marx (Alaska DOT)

1.4. Report Overview

Chapter 1 includes the problem statement, objectives of the project, and the methodology to meet the objectives. Chapter 2 provides the literature review for the connection types incorporated in the research project. Chapters 3 and 4 correspond to a stand-alone refereed journal paper constituting a separate portion of the study. However, for clarity and completeness, all articles include a summary of important background information from the rest of the study. The date of initial submission and the name of the journal are noted at the beginning of each chapter. The final chapter describes a summary and conclusions of the research study (Chapter 5).

To document detailed data and descriptive information that are included in the papers, two appendices are included. Results of the analytical and parametric studies are presented in Appendix A. Appendix B documents the design guidelines that were developed for rebar hinge pocket connections and column to hybrid cap beam grouted duct connections.

CHAPTER 2: PAST RELEVANT STUDIES

2.1. Introduction

Various earthquake-resistant connection types have been explored by researchers through experimental and analytical studies for possible adoption in ABC. These connections (referred to as "ABC connections") include but are not limited to grouted ducts, mechanical bar splice couplers, pocket and socket connections, pipe pin connections, and rebar hinge connections as well as the connection between bridge superstructures and cap beams. The objectives of these studies have been to develop a thorough understanding of the local response of the ABC connections. Due to limitation of test facilities and budget, experimental studies have been mostly limited either to the component level or bridge subassembly testing. Another limitation of these studies has been focused on connection behavior under uni-directional loading. However, to confidently recommend ABC bridges for incorporation in routine bridge design and construction in high seismic regions, investigating the effect of interaction and load distribution among components is essential.

To address this gap a large-scale two-span bridge system with steel superstructure and six ABC connections was investigated experimentally and analytically. The ABC connections used in the bridge model were: (1) column-to-footing rebar hinge pocket connection; (2) column-to-hybrid cap beam grouted duct connection; (3) simple for dead continuous for live (SDCL); (4) panel-to-girder grouted pocket connection; (5) spliced deck panel rebars in the transverse panel-to-panel joints filled with ultra-high performance concrete (UHPC); and (6) spliced deck panel rebars in UHPC-filled panel-to-panel joint over the pier.

This chapter presents a summary review of past studies on the aforementioned ABC connections. Because some of the connections are closely inter-related, the review of past research on connection types: panel-to-girder grouted pocket connection, spliced deck rebars in UHPC-filled transverse joints between adjacent panels and connection between deck panels over the pier.

2.2. Rebar Hinge Pocket/Socket Connections

2.2.1. Introduction

"Pin" or hinge connections are desirable for connecting columns to the footing as they result in smaller and more cost-effective foundations. They may also be used at top of the columns to reduce moment demand in outrigger cap beams. Two-way hinges are free to rotate in any directions and are commonly used in multi-column bents. Rebar hinge connection as a type of a two-way hinge comprises a reinforcement cage with smaller diameter compared to that of the column. A hinge throat (vertical gap) is provided at the interface of the adjoining members to improve the hinge rotational capacity. Rebar hinge is the most commonly used column hinge type in the United States. Although, hinges are intended to be moment free, some moment is developed in the rebar hinge due to the eccentricity of hinge bars relative to the concrete compression force that can be developed in the hinge.

To make the rebar hinge connection suitable for rapid construction, details of the rebar hinges can be combined with those of the pocket/socket connections. In rebar hinge pocket connection (Figure 2-1(a)), precast hinge element integrated with the precast column extended into a corrugated steel pipe embedded in the footing. The gap between the hinge and the pocket is filled with high-strength, non-shrink grout to make the connection monolithic. Another

alternative is rebar hinge socket connection in which the hinge element consists of a rebar cage alone that extends from the column into a footing opening. The opening is filled with concrete with higher compressive strength compared to that of the footing concrete. This connection is called rebar hinge socket connection and is shown in Figure 2-1(b). Yet a third alternative is to leave an opening in the column core and install the column over hinge rebars that extend from the footing and fill the space with grout (Figure 2-1(c)).

Only a few experimental studies have incorporated rebar hinge pocket connections. However, pocket connections for full moment transfer and rebar hinge connections have been the focus of several studies, which are highlighted in this section.

2.2.2. Past Research on Pocket Connections

Pocket connection can be constructed by forming a pocket inside a precast footing or cap beam and extending either the precast column or the extruded reinforcement of the partially precast column into the pocket. In the former method, the gap between the column and the pocket is filled with grout, while in the latter method, the pocket is filled with concrete. Seismic performance of pocket connections has been investigated by several researchers in recent years.

Matsumoto et al. (2001) conducted four full-scale experiments on grout-pocket, grouted-duct, and bolted cap beam-column connections, and two full-scale experiments on bents. The authors reported similar strength and ductility capacity as CIP column-cap beam connections. It was concluded that these connections not only expedited construction, but also resulted in emulative response to that of the monolithic construction.

Restrepo et al. (2011), performed a series of 0.42 scale bent cap to column component tests including a CIP control specimen, a cap pocket full ductility specimen (CPFD), and a cap pocket limited ductility specimen (CPLD). The authors reported considerably more damage in the CPLD compared to the CPFD model. It was concluded that using corrugated steel pipe serving as joint shear reinforcement provided sufficient joint shear resistance when subjected to column overstrength demands. The test results showed that the longitudinal bars of the precast cap beams in the extreme layer yielded which is not acceptable in capacity protected elements.

Haraldsson et al. (2013) showed that the seismic performance of octagonal pocket connections with an embedment length ratio of 1.1 to the column diameter was as good as that of comparable cast-in-place (CIP) systems.

Motaref et al. (2011) conducted a shake table test of a 0.3-scale precast two-column bent. One of the columns comprised a glass fiber reinforced polymer (GFRP) tube filled with concrete. The other column employed ECC in the plastic hinge zone. Both columns were embedded in pockets left in the footing with an embedment length corresponding to 1.5 times the column diameter. Kavianipour and Saiidi (2013) conducted a shake table test of a quarter scale four-span bridge model in which one of the three bents consisted of precast columns constructed with GFRP concrete-filled tubes, embedded to a depth of 1.5 times the column diameter into the footing pockets. In both studies, the embedment length was found to be sufficient to develop the full moment capacity of the columns, while connections and the GFRP tube remained intact. Kavianipour and Saiidi (2013) reported minor surface concrete spalling in the footing area around the columns in the second study.

Mehrsoroush and Saiidi (2016), and Mehraein and Saiidi (2016) tested large-scale two-column bent models, in which columns were embedded in the cap beam pockets to a depth of 1.2 and 1.0 times the column diameter, respectively. Test results demonstrated column-to-cap beam pocket connections behaved as monolithic connections.

Mohebbi et al. (2018a, 2018b) conducted two 0.33-scale shake table tests on a precast bridge column and a precast two-column bent. Square columns were used in the test models. In the single-column model, Unbonded CFRP tendons were used to post-tension the single-column model and UHPC was used in the plastic hinge zone. Column was connected to the footing through a square pocket. The two-column bent model employed UHPC and ECC in the plastic hinges of the columns that were connected to the cap beam with pocket connections. The embedment length of the columns into the pockets was 1.0 times the column dimension. Results showed that the column-footing and column-cab beam pocket connections performed successfully and the integrity was maintained.

2.2.3. Past Research on Rebar Hinge Connections

More than fifty 1/20-scale and fourteen 1/5-scale cantilever columns incorporating rebar hinge detail were tested by Lim and McLean (1991) under cyclic loading. The authors concluded that two-way hinge connections can substantially reduce the moment transfer to the footing, but the moment is not negligible in contrast to design assumptions.

Four 1/6 scale one-way hinge specimens subjected to a constant axial load and variable lateral load were tested under both monolithic and cyclic loads by Saiidi and Straw (1993). Results demonstrated that even for specimens with very low aspect ratio, flexure and not shear controlled the strength of the hinges. It was also found that the concrete at the hinge throat region is capable of developing strains as high as nearly 0.03, and that its compressive strength is approximately 80 percent higher than the measured cylinder strength.

Haroun et al. (1993), tested six 0.4 scale, two-way hinge columns under reverse cyclic lateral loads. The failure mechanism in all specimens was flexural with a high ductility capacity. Pure shear was then applied to three other columns to assess the shear strength. The authors reported that the shear failure mechanism was diagonal tension failure of the entire column, and that the strength of the hinge section might be underestimated by beam shear design theory.

Further experimental research was conducted by Jiang and Saiidi (1995) on one-way hinges. It was concluded that the shear friction method (SFM) is not applicable to hinges and that SFM underestimates the shear capacity of hinges. A preliminary method was hence developed for the design of one-way hinges under lateral load.

Saiidi et al. (2009), tested five one-third scale columns on a shake table under uni-directional loading. The columns incorporated two-way hinges at top. The test parameters were the hinge size, column longitudinal steel ratio, hinge steel ratio, column aspect ratio, and the axial load level. The authors reported that all columns exhibited stable hinging and ductile behavior, and that the classical shear friction mechanism in which two concrete segments slide parallel to each other was not observed in any specimens. It was concluded that under small deformations shear force is resisted by friction only in the compression zone of the hinge rather than the entire hinge. Under large deformations, dowel action of the hinge longitudinal bars provides shear resistance

and prevents the total failure of the hinge. Moment-rotation, and shear-slippage models for two-way hinges were proposed.

Mehraein and Saiidi (2016), performed a shake table test on 1/3.75-scale two-column bent in which rebar hinges connected the column to the pile shaft. The precast hollow column was placed on top of the pile shafts around the rebar hinge, and was filled with SCC after the precast cap beam was placed over the columns. The design and the detailing of rebar hinge was believed to be successful for the connection of column to pile shaft, and led to the ductile behavior of the bent. The concrete at the hinge throat was damaged, but the column and pedestal reinforcement did not yield near the rebar hinge section.

2.2.4. Past Research on Rebar Hinge Pocket/Socket Connections

Mehrsoroush et al. (2016) tested a two-column bent with a combined detail of rebar hinge and pocket connection connecting one of the columns to the cap beam, while the other column was connected to the cap beam through one-piece pipe pin connection. The pier model was tested to failure on a shake table under unidirectional loading. The rebar hinge pocket connection was found to be successful even under high drift ratios.

Mohebbi et al. (2018b), conducted a shake table test on a two-column bent in which precast square columns were connected to the footing using circular rebar hinge pocket connections. A 1.0 in. (25.4 mm) vertical gap corresponding to 3.0 in. (25.4 mm) in a full-scale bridge was provided between the footing and the columns to allow for the rotation of columns. The authors reported that damage in the hinge section was limited to minor spalling of the cover concrete at the hinge gap, and no damage was detected around the rebar hinge pocket connection. Debonding the longitudinal bars of the rebar hinge for $2d_b$ each above and below the footing interface was believed to be effective in spreading yielding to prevent strain concentration and premature bar rupture at the interface.

2.3. Column to Hybrid Cap Beam Grouted Duct Connections

2.3.1. Introduction

In grouted duct connections, the longitudinal bars protruded from a precast or cast-in-place column are extended into individual ducts embedded in the adjoining member. The ducts are then filled with high-strength grout or ultra-high performance concrete. Grouted duct connections are often used for joining columns to the cap beam.

One version of grouted duct connections consists of grouted ducts over part of the cap beam with the rest of bond for the column longitudinal steel provided in a cast-in-place portion. This is referred to as a hybrid grouted duct connection in this study. Hybrid connections allow for making the cap beam superstructure join integral. Only one past research has been conducted on hybrid cap beam connections. Therefore, the following section is mostly focused on grouted duct connections.

2.3.2. Past Research

Raynor et al. (2002) investigated the bond behavior of reinforcing bars of various sizes grouted in ducts subjected to cyclic loading. It was shown that grouted ducts provided enhanced bond strength compared to that of the conventional concrete. Furthermore, the duct provided adequate confinement for bars and thus prevented splitting of the grout.

Pang et al. (2008) tested three 0.4-scale precast columns that were connected to precast bent caps through grouted ducts. The results were compared with a typical cast-in-place (CIP) reference column with similar details. Longitudinal bars of two of the three columns were debonded over a length of $8d_b$ into the cap beam. Authors reported that precast columns showed comparable ductility capacity, lateral load capacity, and energy dissipation capacity to those of the reference CIP column. Debonding of the bars reduced the strain concentration, but did not delay the fracture of bars as intended.

Matsumoto (2008) conducted quasi-static cyclic loading on a 0.42-scale grouted duct column-cap beam connection (GD). No bar or duct pullout or splitting of the grout within the ducts were reported. The hysteretic force-displacement response of the connection resembled that of the reference CIP model up to 3.7% drift ratio. GD model exhibited higher lateral load capacity but lower drift ratio capacity compared to the CIP model.

Tazarv and Saiidi (2014) developed UHPC-filled duct connections to connect columns to shallow cap beam and footings. A half-scale precast column model connected to footing through the new grouted duct detail was tested under cyclic loading. The column was initially hollow but was filled with self-consolidating concrete (SCC) afterward. The performance of the model was satisfactory and emulative of the CIP alternate in terms of the lateral load capacity, drift ratio capacity, and strength and stiffness degradation. Tazarv and Saiidi further extended their studies to determine the bond strength of UHPC-filled ducts. The authors reported that bond strength of UHPC was eight times higher than that of the conventional concrete, and that the required embedment length of the bars in UHPC-filled ducts is at least 50% shorter other grouted duct connections.

Marsh, M. L. et al. (2010) developed a hybrid bent system aimed for integral connections with prestressed girders. The bent employed a two-stage cap beam comprising a lower precast and an upper-part cast-in-place segment. Column bars were partially anchored in the grout-filled ducts embedded in the precast cap beam. The pier model was tested under cyclic lateral loading. Test results were promising; however, the combined effect of the out-of-plane and in-plane loading on the connection was not investigated.

2.4. Simple for Dead, Continuous for Live (SDCL) connection

2.4.1. Introduction

The superstructure-to-substructure integral connection provides the load path to transfer the superstructure moment to the substructure. One advantage of the integral connections is that the cap beam soffit is at the same elevation as or close to the bottom of the girders, and as such larger under-clearance is provided for the bridge. Integral connections can also improve the seismic performance of the bridge through maintaining its integrity and reducing the weight of the superstructure.

Steel superstructures are considerably lighter than the concrete alternative. This can result in enhanced seismic behavior of steel bridges. However, non-integral connections and the need for heavy cap beams can offset the mass reduction provided through using steel girders (Wassef and Davis, 2004). The conventional integral steel girder bridge construction often involves the placement of the middle segment of the steel girders over the pier, connected to the end segments

with bolted or welded field splices that requires temporary supports and increases the onsite construction time.

In the simple for dead and continuous for live load (SDCL) system, the girders span from pier to pier (or abutment to pier) within each span, and are spliced directly over the pier. Girders are simply supported before the deck is in place, but continuous for live load and superimposed dead loads such as the weight of barrier and wearing surface. Past studies on SDCL connection are presented in the following section.

2.4.2. Past Research

The idea of a simple span for dead load and continuous for live load was developed in the 1960's for precast prestressed concrete girders to prevent leakage through the deck joints in simple beam spans (Lampe et al., 2001). The same idea was pursued by researchers to use a pseudo-connection for steel bridges.

Three full-scale tests were carried out to study the behavior of proposed connections (Azizinamini et al. 2005). In the first experiment, the bottom flanges of two adjacent girders were welded over the pier centerline and end bearing plates were welded to the ends of the girders. In the second experiment, girders were simply embedded in the concrete diaphragm. The third specimen was similar to the first one but bottom flanges were not connected. A cyclic load test followed by an ultimate load test was conducted on the specimens. The authors reported that the ultimate moment capacity of the first and third specimens were almost the same and were 1.5 times of that of the second specimen. Ductility of the connections was the highest for the first specimen and the lowest for the second. In the first and third specimens, all tension reinforcement in the deck yielded before the concrete compressive failure of concrete in the diaphragm. However, in the second specimen, concrete compressive failure occurred before all the rebar yielded.

A seismic detail comprising an integral pier connection was proposed for the SDCL connection and its structural behavior and the force transfer mechanism was investigated through analytical studies at the Florida International University (Taghinezhadbilondy, 2016). The proposed connection was evaluated under push-up, push-down, reverse and axial loading. Figure 2-2 shows a schematic view of the connection. The authors reported that under gravity loads, dowel bars and closed stirrups had no effect on the moment capacity of the system. When the FEM was loaded with concentrated push-up forces, the continuity of the bottom flange and tie bars played a major role. The vertical dowel bars were effective but not as much as the tie bars. Under reversal type loading, the only elements that affected the moment capacity were the dowel bars. These dowel bars corresponded to the vertical stirrups referred to as (A_s^{jv}) in Seismic Design Criteria Section 7.4.4.3. A simple design formula for the SDCL seismic detail was developed using a combination of moment-curvature analysis and the Winkler foundation method. Seismic performance of this connection was also tested under cyclic lateral loading. Test results confirmed that the connection was suitable for high seismic regions (Sadeghnejad and Azizinamini, 2017). The model did not include precast elements and also was tested only in one direction. Moreover, the combined effect of out-plane loading and in-plane rotation of the superstructure was not included in the study.

2.5. Deck Panel Connections

2.5.1. Full-depth precast deck panels

Full-depth precast deck panels have been appealing in bridge construction for more than thirty years because they reduce onsite and the total construction time significantly as deck forming, casting, and curing time are eliminated from the critical path of the project. As precast panels are built offsite and under controlled environmental conditions, they offer potential high-quality production, and less volume variations due to shrinkage and temperature during initial curing (Badie and Tadros, 2008). Furthermore, there is an opportunity for the deployment of advanced materials and thus noticeably enhancing the serviceability of deck panels. Although full-depth precast decks are usually more expensive compared to cast-in-place panels in terms of the construction and material, the additional cost is often offset by decreased construction time and less required maintenance (PCI, 2011).

2.5.2. Panel to Girder Pocket Connection

Composite action between the deck and the girder offers many advantages over the non-composite alternate as it leads to shallower depth of the superstructure, longer spans, smaller deflection and less vibration caused by moving traffic, and larger clearance. One of the challenges for the incorporation of prefabricated panels is to provide a full-composite (or sufficiently composite) action between the deck and the girders.

As a part of NCHRP 12-65 Project, Badie and Tadros (2008) proposed a new detail for connection between steel girder and precast panels, in which eight double-headed 1-1/4 in. studs at 48 in. spacing were welded to the girder top flanges. Figure 2-3 shows the connection details. The proposed detail was tested under gravity and lateral loading. Pockets were left in deck panels over the girder lines to accommodate studs. The authors reported that response of the connection was satisfactory in terms of the strength and fatigue capacity. Hollow structural steel (HSS) tubes that were used around the studs were found to be effective in confining the grout surrounding the studs. In addition, it was shown that the 48-in. spacing of the cluster of studs (instead of the 24 in. that is currently specified in AASHTO (2012), Section 6, was adequate to provide a composite action. Furthermore, it was concluded that Article 5.8.4.1 in the AASHTO (2012) can reasonably estimate the horizontal shear capacity of the proposed panel-to girder detail.

Shrestha et al. (2018) conducted a mix of experimental and analytical studies to develop and design prefabricated bridge decks with composite connection to precast girders. A series of pullout and shear tests with various details were undertaken to determine the shear and axial stiffness and strength of headed anchors. Figure 2-4(a) and (b) show the typical test setup for the pullout and shear experiments. A variety of grout types including conventional concrete, Latex Concrete, UHPC, Polyester Concrete, 1428 HP, and EucoSpeed were also examined as the filler material in the pockets. Another variable that was looked into was the group effect of anchors. Shrestha et al. concluded that neither the type of the grout nor the group affected shear and axial capacity of anchors. In terms of the required time and effort for the grout removal, Latex Concrete was the most promising grout type. Overall, all of the grout types but Polyester Concrete and UHPC were recommended for future deck replacement. Another finding of the study was that by using the proposed detail, 70% of a full composite action was achieved.

2.5.3. Joints between Adjacent Deck Panels

Transverse shear keys (joints) between precast panels have to be designed such that they prevent relative vertical displacement between the adjacent panels and provide adequate path for the transfer of the positive moment and vertical shear due to the traffic load (Badie and Tadros, 2008).

There are two main types of transverse shear keys: male to female and female to female shear keys (Figure 2-5). Male-to-female shear keys have been implemented in combination with the longitudinal posttensioning in a few bridges. However, due to the tight tolerances in panel construction, leakage has always been a common challenge in such joints. Grouted female to female joints are most often used. Vertical shear forces applied at the joint are resisted by bearing and bond between the grout and the panel. Inclined surfaces increase the vertical shear strength of the joint (Badie and Tadros, 2008). Roughening the surface of the shear key has been found to enhance the bond between the grout and the shear key surface (Issa et al. 2000).

Longitudinal posttensioning has been used with majority of deck panel systems as a technique to eliminate the joint tensile stresses resulting from traffic load, and hence to prevent cracking and leakage. However, field posttensioning increases the construction time and cost, and complicates the deck placement process.

In the absence of the longitudinal post-tensioning, a wide closure joint is required to provide adequate lap splice length for deck reinforcement. Several researchers have investigated the structural performance of field-cast UHPC connections for bridge deck components. UHPC is a cementitious material with water-to-cementitious material ratio of less than 25%, and a high percentage of steel fibers. Two main reasons that made UHPC a perfect candidate for panel joints were the exceptional bond when cast against previously cast concrete and the ability to shorten the required development length of embedded steel reinforcement significantly (Perry and Royce, 2010). Large cyclic and static flexural and shear loading tests on full-scale field-cast UHPC connections demonstrated that they not only facilitate construction, but also the resulting deck system meets or exceeds the performance requirements of conventional cast-in-place bridges by demonstrating favorable cracking behavior with no sign of interface debonding under cyclic loads (Graybeal 2010, 2014). Furthermore, under the ultimate static loading, the concrete cracking was followed by bar yielding and eventual compressive failure of the conventional concrete. This behavior is similar to monolithically-cast deck panels.

Deck panel joints over the pier in multi-span bridges with continuity for traffic loads are more critical than the joints along the spans, due to the relatively high strains that they could undergo. The deck-to-deck connection are more crucial in integral bridges, as deck bars need to provide an adequate load path for the transfer of the negative moment resulting from seismic lateral loading in addition to that of the service loads. AASHTO (2012) allows for splicing the deck reinforcement over the cap beam. However, Caltrans Memo to Designers 20-9 (2016) prohibits splices inside the critical zones of superstructure capacity-protected components. Critical zones are defined as locations where the moment demand is greater than 75% of the maximum moment. That being said, the common practice has been either to hook the deck bars into the cap beam or to mechanically splice them. Both approaches complicate the construction process and are time-consuming.

Figures

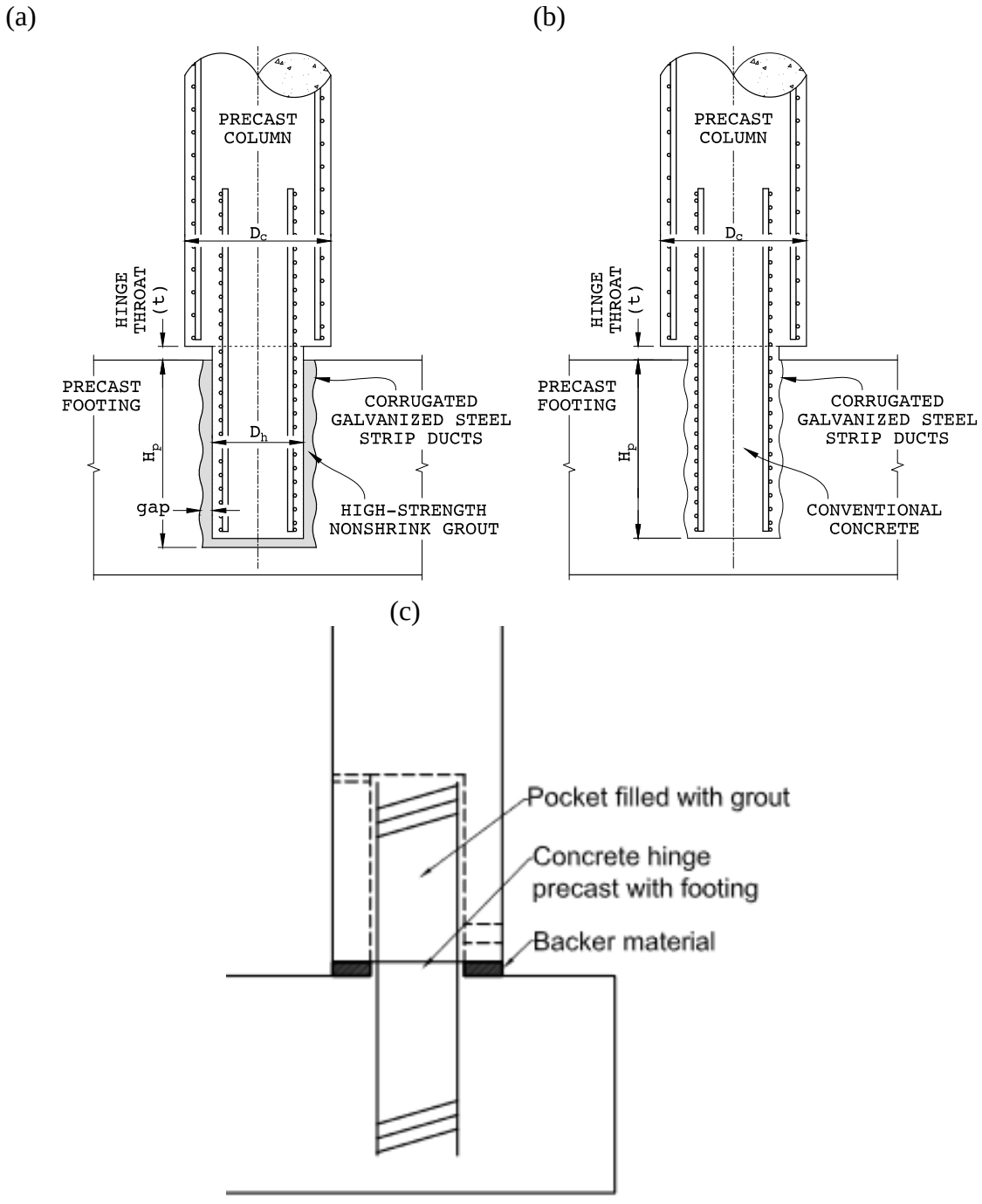

Figure 2.1 column to footing (a) rebar hinge pocket connection, (b) rebar hinge socket connection, (c) rebar hinge pocket connection with pocket left in column

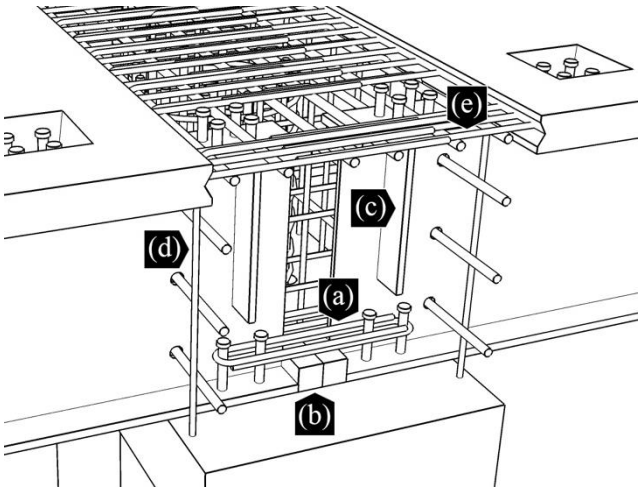

Figure 2.2 Details of the SDCL connection: (a) tie bar, (b) steel block, (c) stiffener, (d) cap beam stirrups (dowel bars), (e) deck longitudinal bars

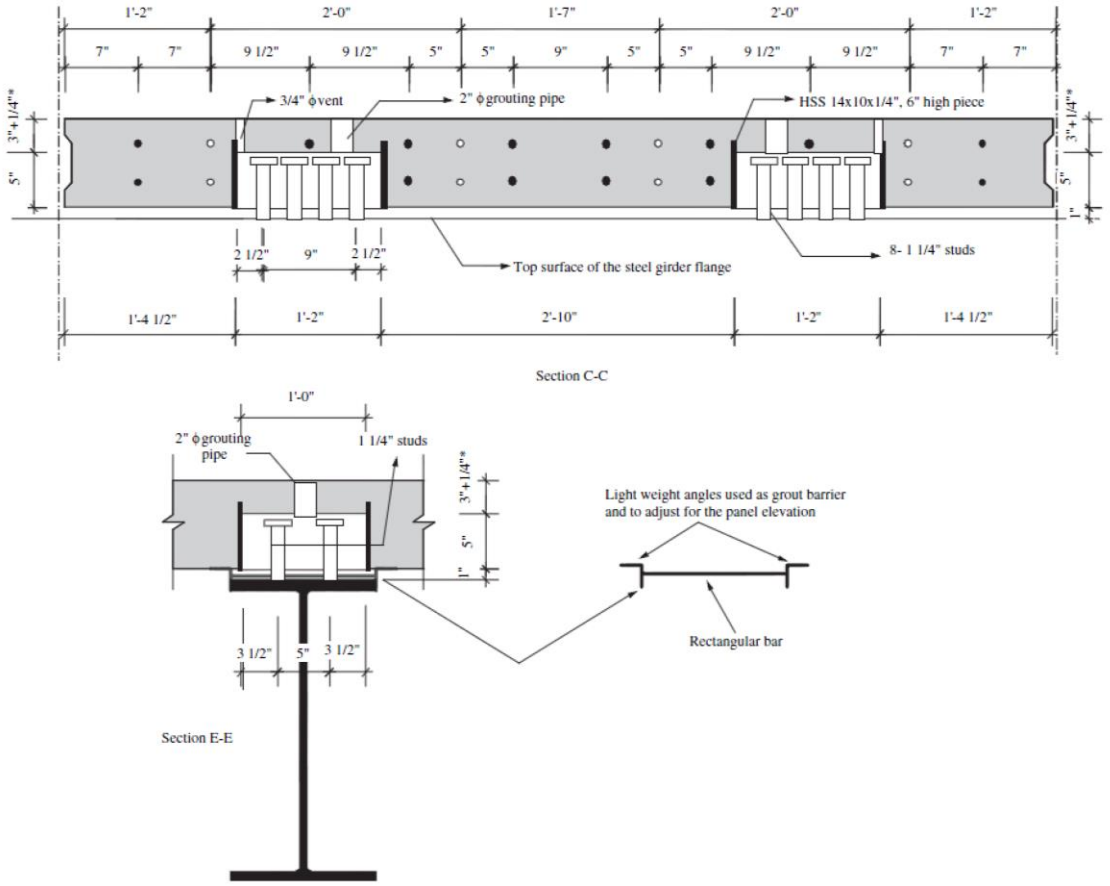

Figure 2.3 Connection between full-depth deck panels and steel plate girder (Badie and Tadros, 2008)

(a) (b)

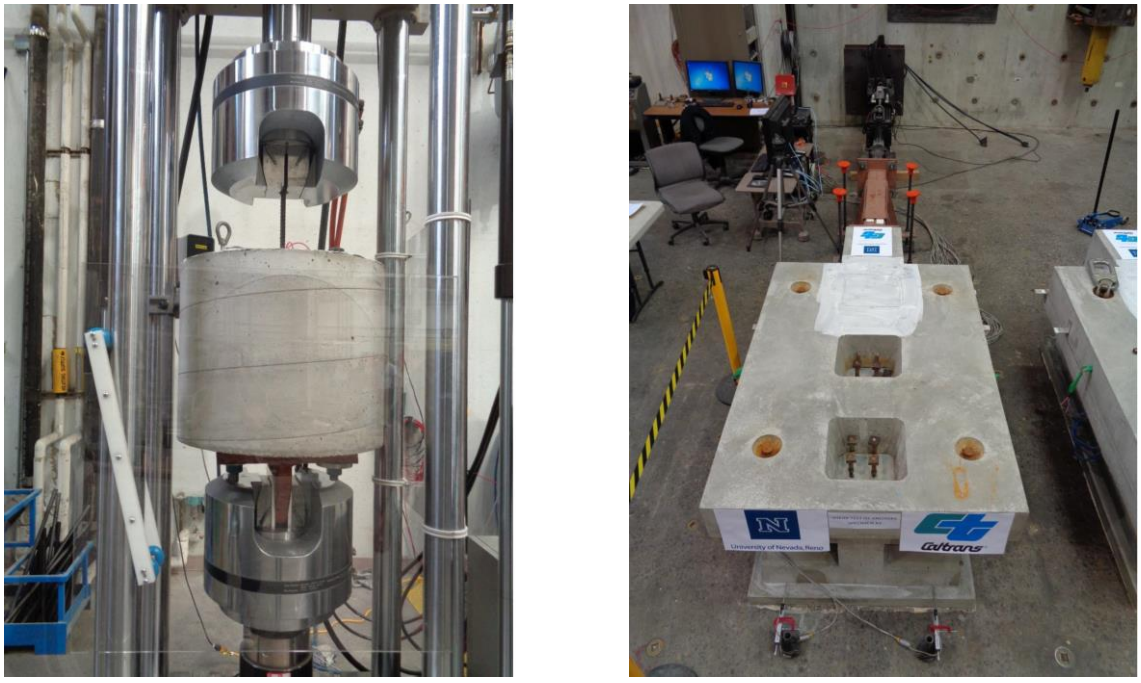

Figure 2.4 Test setup for (a) pullout and (b) shear tests (Shrestha et al. 2017)

(a) (b)

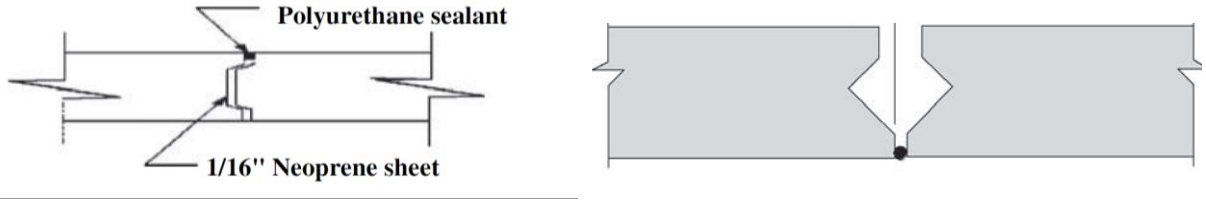

Figure 2.5 Typical detail for (a) male-to-female and (b) female-to-female joints between full-depth panels (Badie and Tadros, 2008)

2.6. References

Azizinamini, A., Yakel, A., & Farimani, M. (2005). Development of a Steel Bridge System-Simple for Dead Load and Continuous for Live Load: Volume 1-Analysis and Recommendations (No. NDOR Research Project Number P542).

Badie, S. S., & Tadros, M. K. (2008). Full-depth Precast Concrete Bridge Deck Panel Systems: Sameh S. Badie and Maher K. Tadros (Vol. 584). Transportation Research Board.

Caltrans, Splices in bar reinforcing steel, Memo to Designers 20-9 (2016), Caltrans, California Department of Transportation, Sacramento, CA

Cheng, Z. Y., Saiidi, M. S., & Sanders, D. (2010). "Seismic Design Method for Reinforced Concrete Two-Way Column Hinges". ACI Structural Journal, 107(5).

Culmo, M. P., Marsh, L., Stanton, J., & Mertz, D. (2017). "Recommended AASHTO Guide Specifications for ABC Design and Construction" (No. NCHRP Project 12-102).

Haraldsson, O. S., Janes, T. M., Eberhard, M. O., and Stanton, J. F. (2013). "Seismic resistance of socket connection between footing and precast column." Journal of Bridge Engineering, 18(9), 910-919.

Haroun, M., Pardoen, G., & Shepherd, R. (1993). Shear strength of pinned columns. Proceedings of the 2nd Annual Seismic Research Workshop.

Issa, M. A., Yousif, A. A., & Issa, M. A. (2000). Experimental behavior of full-depth precast concrete panels for bridge rehabilitation. *Structural Journal*, *97*(3), 397-407.

Kavianpour, F., & Saiidi, M. (2013). Experimental and Analytical Seismic Studies of a Four-Span Bridge System with Composite Piers. University of Nevada, Reno, Department of Civil and Environmental Engineering. Center for Civil Engineering Earthquake Research.

Lim, K. Y., and Mclean, D. I. (1991). "Scale model studies of moment-reducing hinge details in bridge columns." ACI Structural Journal, 88(4), 465-474.

Marsh, L.M., Wernli, M., B.E.Garrett, J.F.Stanton, M.O.Eberhard, and M.D.Weinert. (2011). NCHRP Report 698 "Application of Accelerated Bridge Construction Connections in Moderate-to-High Seismic Regions". Washington, D.C.: National Cooperative Highway Research Program, Transportation Research Board.

Matsumoto, E. E., Mark, C., Waggoner, M. E. K., Vogel, J., & Wolf, L. (2008). "Development of a precast concrete bent-cap system". PCI journal.

Matsumoto, E. E., Waggoner, M. C., Sumen, G., Kreger, M. E., Wood, S. L., & Breen, J. E. (2001). "Development of a Precast Bent Cap System" (No. Report no. RR-1748-2). University of Texas at Austin. Center for Transportation Research.

Mehrsoroush, A., Saiidi, M., & Ryan, K. (2017). "Development of Earthquake-Resistant Precast Pier Systems for Accelerated Bridge Construction in Nevada". (No. 555-14-803).

Mohebbi, A., Saiidi, M. S., & Itani, A. M. (2018a). Shake Table Studies and Analysis of a PT-UHPC Bridge Column with Pocket Connection. Journal of Structural Engineering, 144(4), 04018021.

Mohebbi, A., Saiidi, M. S., & Itani, A. M. (2018b). “Shake Table Studies and Analysis of a Precast Two-Column Bent with Advanced Materials and Pocket Connections”. Journal of Bridge Engineering, 23(7), 04018046.

Mortensen, J., and M. Saiidi, "A Performance-Based Design Method for Confinement in Circular Columns," Civil Engineering Department, University of Nevada, Reno, Report No. CCEER 02-07, November 2002.

Motaref, S., Saiidi, M. S., & Sanders, D. (2013). Shake table studies of energy-dissipating segmental bridge columns. Journal of Bridge Engineering, 19(2), 186-199.

Pang, J., K.P.Steuck, L.Cohagen, Stanton, J., and Eberhard, M. (2008). “Rapidly Constructible Large-Bar Precast Bridge-Bent Seismic Connection’. Olympia, WA: Washington State Department of Transportation. WA-RD 684.2

PCI Design Handbook, (2004), Precast and Prestressed Concrete, 6th edition, MNL 120-04

Perry, V. H., & Mathew Royce, P. E. (2010). Innovative field-cast UHPC joints for precast bridge decks (side-by-side deck bulb-tees), Village of Lyons, New York: Design, prototyping, testing and construction. In Proc., 3rd Int. fib Congress Incorporating the PCI Annual Convention and Bridge Conf (Vol. 1, pp. 1054-1066).

Raynor, D. J., Lehman, D. E., & Stanton, J. F. (2002). Bond-slip response of reinforcing bars grouted in ducts. Structural Journal, 99(5), 568-576.

Restrepo, J. I., M. J. Tobolski, and E. E. Matsumoto, (2011). “Development of a precast bent cap system for seismic regions.” NCHRP Rep. 681. Washington, DC: National Cooperative Highway Research Program.

Sadeghnejad, A., Azizinamini, A., (2017), “Extending the Application of Simple for Dead and Continuous for Live Load Steel Bridge System to ABC Applications in Seismic Regions. Phase II-Experimental” Web-based quarterly Research Seminar, ABC-UTC research center, Florida International University.

Shrestha, G. (2018). Seismic Studies of Superstructure and Substructure Connections for Accelerated Bridge Construction (Doctoral dissertation).

Steuck, K., Stanton, J., and Eberhard, M. (2009). “Anchorage of Large-Diameter Reinforcing Bars in Ducts”. ACI Structural Journal, Volume 106, No. 4, pp. 506-513.

Taghinezhadbilondy, R. (2016). Extending Use of Simple for Dead Load and Continuous for Live Load (SDCL) Steel Bridge System to Seismic Areas.

Tazarv, M. and Saiidi, M.S. (2014). “Next Generation of Bridge Columns for Accelerated Bridge Construction in High Seismic Zones.” Center For Civil Engineering Earthquake Research, Department of Civil and Environmental Engineering, University of Nevada, Reno, Nevada, Report No. CCEER-14-06, 400 pp.

Wassef, W. G., & Davis, D. (2004). NCHRP REPORT 527. Integral Steel Box-Beam Pier Caps. Transportation Research Board of the National Academies.

CHAPTER 3: PRETEST ANALYSIS OF SHAKE TABLE RESPONSE OF A TWO-SPAN STEEL GIRDER BRIDGE INCORPORATING ABC CONNECTIONS

This chapter is a stand-alone paper that is accepted for publication in FSCE Journal (Frontiers of Structural and Civil Engineering)

Abstract

This paper presents pretest analysis of a shake table test model of a 0.35-scale, two-span, steel plate girder bridge. The objective of pretest analysis was to obtain an insight on the seismic response of the bridge model during the shake table tests. The bridge included seat type abutments, full-depth precast deck panels, and a two-column bent in which columns were pinned to the footing and integral with superstructure. Six ABC connections were incorporated in the bridge model. An analytical model was developed in OpenSees and was subjected to ten input bi-directional earthquake motions including near-fault and far-field records. The overall seismic response of the bridge was satisfactory for all the earthquake records at 100%, 150%, and 200% design level. All connections and capacity-protected components remained elastic, and the average ductility capacity surpassed the ductility demand even at 200% design level. Using experimental fragility curves developed for RC bridge columns, it was predicted that there was a probability of 45% that columns would undergo the imminent failure in the last run and a probability of 30% for their failure.

3.1. Introduction

Bridge construction often leads to traffic delays, compromises the safety of highway workers and the traveling public, and could affect the regional economy and psychological health. Accelerated bridge construction (ABC) is a technique which utilizes prefabricated bridge elements to limit the onsite construction time. Because precast members are built offsite and under controlled environmental conditions, ABC provides an opportunity to use novel materials. In moderate and high seismic regions, it is of great importance to make sure that prefabricated elements are connected properly to guarantee bridge integrity, adequate load path, and constructability.

Several researchers have investigated the seismic performance of various connections appropriate for ABC (hereby referred to as ABC connections) in the past [1,2,3,4,5,6]. These previous studies have been on components consisting of single or a subassembly of part of the bridge rather than the entire bridge system. Moreover, the unrealistic type of loading (such as uni-directional loading) and test setup (such as inverse test set up) could impose unrealistic demands on the connections. Integrating different promising ABC connections in a single bridge under realistic seismic loading could reveal issues with construction and seismic performance that would not be otherwise known. The focus of the study discussed in this article was on combining in one bridge model six ABC connection types used in different parts of the bridge: (1) Rebar hinge pocket connection (used for connecting columns to the footing); (2) Grouted duct connection (used for connecting columns to the cap beam); (3) Seismic simple for dead continuous for live (SDCL) girder-to-cap beam connection; (4) Girder-to-deck grouted pocket connection; (5) Joints filled with ultra-high performance concrete (UHPC) between deck panels; and (6) deck panel UHPC-filled connection above the cap beam.

A rebar hinge connection is a two-way hinge detail typically used at the base of columns in multi-column bents. Two-way hinge connections reduce the transferred moment to the foundations leading to smaller and less expensive foundations. Rebar hinge connections comprise a cluster of bars placed in a pattern with a smaller diameter compared to the column diameter. Mehrsoroush, et al. [7] and Mohebbi et al. [8] performed shake table tests on two-column bents incorporating rebar hinge connections that were embedded in the pockets left in the footing or cap beam.

A two-stage hybrid cap beam (consisting of a precast and cast-in-place segment), as part of a proposed precast bent system aimed for integral bridges with prestressed girders, was tested under cyclic lateral loading [9]. The cap beam included a lower precast cap beam installed first to support the girders and a cast-in-place upper portion to integrate the pier and superstructure. Column longitudinal bars extended into grouted ducts incorporated in the precast cap beam.

A seismic detail of cap beam to girder connection for integral steel bridges was developed at Florida International University in which girders were simply supported for the dead load and continuous for the live load (SDCL). Seismic performance of the connection was experimentally investigated under cyclic lateral loading, confirming that the connection was well suited for seismic applications [10].

To provide composite action between full-depth precast deck panels and steel girders, shear studs need to be clustered in groups, and pockets need to be left in the panels to accommodate studs [11]. Shreshta et al. [12] used different materials in the pockets connecting deck to precast girders. Authors reported that the type of grout used in the pockets does not affect shear and axial capacity of studs.

UHPC is a cementitious material with water-to-cementitious material ratio of less than 25%, and a high percentage of steel fibers. Several researchers have used UHPC in joints connecting prefabricated deck panels because of its superior bond strength to reduce the required lap splice length for deck longitudinal reinforcement, thereby enabling the use of narrower joints [13,14].

Component studies have provided invaluable information on the local behavior of connections, which helps formulating seismic design guidelines for ABC connections. However, to confidently recommend ABC bridges for adoption in routine bridge design and construction in high seismic regions, a comprehensive study of ABC bridge systems and the effect of interaction and load distribution among components is essential. For example, it is not known how SDCL connections behave under seismic loading when the girders are integrated with a hybrid cap beam and column grouted duct connection. Another example is possible in-plane rotations of the superstructure when columns are pinned to the footing through rebar hinge pocket connections, and the bridge is under bi-directional loading.

A large-scale, two-span ABC bridge model with steel girders was designed, constructed, and tested on the shake tables of the University of Nevada, Reno. The study was aimed at investigating the seismic response of a bridge system integrating six ABC connections under combined gravity and bi-directional horizontal seismic loading. Another objective was to evaluate the feasibility of the construction methods and the adequacy of some of the emerging design methods for ABC connections.

This article focuses on pretest analytical studies of the model, which aimed at providing beneficial input for the design of the bridge model and the experimental program. Furthermore, seismic performance of the bridge model was investigated under a large number of input earthquake motions including near-fault and far-field records to evaluate its ductility capacity and damage potential in connections. Design, construction, testing, and measured and calculated response of the bridge model are discussed elsewhere.

3.2. Bridge Model Description

The elevation of a typical two-span highway bridge is shown in Fig. 1. This bridge was used as the prototype. The width of the prototype superstructure section was 7.8 m (31 ft). The axial load index (ALI) for the columns, defined as the dead load divided by the product of the nominal concrete compressive strength and the gross cross-sectional area of each column was 0.057. The prototype bridge was scaled down to 0.35 to enable testing on shake tables at the University of Nevada, Reno. Fig. 2 shows a 3-dimensional representation of test setup. The geometric configuration and general dimensions of the bridge model are shown in Fig. 3. The bridge model incorporated two equal spans of 10.6 m (34 ft – 8 in.), a two-column bent, full-depth precast deck panels, and seat type abutments. The skew angle was zero at both abutments. Schematics of column-to-cap beam and column-to-footing connections are shown in Fig. 4. The columns were integral with the superstructure but hinged at the base through two-way hinges embedded in pockets formed in the footing. For girders to be simply supported for dead load and continuous for seismic loads, the cap beam was constructed in two stages, a lower and an upper part, with the former being precast and the latter being cast-in-place. The girders were supported on the precast part. Fig. 5 shows cap beam details before and after casting concrete on top of stage I cap beam. The longitudinal column bars passed through grouted ducts embedded in the precast cap beam and extended into the CIP part of the cap beam. To duplicate the column axial load index and stresses of the prototype bridge, extra masses were superimposed on the superstructure in form of lead pallets and concrete mass. Current United States bridge seismic design codes, such as AASHTO [12] and Caltrans SDC [16], do not include the contribution of the backwall as well as the foundation supporting the abutment in the seismic design of the bridges. The assumption of the abutment back walls to be sacrificial and shear off even under small earthquakes is to avoid any damage to the abutment pile foundation, which is hard to inspect and repair. Furthermore, previous detailed analytical studies conducted by Zadeh and Saiidi [17] concluded that elimination of the abutment interaction does not change the seismic response significantly. There is only a slight reduction in the peak displacements while maintaining the overall displacement pattern.

All components of the bridge model were designed based on AASHTO LRFD [16], and AASHTO Guide Specifications for LRFD Seismic Bridge Design [18], and emerging design methods for ABC connection based on previous studies. The bridge model was assumed to be located in Los Angeles area, Lake Wood, with the latitude and longitude of 33.84926 N, and 118.0952 W, respectively, and site class D. Design spectrum was developed utilizing United States Geological Survey (USGS), U.S. Seismic Design Maps web application [19]. AASHTO 2009 [20] was selected in the application to provide the seismic design parameter values. The time axis of the spectrum was compressed by a factor of 1.69, corresponding to the inverse of the square root of the dimensional scale factor. Design spectrum is shown in Fig. 6. The bridge components were designed such that inelastic deformations mainly occur in columns and the

superstructure and footing remain essentially elastic with no yielding or damage during shake table testing. The essentially elastic elements are referred to as "capacity protected". For capacity protected elements, inelastic response is limited to minor cracking and/or material strains that will not significantly diminish the component's stiffness. The columns were designed based on the force-based approach according to AASHTO LRFD [18], and the design was checked using the displacement-based approach in accordance to AASHTO Guide Specs [15].

Two-way hinge connections were designed based on the procedure developed by Saiidi et al. [21]. The footing incorporated two corrugated steel pipes as pockets for rebar hinge elements. Column embedment length in the footing was 1.25 times the required tension development length of the column longitudinal bars, and 1.18 times the column cross sectional dimension. The lower (precast) cap beam was designed for the construction loads. The lower cap beam incorporated 24, 51-mm (2-in.) diameter corrugated galvanized metal ducts that were later filled with high-strength nonshrink grout. The entire cap beam was designed for seismic loading. Table 1 lists the design properties of bridge components.

A uniform cross section was used for girders throughout the bridge length. The girders were designed for Strength I, and Service I load combination in accordance to chapter 6 of Bridge Design Specifications [18]. The connection of the girders to the cap beam was designed and detailed according to SDCL connection that was developed [Fig. 5] by Taghinezhadbilondy et al. [22]. The tie bars were designed to resist the vertical component of the seismic forces. Two steel blocks welded to the girder bottom flanges were used to improve the negative moment capacity of the connection. Dowel bars (cap beam stirrups), as the main load carrying mechanism under reverse loading, were designed based on the established Caltrans [16] design provisions for capacity protected elements.

The deck in the prototype bridge was designed considering HL93 loading as the live load, and 2.39 kPa (50 PSF) as the wearing surface. The required reinforcement area was then scaled down for the deck panels in the test model. The bridge model included 22 precast deck panels joined together with transverse female-to-female joints. The girders were connected to the deck panels using clusters of four shear studs welded to the girder top flange and embedded in grout-filled deck pockets left in the precast deck panels. Shear studs were designed for Strength and Fatigue limit states. UHPC was used in the panel joints to decrease the required lap splice length for deck longitudinal bars. Although lap splice length was sufficient for deck reinforcement over the pier using normal strength grouts, UHPC was used in the upper 70 mm (2 ¾ in.) of the cap beam to match the deck thickness.

3.3. Pretest Computational Analyses

Pretest analytical studies were conducted to estimate design forces for preliminary design of the bridge components, determine linear and nonlinear seismic response of the bridge, verify that the capacity protected elements remain in the elastic range, and determine the suitable ground motion and the loading protocol for the shake table tests. The CSiBridge [23] and the Open System for Earthquake Engineering Simulation (OpenSees) [24], finite element packages were used in the pretest studies, with the former for linear analysis and the latter for nonlinear analysis, as explained in subsequent sections.

3.3.1. Modeling Method

A 3-dimensional computational model of the prototype bridge was created using CSiBridge software [Fig. 7]. Linear analysis under Strength I, Service I, Extreme Event I, and Fatigue I limit states (according to AASHTO [17]) was conducted for the force-based design of columns, design of steel plate girders and shear studs. Shell elements, with automatically generated meshes, were used to model the deck panels. The girders, cap beam, and columns were modeled using "Frame" elements. Since the bridge was supported on seat type abutments, translation of the abutment bearing in all directions but vertical, was unrestrained. The girder to deck shear connectors were modeled using flexible link elements. The shear and axial stiffness values of the link elements were based on the measured data obtained by Shrestha et al. [12] using full-scale slab-girder connection tests. Fig. 8 shows the force-displacement plots of connectors. The column to cap beam connection was through "Rigid Links". All the translational and rotational components of the cap beam link elements were fixed to represent integral connections.

OpenSees was used for nonlinear static analysis (pushover) and nonlinear dynamic response history analysis (RHA). A schematic view of the OpenSees model is presented in Fig. 9. The OpenSees model was composed of linear beam column elements combined with nonlinear column fiber section elements that connected a three-dimensional assemblage of nodes. Nodes and elements were located at center of gravity of the bridge components. All nonlinear deformations in the computer model were assumed to take place in the columns.

The superstructure was modeled using Enhanced Beam-Stick model [25]. A grillage was used to represent the deck and the girders. "ElasticBeamColumn*"* elements were used to model deck and girder elements. The longitudinal elements representing the deck were connected through elastic transverse beams. A modification factor of 0.5 was assigned to the longitudinal and transverse beams for torsional constant. Since there is no interaction between axial force and bending moment in two perpendicular directions in the grillage, poisson's ratio of grillage beams was set equal to zero [26]. The deck elements were treated as cracked members by assigning 40% of the gross section rigidity to the deck elements [27].

To capture nonlinear effects in the columns and rebar hinges, force-based beam column elements were used, which allow for the distribution of plasticity along the length of the member. The defined "aggregator" option in OpenSees was used to add cracked section shear and torsional properties to the column fiber element sections. Rebar hinge elements were fixed to the base, and the girders were supported on rollers at the abutments. The girders were connected to the cap beam by means of rigid links. Deck to girder connection was modeled by "twoNodeLink" elements. The axial and horizontal shear properties were defined for the link elements, each representing a cluster of four studs. The axial stiffness of the link element was defined using elastic bilinear uniaxial material object and shear stiffness was defined using multi-linear elastic uniaxial material object.

The superstructure mass was lumped at the nodes defined at 25 points along the length of each girder. The superimposed masses were lumped at the nodes defined at the center of each concrete block or lead pallet. The center of mass node for each superimposed load was connected with a rigid beam column element vertically to the centerline of the superstructure.

The expected material properties were used in the analysis. Grade 60 reinforcement steel [with the expected yield stress of 469 MPa (68 ksi) per SDG [16]] was specified for mild steel reinforcement, and the specified 28-day compressive strength of concrete was 27.6 MPa (4 ksi) with the expected compressive strength of 35.9 MPa (5.2 ksi). The concrete behavior was modeled using "Concrete02", which is a concrete model with tensile strength and linear tension softening. "ReinforcingSteel" material was used to model the longitudinal bars of the column. Damping was specified using mass and stiffness proportional coefficients that were calculated for two percent damping. The P-delta effects were included in the analysis. "UniformExcitationPattern" command, which applies the same ground motion record at different support points, was used to apply ground motion accelerations in the transverse and longitudinal directions.

3.3.2. Linear Analysis

Results of the linear analysis under different limit states were utilized for the design of the bridge components. Detailed description of the design procedure is discussed elsewhere. Modal analysis of the prototype bridge assuming cracked section properties for columns showed that the first three modes were in-plane rotation, longitudinal (along traffic), and transverse with periods of 3.5, 0.67, and 0.59 s, respectively. Fig. 10 presents the first three mode shapes.

3.3.3. Nonlinear Static Analysis

Nonlinear static analysis (pushover) was conducted in each of the transverse and longitudinal directions of the bridge model to obtain the capacity curves. The results are shown in Fig. 11. The columns were assumed to fail when either strain in an edge fiber in the core concrete reaches 125% of calculated ultimate concrete compressive strain (ε_{cu}) obtained from the Mander's confinement model [28], or a longitudinal bar strain reaches the ultimate tensile strain (ε_{su}). Using these criteria, the calculated displacement ductility capacity of the bent was 5.7 and 6.2 in the longitudinal and transverse directions, respectively. The ultimate displacement was controlled by the core concrete failure in both directions. The capacity curves were idealized by an elastoplastic relationship to estimate the plastic shear force and the effective yield displacement. The elastic portion of the idealized curve passed through the point marking the first longitudinal bar yielding. The idealized plastic lateral force was obtained by balancing the areas between the calculated and the idealized curves beyond the first reinforcing bar yield point.

Based on the dynamic mass [64.4 Metric ton (142 kips)] and the effective initial stiffness of the pier, the effective natural period of the bridge model was 0.44 s and 0.41 s, in the longitudinal and transverse directions of the bridge, respectively. The slope of the first branch of the idealized bilinear pushover curve was regarded as the effective initial stiffness of the pier.

3.3.4. Response History Analysis

Response history analyses were conducted on the bridge model using OpenSees to evaluate its ductility capacity and damage potential in connections and capacity protected members. The bridge was analyzed under a large number of near-fault and far-field ground motions (GMs) of different intensities.

Two horizontal components of 5 near-fault and 5 far-field GMs, selected from the Pacific Earthquake Engineering Research Center (PEER) strong ground motion database (NGA-West2 program), were used as the input GMs in the analyses. The parameters that were used in the

selection of GMs were: (1) VS30 (average small strain shear wave velocity in the upper 30.48 m (100 ft) of the soil column); (2) earthquake magnitude; and (3) distance to fault (Rjb). The range of VS30 between 200 m/s (656 ft/s) to 360 m/s (1181 ft/s), corresponding to site class D and earthquake magnitude greater than six was assumed in the selection of GMs. The Rjb between 0 to 15 km (0 to 9.3 miles) and 15 to 30 km (9.3 to 18.6 miles) was used to distinguish near-fault and far-field ground motions [29]. Table 2 lists the selected GMs. In this table, NGA is the new generation attenuation number and PGA is the peak ground acceleration. For scaling considerations, the duration of the motions was shortened by a factor of 1.69.

Although the use of a large number of records may improve estimates of the average demands obtained from RHA, this approach may not be practical. To minimize the statistical dispersion and maximize the accuracy in the response parameters estimated from RHA under relatively small number of records, ground motions were scaled to the target design spectrum. The scaling was applied to the spectral acceleration at the fundamental period of the bridge $S_a(T_1)$. The response spectra for the input motions were calculated for 5 percent damping. Each component of the records was then scaled to match the design spectral acceleration at the average of the longitudinal and transverse periods of the bridge (0.43 sec) that were based on the effective stiffnesses obtained from pushover analyses. To use the same scale factor for both components of each GM, the average of the two scale factors were utilized. Fig. 12 shows the response spectra for the ten scaled records superimposed on the design spectrum for each direction. The records were further multiplied by 1.5 and 2.0 to represent 150% and 200% versions of the design earthquake.

A total of 30 response history analyses were conducted on the bridge model under bi-axial horizontal excitations simultaneously in the transverse and longitudinal directions. The component with higher PGA was applied in the longitudinal direction to place relatively high demands on the superstructure-substructure connections.

The maximum and residual drift ratios for each GM at 100%, 150%, and 200% design level and in both directions are listed in Table 3. Theoretical failure occurred for N1 and N3 at 150% and 200% design level, and for F1 at 200% design level, which corresponds to the ductility demand exceeding the ductility capacity. The analyses were stopped when the theoretical failure occurred. Therefore, the residual displacement is not specified for these motions. It can be seen from the table that near-fault motions are more demanding in terms of the maximum and residual drift ratios compared to far-field motions. For instance, residual drift ratio for all the far-field motions were less than 1%, which was considered negligible [30]. However, N2 and N5 led to residual drift ratios of more than 1% at 200% design level. Moreover, the effect of near-fault ground motion tended to be more severe under higher-amplitude motions (for instance the 200% versions of the design level earthquake compared to 150% and 100% design level).

Table 4 lists the maximum and average values for critical response parameters under the 10 earthquake records set in addition to associated capacities. The response parameters consisted of the maximum values of cap beam shear, positive and negative moment in the cap beam, shear in the deck to girder connectors, and positive and negative moment in the superstructure. All capacity to demand ratios were equal or more than one. which indicates that cap beam, superstructure, and deck to girder connectors remained elastic even under 200% design level. It is worth noting that the calculation of the cap beam moment capacities was based on the first

reinforcing bar yield and with cap beam side reinforcement being ignored. Therefore, C/D = 1.0 (for cap beam negative moment) corresponds to the yielding of the first rebar in the cap beam. Moreover, with an overstrength factor of 1.2 to obtain the cap beam flexural demand and nominal material properties to obtain its flexural capacity [16], essentially elastic behavior is ensured by using resistance factor equal to 1.0 (C/D=1.0).

3.4. Bridge Model Response Prediction for the Test Input Records

Results of the RHA under the earthquake set were examined to determine the input motion in the shake table test. The 142-degree and 52-degree horizontal components of the Sylmar convertor station ground motion record obtained during the 1994 Northridge, California earthquake (referred to N2 in this paper) was selected as the input ground motion in the shake table test. The reason for this selection was in part because this motion was one of the more critical motions among the earthquake records. Another important reason was so comparisons could be made with the response of a similar two-span ABC bridge model (Calt Bridge-1) with concrete superstructure that had been tested on a shake table, under the same motion [31].

The component with higher PGA (the 142-degree) was applied in the longitudinal direction. The amplitude of the design earthquake was determined so that the peak resultant displacements obtained from the nonlinear dynamic analysis and that obtained from the orthogonal combination of the design displacement demands were approximately the same. As a result, the acceleration records for each component were further scaled by a factor of 0.6 to build the target design earthquake (TDE). The time scaled acceleration, velocity, and displacement histories for the target design earthquake are shown in Fig. 13. The response spectra for the two components of the TDE and their square root of sum of squares (SRSS) resultant under 5% damping is shown in Fig. 14.

The number of earthquake runs and associated scale factors were selected so that different damage states of the bridge were captured. The desired maximum displacement in each run was such that the pushover curve can be produced based on the envelope of the hysteresis curve in each direction to represent the overall nonlinear behavior of the bridge. The loading protocol started with 0.3×Sylmar to capture the elastic response and followed by 0.65×Sylmar and 1.0×Sylmar, continued to 2.0×Sylmar with 0.25×Sylmar increments to capture. Table 5 lists the scale factors for different motions and the associated PGA values. The target shake table accelerations in the longitudinal and transverse directions are shown in Fig. 15. Response history analysis was conducted under a spliced record that combined in sequence all the records in the loading protocol. Sufficient gap with zero amplitudes were included in the beginning and at the end of each earthquake record to assure that the test model comes to complete rest after each run. The spliced record corresponded to the motion that the bridge model would undergo during the tests.

The displacement histories of top of the columns in the longitudinal and transverse directions are illustrated in Fig. 16. To identify the maximum bent displacement demand, the resultant of longitudinal and transverse displacement histories was calculated and is also shown in Fig. 16. The peak resultant displacement [157 mm (6.2 in.)] corresponding to resultant drift ratio of 7.4%, is only about 20% higher than the peak longitudinal and transverse direction values meaning that the maximum displacements in the two directions do not occur at the same time. The displacement ductility demand was estimated by dividing the resultant displacement by the bent

yield displacement obtained from the idealized pushover curves. The maximum ductility demand was approximately 10.3.

The force-displacement hysteresis curves as well as the associated backbone curves under the spliced motion in both the longitudinal and transverse directions are shown in Fig. 17. The force-displacement response of the bridge model indicated stable hysteretic behavior with ample energy dissipation. The dissipated energy increased in successive runs due to the higher displacements and insignificant strength degradation.

3.5. Expected Damage States

To predict the extent and type of the apparent damage in the columns of the bridge model after each earthquake run and how these compare with that of conventional bridge columns, the damage states defined by Vosooghi and Saiidi [32] were utilized. Their database included 32 cast-in-place bridge large-scale columns tested either on shake tables or under lateral quasi-static loading. Although only eight columns were tested under bi-directional loading, it was believed that the fragility curves could be applicable to the columns of the bridge model in the current study because resultant drift ratios were used in this part of the analysis. Furthermore, the amplitude of the motion was not considered as a parameter in developing the fragility curves, and the correlation between the selected response parameters and damage states were independent of the amplitude of the motion.

Table 6 lists the damage states and the associated extent of apparent damage. Fig. 18 shows photos of the apparent damages for each damage state. One of the key response parameters that can be used to indicate the probability that a component will be damaged to a given DS is the maximum drift ratio (MDR). MDR that was used in this study was based on the resultant displacements to predict damage state after each run. Table 7 lists the predicted probability of occurrence for each damage state in each run. It can be seen that in the third run, there was a probability of 60% for the formation of the flexural cracks in the columns (DS-1) and a 10% probability for minor spalling and possible shear cracks (DS-2). For the fourth run there were 90% and 60% chance for the columns to be in the DS-1 and DS-2, respectively, and a 10% chance for extensive cracks and spalling (DS-3). In Run 5, in which the ductility demand surpassed the ductility capacity of the bridge in both directions, lateral and/or longitudinal reinforcing bars were expected to be visible by a 50% probability. Moreover, there was a 25% chance for the compressive failure for the concrete core edge (imminent failure) during this run. In Run 6, there were 95%, 70%, 40%, and 20% probability of occurrence for DS-3, DS-4, DS-5, and failure, respectively. Finally, the last run, in which the first longitudinal bar reached the ultimate tensile strength in the model, the probability of DS-4 occurrence was increased to 75%. In addition, there were 45% probability of imminent failure and 30% probability of complete column failure.

3.6. Conclusions

The following conclusions were drawn based on the information and discussions presented in this paper.

1. All the components of the two-span bridge test model exhibited satisfactory seismic performance under a large number of input earthquake motions that included near-fault and far-field records.

2. Near-fault motions were more demanding in terms of the maximum and residual drift ratios compared to far-field motions. For instance, residual drift ratio for all the far-field motions were less than 1% which was considered negligible. However, N2 and N5 led to residual drift ratios of more than 1% at 200% design level.
3. The effect of near-fault ground motion tended to be more severe under higher-amplitude motions (for instance the 200% versions of the design level earthquake compared to 150% and 100% design level).
4. The theoretical failure occurred in five out of the 30 response history analyses. These included N1 and N3 at 150% and 200% design level, and N1, N3, and F1 at 200% design level.
5. Vosooghi and Saiidi's fragility curves were used to predict damage states of the bridge model during the shake table test. It was concluded that columns would pass DS-1 in the third run and DS-2 in the fourth run. In the last run, there were 75% and 45% chance that columns would be in DS-4 and DS-5 (imminent failure), but there was only a 30% chance that columns would fail.

Detailed description of the design methods and construction sequence of the bridge model, as well as observed damages during the shake table test were developed but will be presented elsewhere [33]. Moreover, measured experimental results of the shake table test will be presented in a separate manuscript [34].

3.7. Acknowledgement

The study presented in this article was supported by the Accelerated Bridge Construction University Transportation Center (ABC-UTC) at the Florida International University (FIU). This study would not have been possible without the assistance and advice of the UNR Earthquake Engineering Laboratory staff Dr. Patrick Laplace, Chad Lyttle, Todd Lyttle, and Mark Lattin. The support and advice of ABC-UTC director, Dr. Atorod Azizinamini, is greatly appreciated. Thanks are due to Mojtaba Alian, Jose Benjumea Royero, Jared Jones, Amir Sadeghnezhad, Dr. Alireza Mohebbi, and Dr. Ali Mehrsoroush. The authors would like to thank Lafarge North America Inc. for donating UHPC material, C&K Johnson Industries for donating corrugated metal ducts, Reno Iron Works for fabrication of steel girders at a reduced cost, and NSBA for donating steel material for the girders, cross frames, and other accessories.

3.8. References

[1] Matsumoto, E.E., Waggoner, M.C., Sumen, G. and Kreger, M.E. (2001). "Development of a Precast Bent Cap System," Center for Transportation Research, The University of Texas at Austin: FHWA Report No. FHWA/TX-0-1748-2.

[2] Restrepo, J.I., Tobolski, M.J. and Matsumoto, E.E. (2011). "Development of a Precast Bent Cap System for Seismic Regions," NCHRP Report 681, Washington, D.C.

[3] Tazarv, M., Saiidi, M. (2014). Next generation of bridge columns for accelerated bridge construction in high seismic zones. Center for Civil Engineering Earthquake Research, Department of Civil and Environmental Engineering, University of Nevada, Reno, Nevada, Report No. CCEER-14-06.

[4] Motaref, S., Saiidi, M., and Sanders, D. (2011). "Seismic Response of Precast Bridge Columns with Energy Dissipating Joints," Center for Civil Engineering Earthquake

Research, Department of Civil and Environmental Engineering, University of Nevada, Reno, Report No. CCEER-11-01.

[5] Mehrsoroush, A., and Saiidi, M. (2016). "Cyclic Response of Precast Bridge Piers with Novel Column-Base Pipe Pins and Pocket Cap Beam Connections." J. Bridge Eng., 10.1061/(ASCE)BE.1943-5592.0000833, 04015080

[6] Mehraein, M., and Saiidi, M. (2016). "Seismic Performance of Bridge Column-Pile-Shaft Pin Connections for Application in Accelerated Bridge Construction." Rep. No. CCEER-16-01, Center for Civil Engineering Earthquake Research, Dept. of Civil and Environmental Engineering, Univ. of Nevada, Reno, NV.

[7] Mehrsoroush, A., Saiidi, M., & Ryan, K. . (2017). Development of Earthquake-Resistant Precast Pier Systems for Accelerated Bridge Construction in Nevada (No. 555-14-803).

[8] Mohebbi, A., Saiidi, M., and Itani, A., "Development and Seismic Evaluation of Pier Systems w/Pocket Connections, CFRP Tendons, and ECC/UHPC Columns," Center for Civil Engineering Earthquake Research, Department of Civil and Environmental Engineering, University of Nevada, Reno, Nevada, Report No. CCEER-17-02, June 2017

[9] Marsh, M. L., Stanton, J. F., Eberhard, M. O., Haraldsson, O., & Khaleghi, B. (2010). A precast bridge bent system for seismic regions.

[10] Sadeghnejad, A., Azizinamini, A., (2017), "Extending the Application of Simple for Dead and Continuous for Live Load Steel Bridge System to ABC Applications in Seismic Regions. Phase II-Experimental" Web-based quarterly Research Seminar, ABC-UTC research center, Florida International University.

[11] Badie, S. S, and Tadros, M. K, (2008). "Full-Depth Precast Concrete Bridge Deck Panel Systems", Report 584 by National Cooperative Highway Research Program.

[12] Shrestha, G., Itani, A., and Saiidi, M. (2017) "Seismic Performance of Precast Full-Depth Decks in Accelerated Bridge Construction" Center for Civil Engineering Earthquake Research, Department of Civil and Environmental Engineering, University of Nevada, Reno, Report No. CCEER-17-05.

[13] Graybeal, B. (2010). "Behavior of Field-Cast Ultra-High Performance Concrete Bridge Deck Connections under Cyclic and Static Structural Loading," Federal Highway Administration, Report No. FHWA-HRT-11-023.

[14] Graybeal, B., (2014), "Design and Construction of Field-Cast UHPC Connections", Federal Highway Administration Publication No. FHWA-HRT-14-084. Pp. 1-36.

[15] American Association of State Highway and Transportation Officials (AASHTO). (2014). "Guide Specifications for LRFD Seismic Bridge Design", Washington, D.C.

[16] Caltrans. Seismic Design Criteria (SDC). (2013). version 1.7. California Department of Transportation, Sacramento, CA

[17] Sadrossadat-Zadeh, M. and Saiidi, M., "Analytical Study of NEESR-SG 4-Span Bridge Model Using OpenSees," Center for Civil Engineering Earthquake Research, Department of Civil Engineering, University of Nevada, Reno, Nevada, Report No. CCEER-07-03, January 2007.

[18] American Association of State Highway and Transportation Officials (AASHTO), (2012). AASHTO LRFD Bridge Design Specifications, 6th edition.

[19] US Seismic Design Maps, Earthquake hazard Program, https://earthquake.usgs.gov/designmaps/us/application.php, 2016, [accessed January 2016]

[20] mbsen, R. A. (2009). AASHTO guide specifications for LRFD seismic bridge design. AASHTO

[21] Saiidi, M. S., Cheng, Z. Y., & Sanders, D. (2009). "Experimental Study of Two-Way Reinforced Concrete Column Hinges under Seismic Loads". ACI Structural Journal, 106(3), 340.

[22] Taghinezhadbilondy, R., Yakel, A., and Azizinamini, A., (2016), "Extending Use of Simple for Dead Load and Continuous for Live Load (SDCL) Steel Bridge System to Seismic Areas". Dept. of Civil and Environmental Engineering, Florida International University, Miami, FL.

[23] CSiBridge (V19.2.2, 2016), CSI Computer & Structures Inc. Integrated 3-D Bridge Analysis, Design, and Rating. Berkeley (CA): Computer & Structures, Inc.

[24] McKenna, F., Fenves, G., and Scott, M., "Open System for Earthquake Engineering Simulation (OpenSees)", Berkeley, California: Pacific Earthquake Engineering Research Center, 2000.

[25] Amirihormozaki, Ebrahim, Gokhan Pekcan, and Ahmad Itani. "Analytical modeling of horizontally curved steel girder highway bridges for seismic analysis." Journal of Earthquake Engineering 19.2 (2015): 220-248.

[26] Hambly, E. C. [1990] Bridge Deck Behaviour, 2nd ed.

[27] Carden, L. P., Itani, A., and Buckle, I. G. (2005) "Seismic load path in steel girder bridge superstructures," Center for Civil Engineering Earthquake Research, Dept. of Civil Engineering, University of Nevada, Reno, Nevada, Report No. CCEER-05-03.

[28] Mander, J. B., Priestley, M. J., & Park, R. (1988). Theoretical stress-strain model for confined concrete. Journal of structural engineering, 114(8), 1804-1826.

[29] Alavi, B., & Krawinkler, H. (2000, January). Consideration of near-fault ground motion effects in seismic design. In Proceedings of the 12th World Conference on Earthquake Engineering (p. 8).

[30] Japan Road Association (2000), Design Specifications for Highway Bridges, Part Seismic Design (English edition).

[31] Bridge System Seismic Research for Accelerated Bridge Construction (ABC), https://wolfweb.unr.edu/homepage/saiidi/caltrans/abc-systems.html, 2018, [accessed 2 August 2018]

[32] Vosooghi, A., and Saiidi, M. S., (2012). "Experimental fragility curves for seismic response of reinforced concrete bridge columns." ACI Struct. J. 109 (6), 825–834.

[33] Shoushtari, E., Saiidi, M., and Itani, A., Moustafa, M. (2018) "Design, construction, and Shake Table Testing of a Steel Girder Bridge System with ABC Connections", ASCE Journal of Bridge Engineering, Manuscript submitted for publication

[34] Shoushtari, E., Saiidi, M., and Itani, A., Moustafa, M. (2018) "Seismic Performance of a Two-Span Steel Girder Bridge with ABC Connections under Earthquake Loading", Manuscript in preparation.

Table 3.1 Design properties of bridge components

Scale factor	0.35
Span length	10.6 m (34 ft-8 in.)
Width of the bridge	3.4 m (11 ft)
Number of girders in each span	4
Column diameter	406 mm (16 in.)
Column height	2.1 m (84 in.)
Axial load index (dead load)	5.7%
Column longitudinal bar	12#5 [dia.= 16 mm (0.625 in.)]
Column longitudinal steel ratio	1.83%
Column transverse steel	#3 [dia.= 9.5 mm (0.375 in.)] @ 63 mm (2.5 in.)
Column transverse steel ratio	1.25%
Rebar hinge longitudinal bar	6#5 [dia.= 16 mm (0.625 in.)]
Rebar hinge longitudinal steel ratio	2.40%
Rebar hinge transverse steel	#3 [dia.= 9.5 mm (0.375 in.)] @ 38 mm (1.5 in.)

Table 3.2 Input ground motions for response history analysis

rec#	NGA#	Event name	PGA	Magnitude	Scale Factor
N1	RSN4116-H1	Parkfield-02_CA	1.31	6.0	0.65
	RSN4116-H2		0.58		
N2	RSN1084-H1	Northrdige-01	0.62	6.7	0.50
	RSN1084-H2		0.93		
N3	RSN1120-H1	Kobe Japan	0.62	6.9	0.66
	RSN1120-H2		0.98		
N4	RSN1503-H1	Chi-Chi Taiwan	0.79	7.6	0.74
	RSN1503-H2		0.58		
N5	RSN1602-H1	Duzce Turkey	0.75	7.1	0.79
	RSN1602-H2		0.82		
F1	RSN338-H1	Coalinga-01	0.26	6.4	1.67
	RSN338-H2		0.28		
F2	RSN778-H1	Loma Prieta	0.27	6.9	1.24
	RSN778-H2		0.28		
F3	RSN995-H1	Northridge-01	0.23	6.7	1.59
	RSN995-H2		0.36		
F4	RSN1116-H1	Kobe_ Japan	0.23	6.9	1.46
	RSN1116-H2		0.23		
F5	RSN1203-H1	Chi-Chi_ Taiwan	0.27	7.6	1.05
	RSN1203-H2		0.20		

Table 3.3 Maximum and residual drift ratios

Design level	Motion	Maximum drift ratio		Residual drift ratio	
		Longitudinal	Transverse	Longitudinal	Transverse
100%	N1	3.5%	3.2%	0.0%	0.2%
	N2	0.6%	0.5%	0.1%	0.0%
	N3	1.4%	2.1%	0.0%	0.1%
	N4	0.9%	1.1%	0.0%	0.0%
	N5	2.0%	1.1%	0.3%	0.2%
	F1	1.5%	1.3%	0.0%	0.0%
	F2	1.4%	1.0%	0.0%	0.1%
	F3	1.2%	0.9%	0.1%	0.0%
	F4	1.1%	1.4%	0.1%	0.0%
	F5	1.4%	0.9%	0.0%	0.0%
	Max. (N)	3.0%	3.2%	0.3%	0.2%
	Max. (F)	1.5%	1.4%	0.1%	0.1%
	Ave. (N&F)	1.5%	1.4%	0.1%	0.1%
150%	N1 (failure)‡	4.1%	4.4%	N/A	N/A
	N2	2.1%	1.8%	0.1%	0.0%
	N3 (failure)	3.9%	4.7%	N/A	N/A
	N4	2.0%	1.9%	0.3%	0.1%
	N5	2.3%	1.4%	0.3%	0.2%
	F1	2.2%	3.8%	0.3%	0.3%
	F2	1.9%	3.1%	0.3%	0.8%
	F3	1.6%	1.3%	0.1%	0.0%
	F4	1.7%	1.9%	0.2%	0.1%
	F5	2.3%	1.5%	0.2%	0.1%
	Max. (N)	4.1%	4.7%	0.3%	0.2%
	Max. (F)	2.3%	3.8%	0.3%	0.8%
	Ave. (N&F)	2.4%	2.6%	0.2%	0.2%
200%	N1 (failure)	4.8%	4.8%	N/A	N/A
	N2	3.8%	3.6%	0.3%	**1.0%**†
	N3 (failure)	3.6%	3.5%	N/A	N/A
	N4	4.2%	4.6%	0.9%	0.6%
	N5	2.3%	2.9%	**1.2%**	0.6%
	F1 (failure)	2.8%	5.3%	N/A	N/A
	F2	1.9%	4.3%	0.8%	0.9%
	F3	2.8%	2.2%	0.2%	0.1%
	F4	2.0%	2.5%	0.5%	0.2%
	F5	3.0%	2.1%	0.5%	0.3%
	Max. (N)	4.8%	4.6%	1.2%	1.0%
	Max. (F)	3.0%	5.3%	0.8%	0.9%
	Ave. (N&F)	3.1%	3.6%	0.6%	0.5%

† Bold values show the residual drift ratios more than 1%.

‡ The analyses were stopped after the theoretical failure happened.

Table 3.4 Maximum demands and capacities

Demand type	Max. Demand	Capacity	C/D Ratio
Cap beam shear [kN (kips)]	414 (93)	676 (152)	1.6
Cap beam positive moment [kN-m (k-ft)]	225 (166)	366 (270)	1.6
Cap beam negative moment [kN-m (k-ft)]	373 (275)	366 (270)	1.0
Shear in a cluster of stud [kN (kips)]	67 (15)	165 (37)	2.5
Superstructure positive moment [kN-m (k-ft)]	507 (374)	2,684 (1,980)	5.3
Superstructure negative moment [kN-m (k-ft)]	217 (160)	2,556 (1,885)	11.7

Table 3.5 Loading protocol for shake table test

Run #	Test type	Factor	PGA (g, long.)	PGA (g, trans.)	%DE
WN1-L	White Noise – Long.				
WN1-T	White Noise – Trans.				
1	EQ record	0.18	0.278	0.187	30%
WN2-L	White Noise – Long.				
WN2-T	White Noise – Trans.				
2	EQ record	0.39	0.602	0.406	65%
WN3-L	White Noise – Long.				
WN3-T	White Noise – Trans.				
3	EQ record	0.60	0.926	0.624	100%
WN4-L	White Noise – Long.				
WN4-T	White Noise – Trans.				
4	EQ record	1.50	1.158	0.780	125%
WN5-L	White Noise – Long.				
WN5-T	White Noise – Trans.				
5	EQ record	0.90	1.389	0.936	150%
WN6-L	White Noise – Long.				
WN6-T	White Noise – Trans.				
6	EQ record	1.05	1.621	1.092	175%
WN7-L	White Noise – Long.				
WN7-T	White Noise – Trans.				
7	EQ record	1.20	1.852	1.248	200%

Table 3.6 Damage states and associated apparent damage [32]

Damage state	Apparent damage
DS-1	Flexural cracks
DS-2	Minor spalling and possible shear cracks
DS-3	Extensive cracks and spalling
DS-4	Visible lateral and/or longitudinal reinforcing bar
DS-5	Compressive failure of the concrete core edge (imminent failure)

Table 3.7 Predicted apparent damage of columns in the shake table test

Run No.	Max. Resultant Disp., mm (in.)	Ductility Demand	Max. Resultant Drift Ratio	Probability of occurrence for each damage state					
				DS-1	DS-2	DS-3	DS-4	DS-5	Failure
1	4 (0.15)	-	0.2%	0%	0%	0%	0%	0%	0%
2	13 (0.5)	-	0.6%	0%	0%	0%	0%	0%	0%
3	38 (1.5)	2.5	1.8%	**60%**	10%	0%	0%	0%	0%
4	66 (2.6)	4.3	3.1%	90%	**60%**	10%	0%	0%	0%
5	114 (4.5)	7.5	5.4%	100%	100%	90%	**50%**	25%	3%
6	147 (5.8)	9.7	6.9%	100%	100%	95%	**70%**	40%	20%
7	157 (6.2)	10.3	7.4%	100%	100%	100%	**75%**	45%	30%

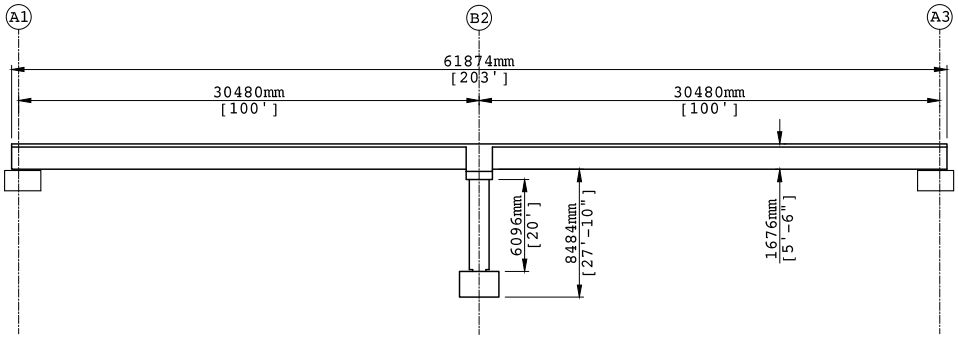

Figure 3.1 Prototype bridge configuration

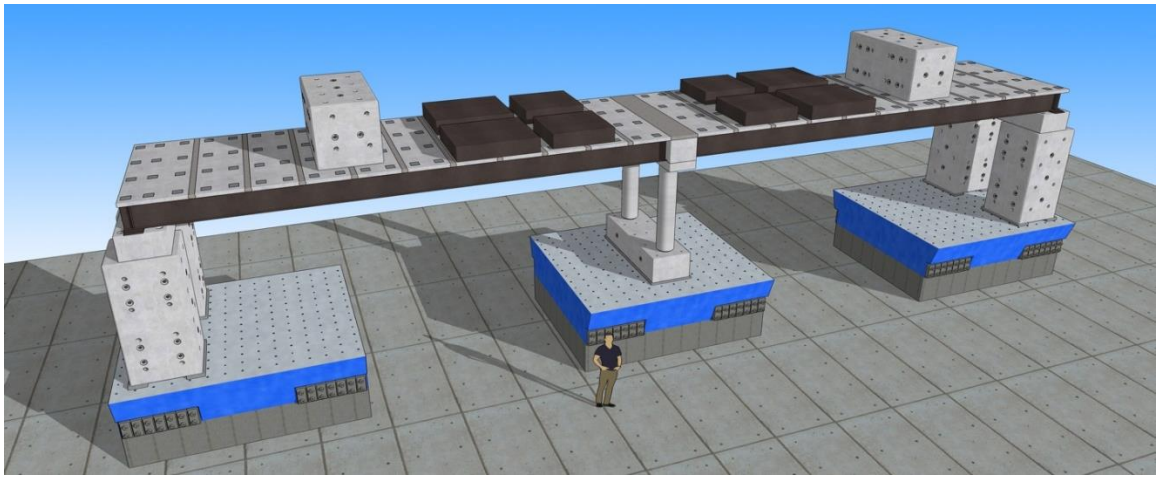

Figure 3.2 Test setup

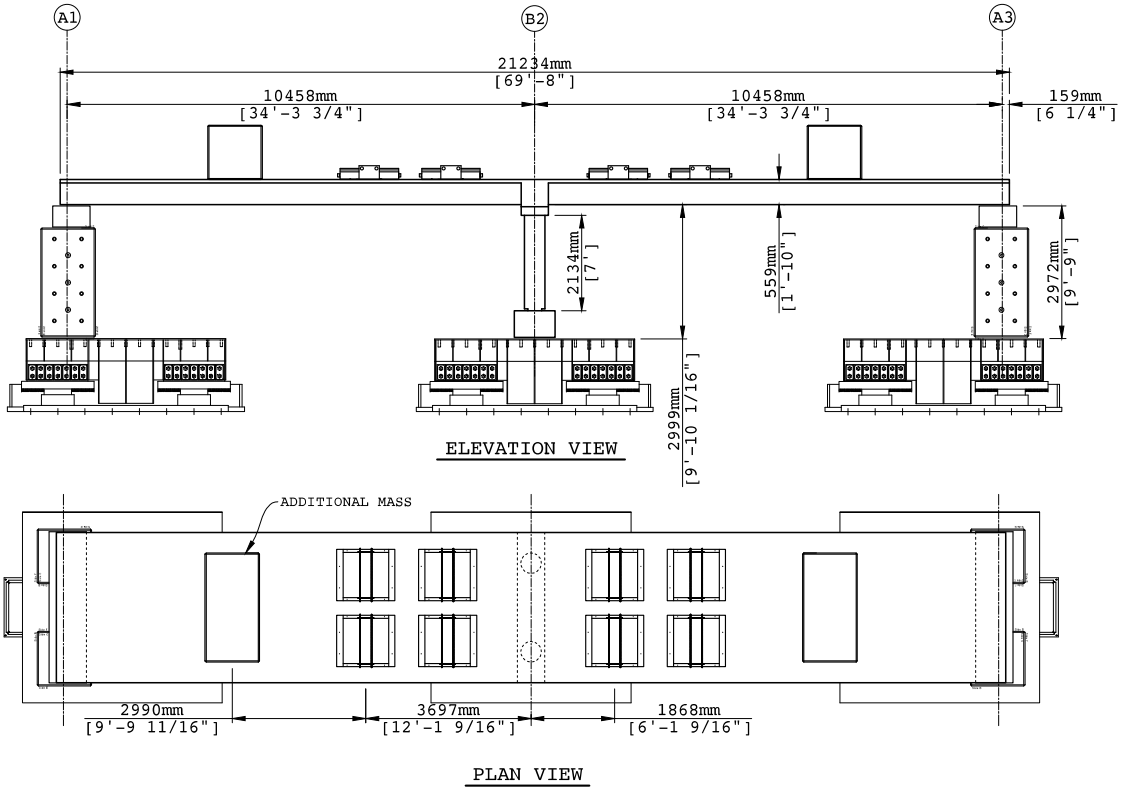

Figure 3.3 Geometric details of the bridge model

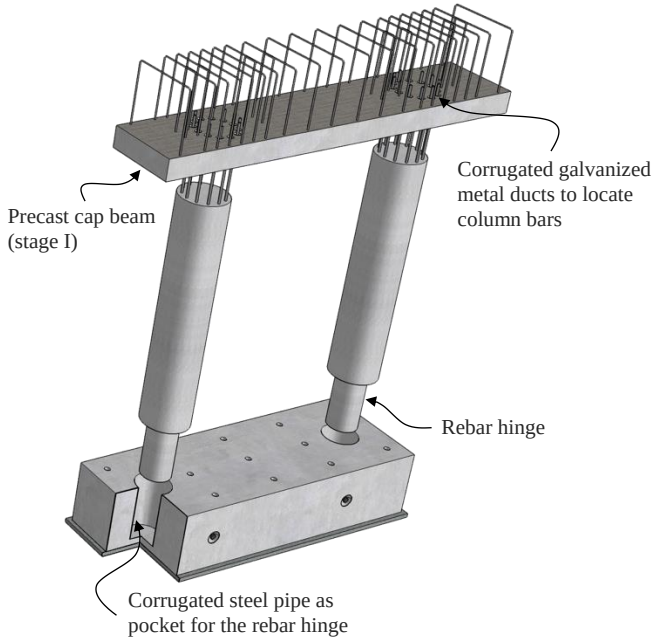

Figure 3.4 Column-to-footing and column-to-cap beam connection

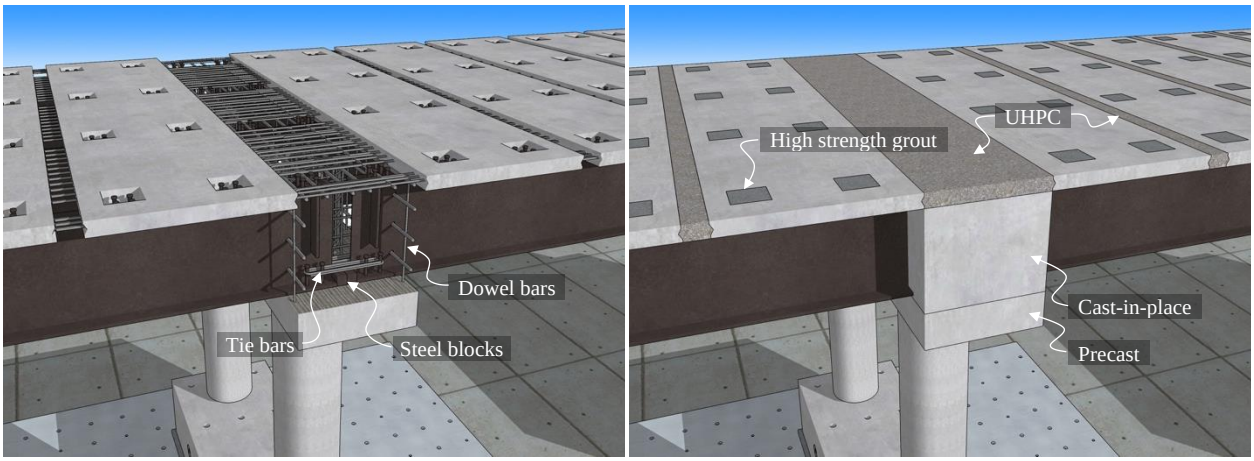

Figure 3.5 Superstructure over pier cap before and after pouring UHPC, grout, and conventional concrete

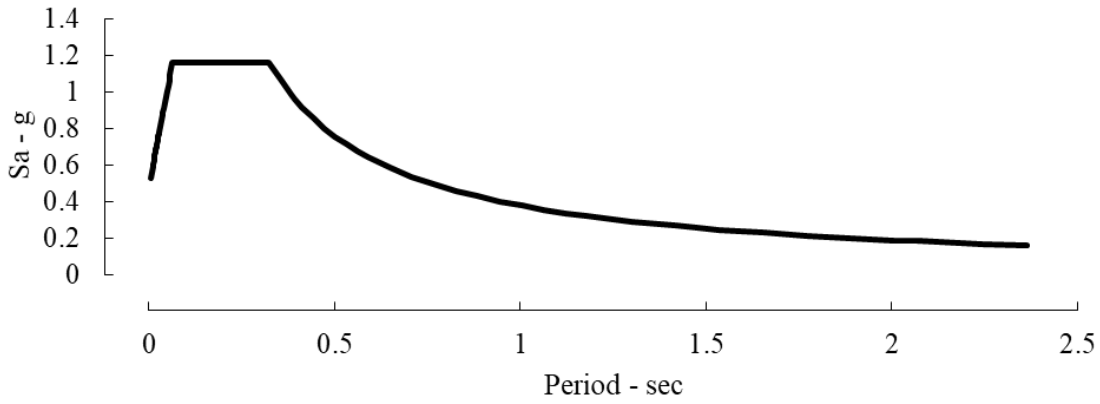

Figure 3.6 Design spectrum

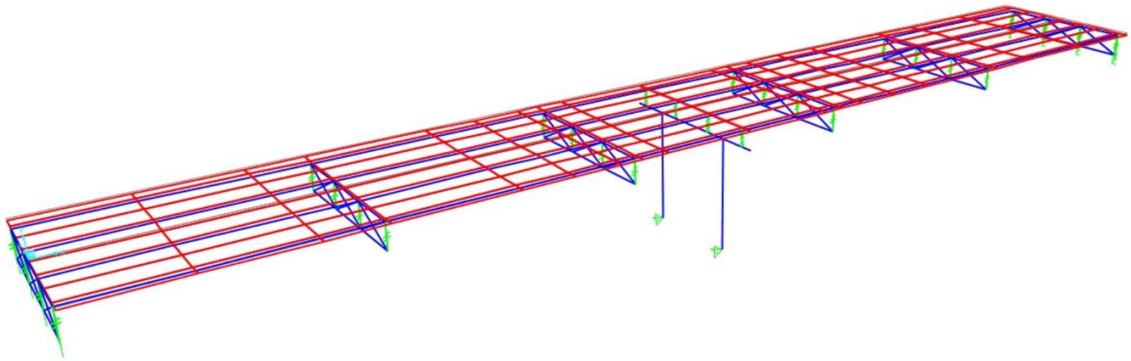

Figure 3.7 CSiBridge model

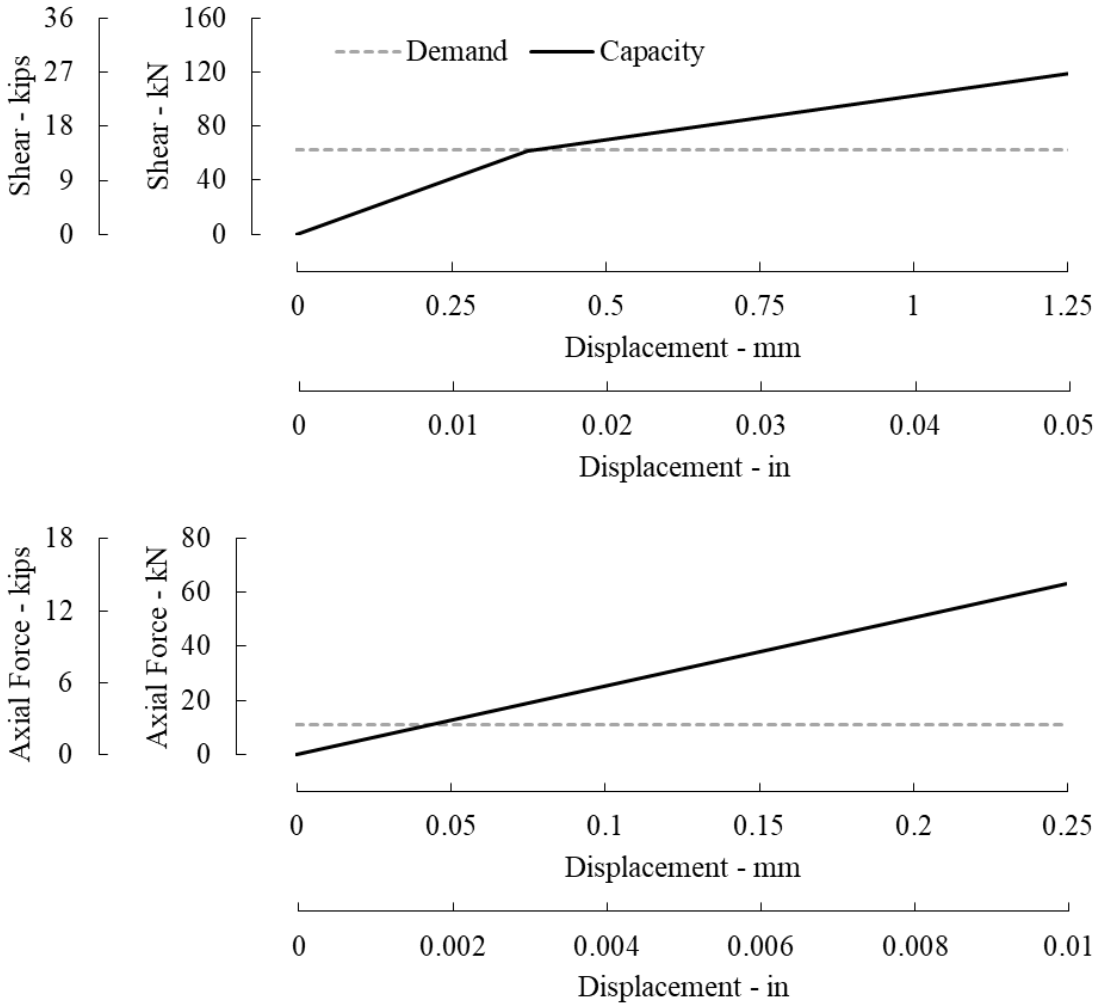

Figure 3.8 Shear and axial force displacement behavior of shear connectors

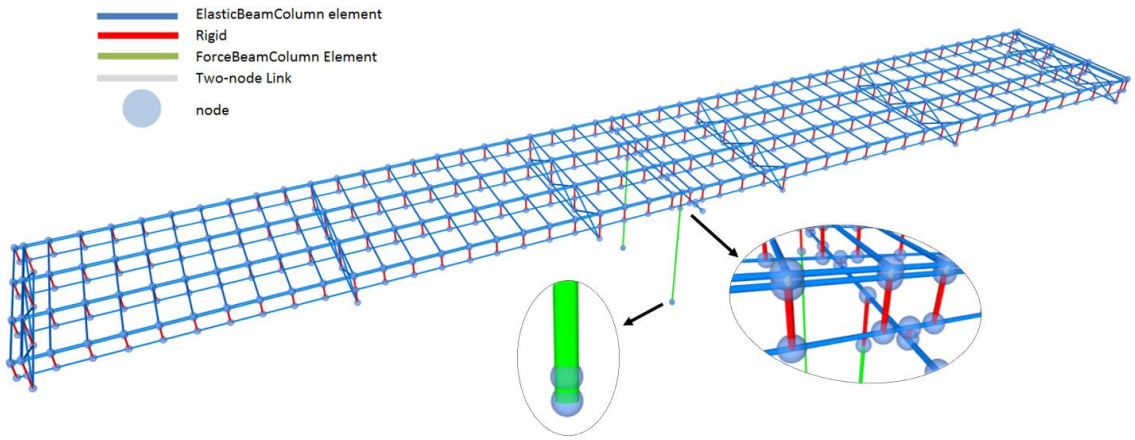

Figure 3.9 Schematic view of the OpenSEES model

(a)

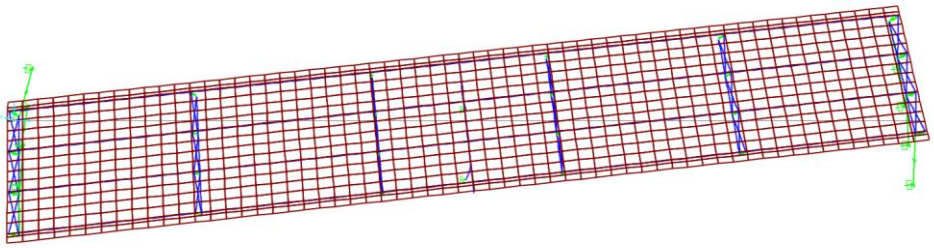

(b)

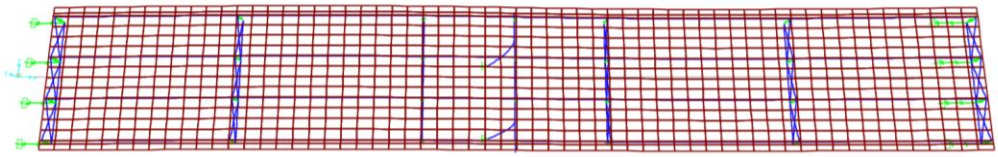

(c)

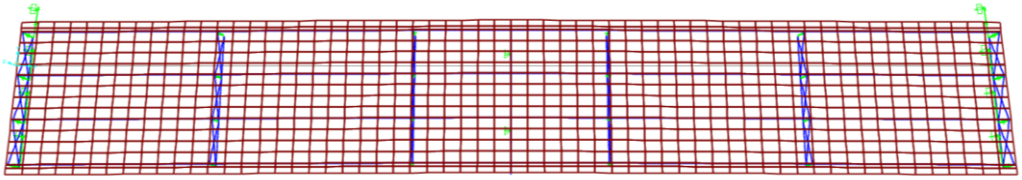

Figure 3.10 First three vibrational mode shapes of the bridge model (a) first mode (In-plane rotation) (b) second mode (Longitudinal) (c) third mode (Transverse)

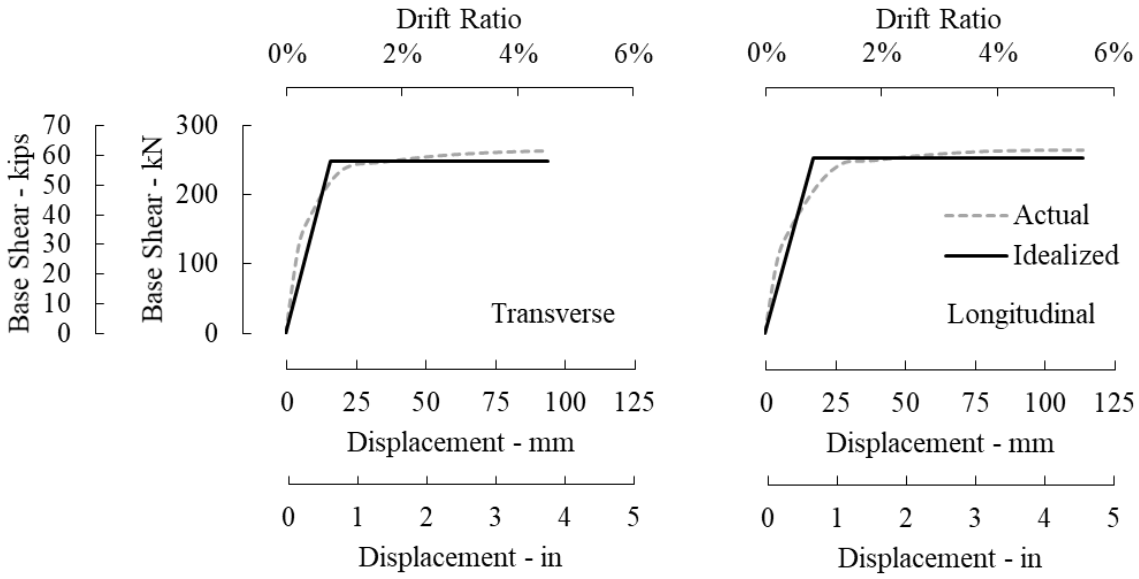

Figure 3.11 Capacity curves in two directions

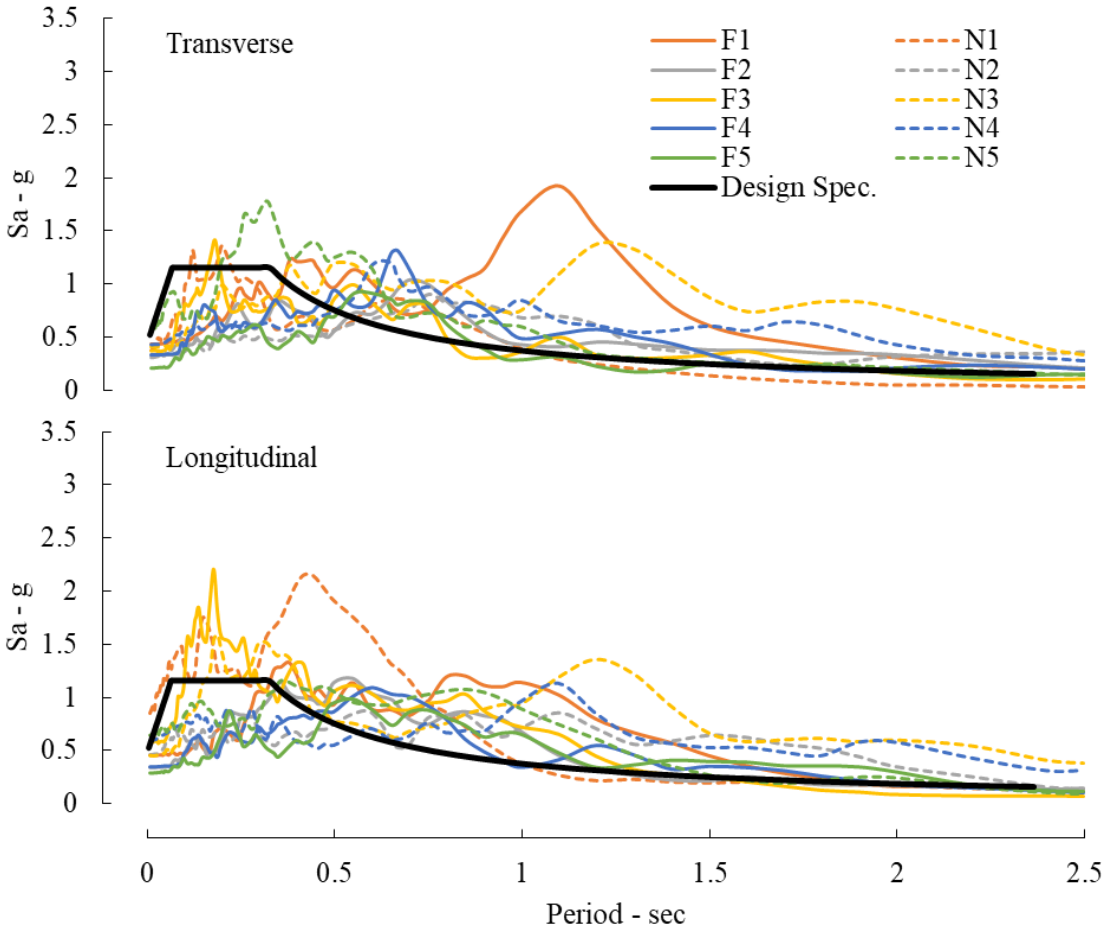

Figure 3.12 Response spectra for the ten scaled records superimposed on the design spectrum for transverse (top) and longitudinal (bottom) directions

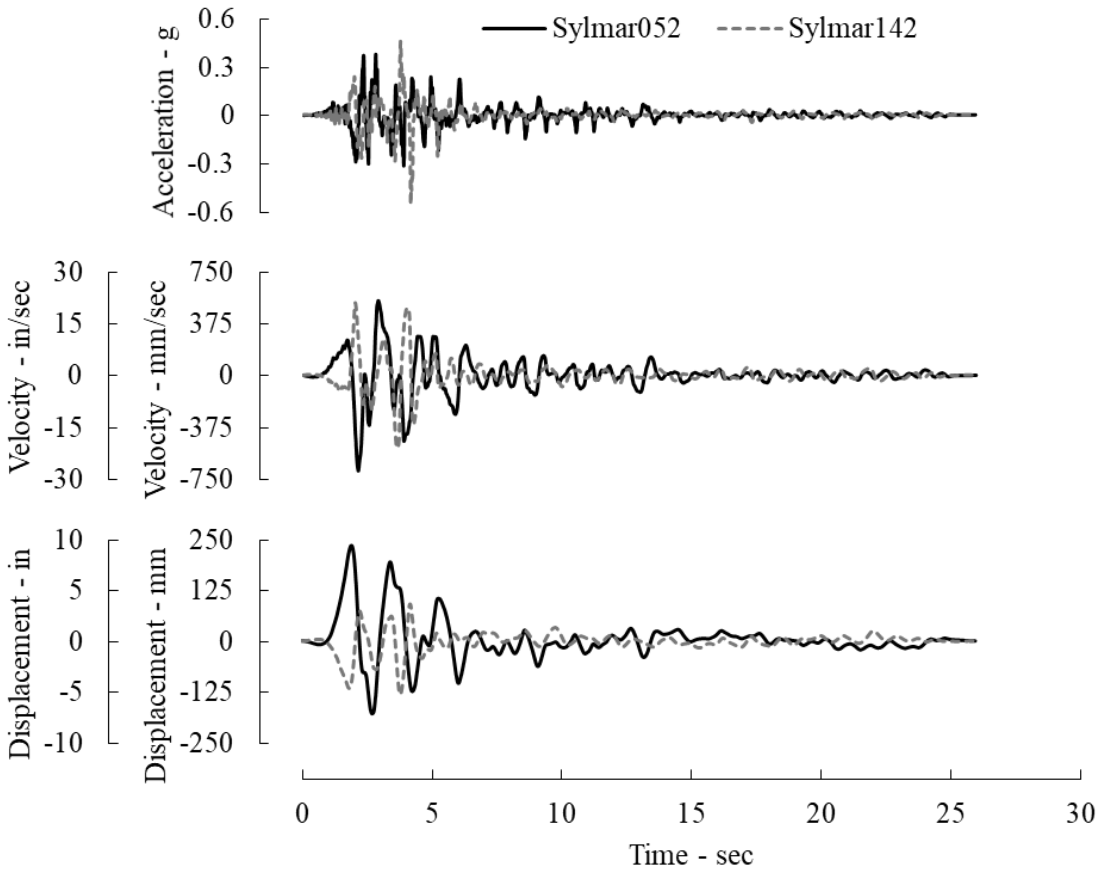

Figure 3.13 Time scaled acceleration, velocity, and displacement histories for TDE

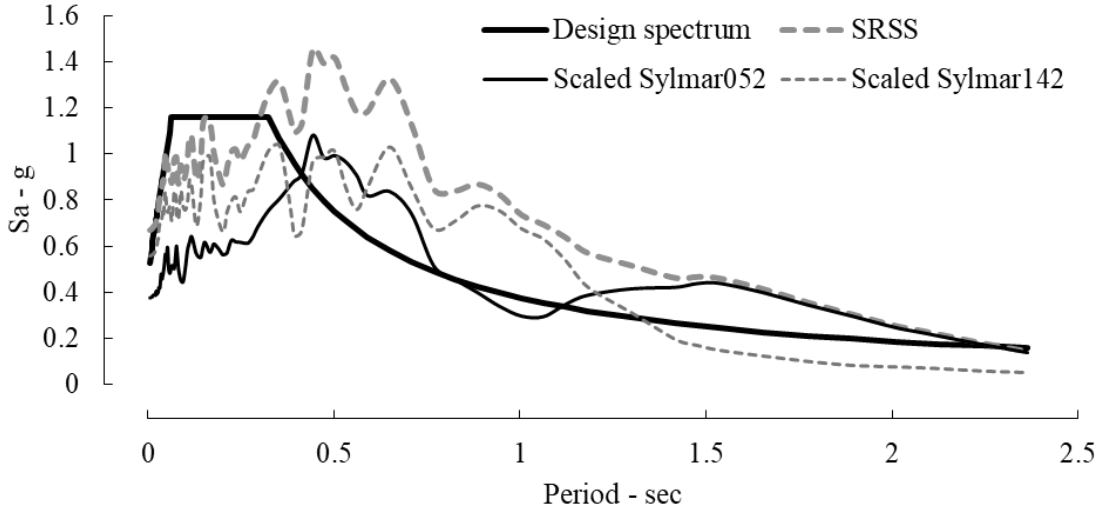

Figure 3.14 Design response spectrum and response spectra for the two components of TDE and their SRSS resultant

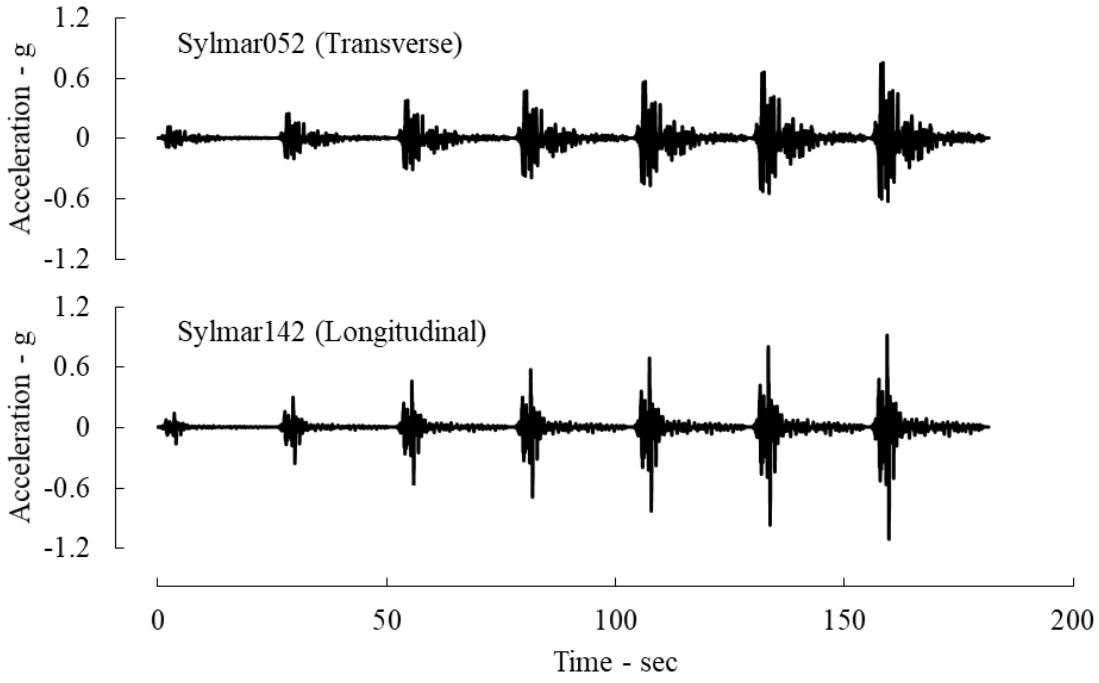

Figure 3.15 Target shake table acceleration histories

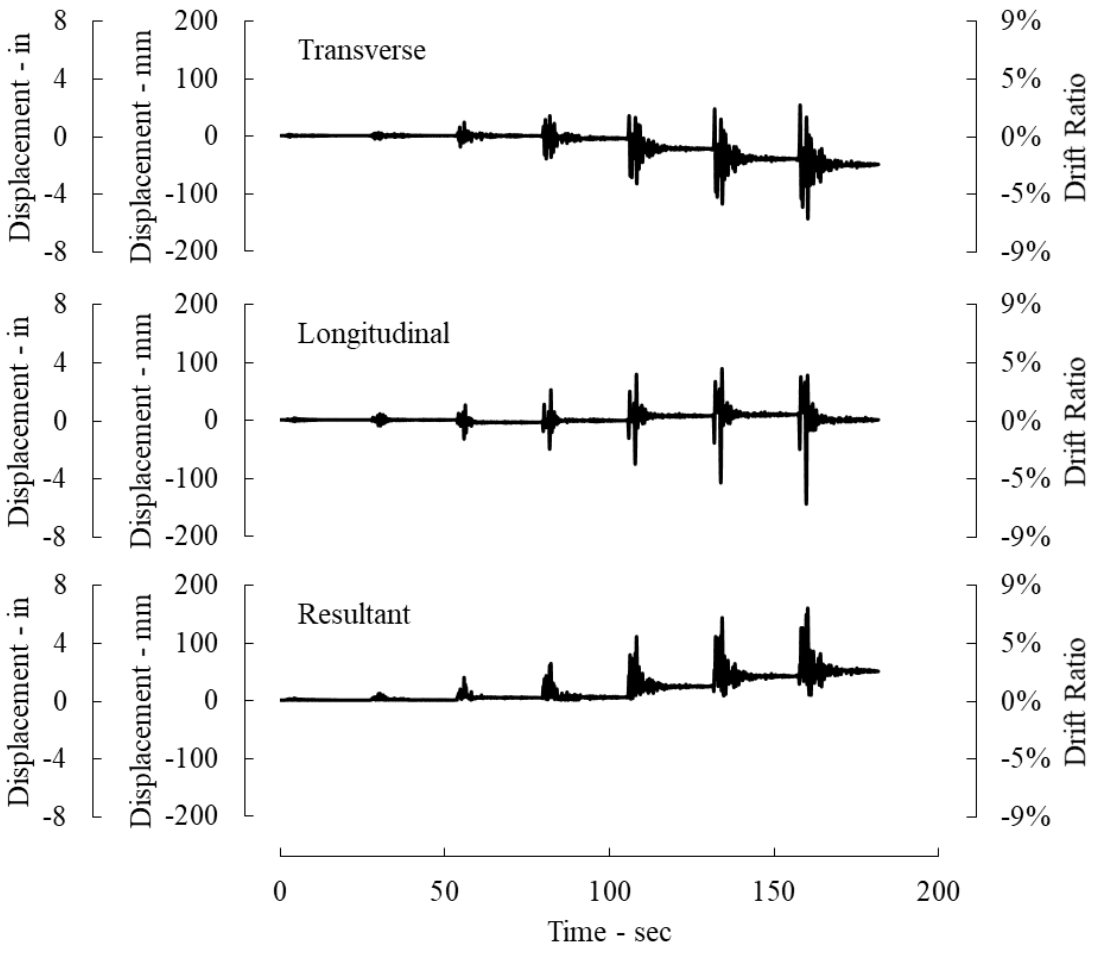

Figure 3.16 Predicted bent displacement response in the transverse (top) and longitudinal (middle) directions and bent resultant displacement (bottom)

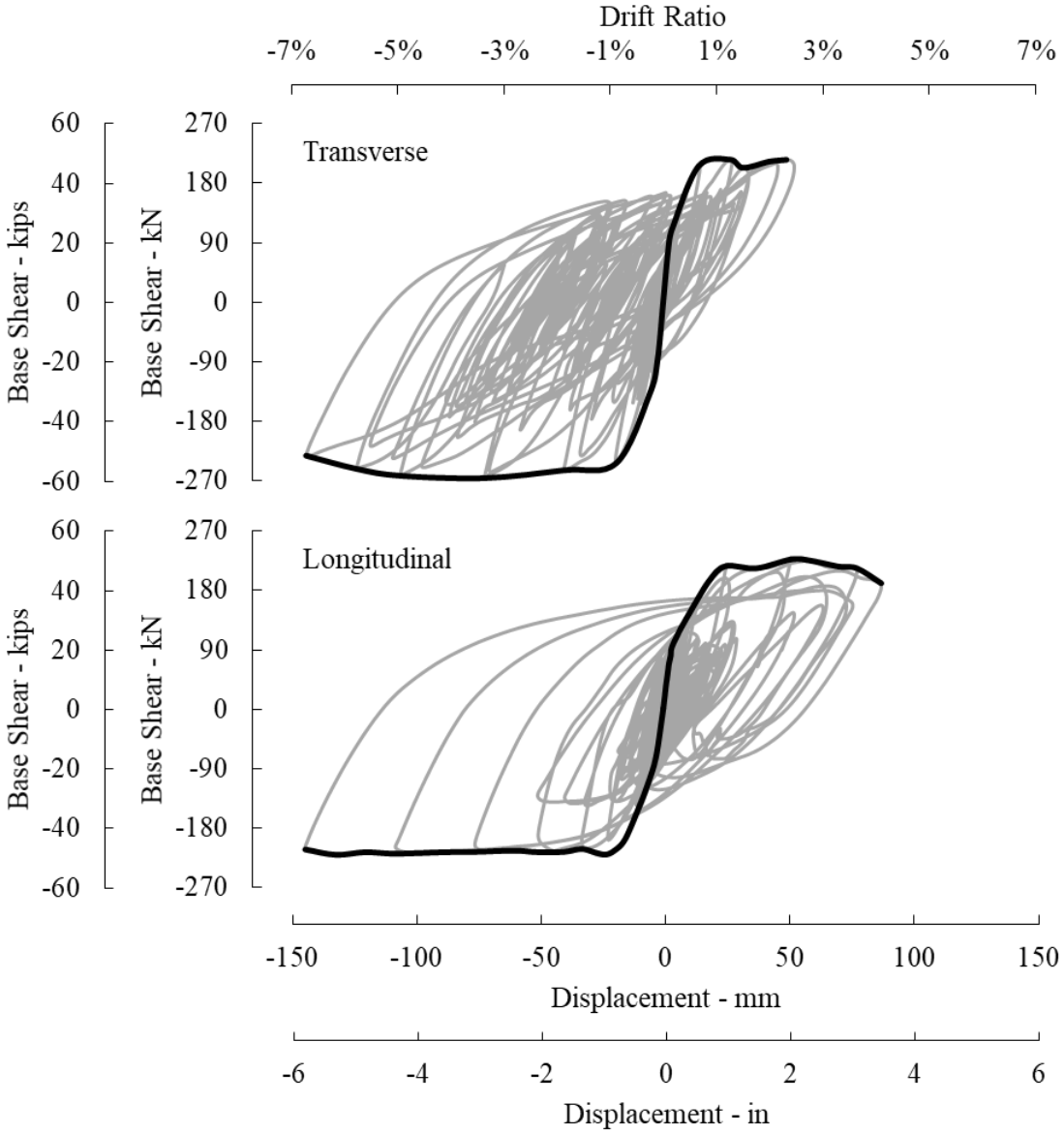

Figure 3.17 Bent hysteresis curves in the longitudinal and transverse directions and associated backbone curves

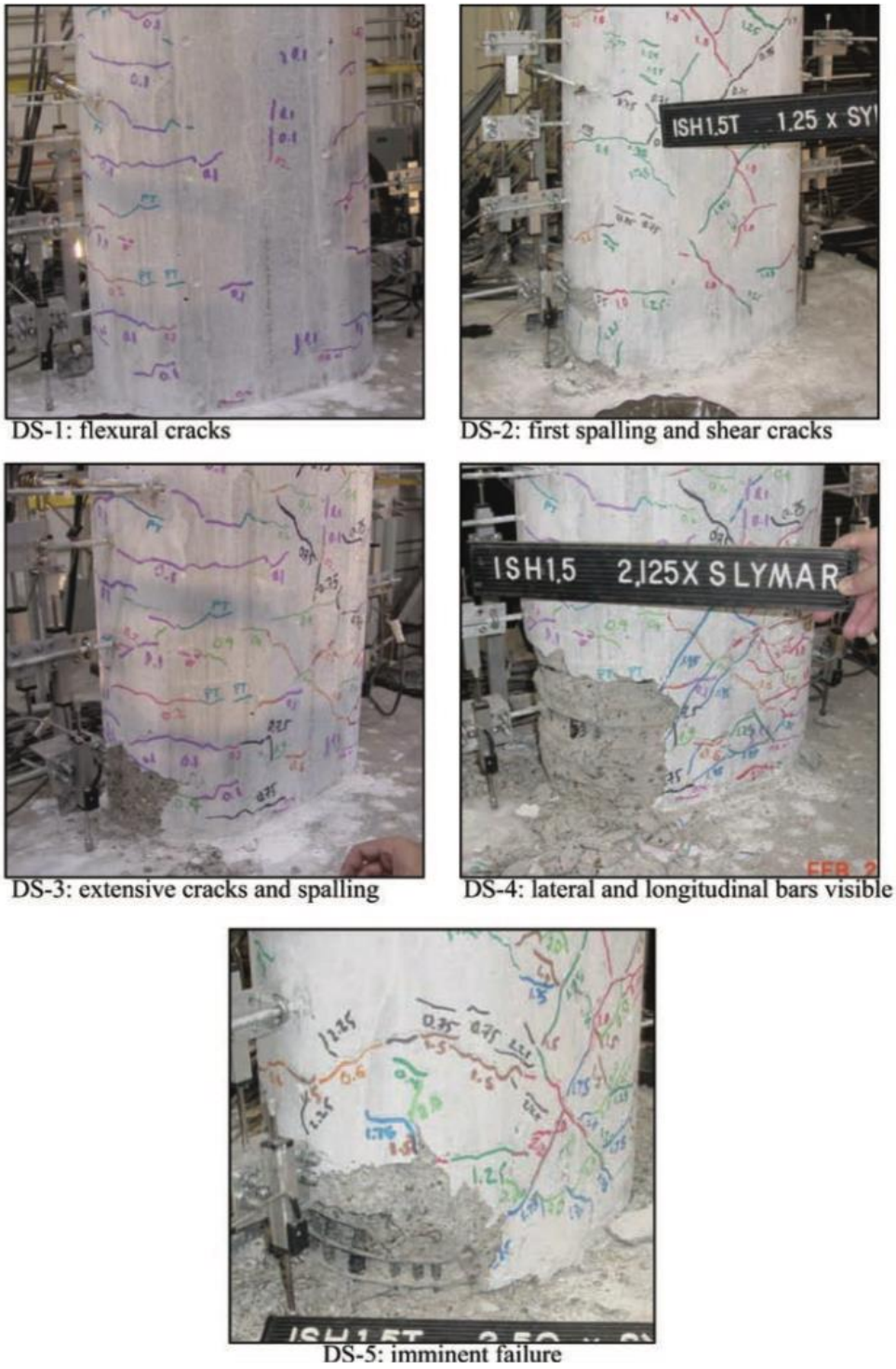

Figure 3.18 Five distinct damage states in the RC bridge columns (Vosooghi and Saiidi, 2012)

CHAPTER 4: ANALYTICAL STUDIES AND DESIGN OF STEEL PLATE GIRDER ABC BRIDGES UNDER SEISMIC LOADS

This chapter is the first draft of a stand-alone paper that will be submitted to the Engineering Structures – Elsevier Journal

ABSTRACT

Despite the numerous advantages that accelerated bridge construction (ABC) offers over the conventional construction, bridge officials in moderate and high seismic areas have not been confident to embrace it. This is due to the insufficient research data and guidelines for seismic design of prefabricated members and connections, as well as the reliable analytical modeling methods for ABC bridges. The main objective of the current study was to address this issue through analytical investigations of a two-span bridge system with six ABC connections that was tested on shake tables at the University of Nevada, Reno. A three-dimensional finite element model was developed in OpenSees. The analytical model was found to be adequate to capture the overall seismic response of the bridge model. The effects of the vertical ground motions and bi-axial excitations on the seismic response of bridge elements and connections were investigated and found that some of the response parameters can be significantly affected by near-fault earthquakes. Design implications were developed based on the results of the shake table test, previous studies on the connections, and the parametric studies. The article also presents design guidelines for the rebar hinge pocket connection and hybrid grouted duct connection.

4.1. Introduction

Accelerated bridge construction (ABC) utilizes prefabricated elements to lessen field construction time and traffic disruptions that are typical issues with conventional construction. Furthermore, ABC provides the opportunity for concurrent execution of project tasks and improves the safety of workers and the traveling public through reduction of their exposure to construction activities. The primary concern for the incorporation of ABC techniques is maintaining the structural integrity of the bridge system while desirable performance is achieved under strong seismic excitations. Past research [1,2,3, and 4] has provided a certain level of understanding and confidence on the component-level performance of many connection types appropriate for ABC (so-called "ABC connections"). However, to examine the holistic behavior of ABC bridges and study the effect of interaction and load distribution among components, prefabricated elements and ABC connections should be included in a single bridge system and tested under realistic seismic excitations. Furthermore, to facilitate the adoption of ABC bridges in moderate and high seismic areas, development of simple yet sufficiently accurate analytical modeling procedures and seismic design guidelines for ABC bridge systems is essential.

In an attempt to address the above mentioned issue, six of the more promising ABC connection types were included in a two-span bridge model in this study: (1) rebar hinge pocket connection, (2) hybrid grouted duct connection, (3) Simple for dead continuous for live (SDCL) girder-to-cap beam connection, (4) girder-to-deck grouted pocket connection, (5) ultra-high performance concrete (UHPC)-filled joints between the deck panels, and (6) deck panel UHPC-

filled connection above the (CIP) portion of the cap beam. The bridge model was designed and tested on shake tables at the University of Nevada, Reno. Detailed discussion of the previous parts of the study including pretest analytical studies, construction and shake table testing of a large-scale two-span steel girder bridge were presented elsewhere. This paper explains the development and validation of the analytical model and the subsequent parametric studies. Parametric studies included Design implications from measured and calculated data, and step-by-step seismic design guidelines for rebar hinge pocket connection and hybrid grouted duct connections are presented. A summary of the previous parts of the research study are also included for completeness.

4.2. Past Research

To make a viable hinge for ABC, details of the rebar hinge connection [5] can be combined with those of the pocket connection [6,7] which is called rebar hinge pocket connection. This connection type can be built by extending the precast hinge element, which is cast integrally with the column, into the pockets left in the adjoining member and grouting the gap around hinge in the pocket. Shake table tests conducted by Mehrsoroush et al. (2016) and Mohebbi et al. (2018) [8,9] showed promising seismic performance of the rebar hinge pocket connections connecting precast columns to the cap beam and footing, respectively.

Marsh, M. et al. 2010 [10] developed a precast bent system intended for integral connections with prestressed girders in which column bars were partially anchored in the ducts embedded in a precast portion of the cap beam and extended further into a cast-in-place portion. This type of connection is referred to as "hybrid grouted duct connection" in this study. Cyclic lateral test of the connection confirmed that it was suitable for seismic applications.

Taghinezhadbilondy et al. (2016) [11] developed a cap beam to girder connection detail appropriate for integral steel bridges in which girders were simply supported for the dead load and continuous for the live load (SDCL). The connection performed well under cyclic lateral loading (Sadeghnejad and Azizinamini, 2017 [12]).

To make a composite action between steel girders and full-depth precast deck panels, pockets need to be left in deck panels over the girderlines to accommodate clusters of studs (Badie and Tadros 2008 [13], Shrestha et al. 2017 [14]). Ultra-high performance concrete (UHPC) have been employed in the joints between precast deck panels because of its superior bond strength and the ability to reduce the required splice length for deck reinforcements of adjacent panels (Graybeal 2010, 2014 [15,16]). Deck panel joints over the pier in multi-span integral bridges are more critical compared to those along the spans due to the higher strains that they experience during earthquakes. The common practice for these joints has been either to hook the deck bars into the cap beam or to mechanically splice them. Both approaches complicate the construction process and are time-consuming.

Vertical ground motions (VGM), when combined by the horizontal components, may significantly amplify some response parameters of the bridge. Lee and Mosalam [17] showed that VGM amplifies column tensile forces which in turn results in the degradation of column shear strength. Another response parameter which is sensitive to the vertical component of the ground motions is the moment demand in the superstructure at the pier or in the mid-span (Wang et al. 2013; Kunnath et al. 2008) [18 and 19]. Kim et al. [20] (2011) investigated the correlation

between the time interval between vertical peak ground acceleration (PGA_V) and horizontal peak ground acceleration (PGA_H) and the column forces. They concluded that Shorter interval increase the variations in column axial forces. No clear trend was noticed for column shears. Another contributing factor to the extent of amplifications of response parameters is the ratio between PGA_V and PGA_H, typically known as V/H [17, 18, 19, 20].

4.3. Summary of the Experimental Investigation

The experimental studies, as the core of this research study, aimed at providing conclusive observations and recorded data to assess the response of the ABC bridge system. They served as the underlying foundation for the analytical phase including calibration, parametric studies, and development of the design guidelines.

4.3.1. Bridge Model Description

A 0.35-scale two-span steel girder bridge model was constructed and tested on shake tables. The elevation and plan view of the test model is shown in Fig. 1. The bridge model incorporated two equal spans of 10.6 m (34 ft – 8 in.), a two-column bent, full-depth precast deck panels, and seat type abutments. Skew angle at both abutments was zero. Shear keys and the abutment backwalls were assumed to be sacrificial. The width of the superstructure section was 3.1 m (11 ft). The axial load index (ALI) for the columns, defined as the dead load divided by the product of the nominal concrete compressive strength and the gross cross-sectional area of each column was 0.057. Test setup is shown in Fig. 2. The extra masses on the superstructure were provided for similitude requirements.

Columns were integral with the superstructure but pinned to the footing using rebar hinge pocket connections. Cap beam was constructed in two segments to make the girders simply supported for the dead loads but continuous for seismic loads and the part of the extra mass that represented live loads and the weight of the wearing surface. The first portion of the cap beam was precast and served as the support for the girders. The second portion was cast-in-place and integrated girders with the pier. Columns bars were anchored in grouted ducts that were embedded in the precast cap beam and extended further in the upper-part cap beam. All the bridge components and connections were designed in accordance to AASHTO LRFD [21], AASHTO Guide Specifications for LRFD Seismic Bridge Design [22], and previous research data covered in Section 2. The design strategy was to limit the nonlinearity to column plastic hinges, while the other components and connections remained essentially elastic with no yielding or damage (also referred to as “capacity protected”). Table 1 lists select design properties of the bridge. Thorough explanation of the design and construction procedures for the bridge model components and connections are presented in Shoushtari et al. 2019 [23].

4.3.2. Test Results

Eight bi-directional shake table motions simulating 1994 Northridge-Sylmar earthquake record with increasing amplitudes, were simulated in the test using the central shake table (Fig 1). The other two shake tables were stationary. Table 2 lists peak ground accelerations in the longitudinal and transverse directions of the bridge for each run. Also included are the ratios of the earthquake runs as percentages to the design earthquake (DE), where the DE was defined such that the peak

resultant displacement obtained from the nonlinear dynamic analysis and the orthogonal combination of the design displacement demands were the same.

The bridge model performance was satisfactory and comparable to cast-in-place bridges. As envisioned in the design, plastic hinges were formed at top of the columns, while cap beam, deck panels, and ABC connections incorporated in the superstructure remained elastic. The maximum resultant drift ratio of the bridge model was 6.9%. Figure 3 shows bent measured force-displacement relationship in the transverse and longitudinal directions. The fundamental periods of the bridge model in the transverse and longitudinal directions were 0.62 and 0.57 sec., respectively. Design and detailing of the rebar hinge pocket connections and hybrid grouted duct connections ensured the full moment transfer, while maintaining the integrity of the connections.

No bar fracture, gap closure, or damage to the pocket connection was noticed in the hinge connection. No sign of duct or bar pullout was noticed in the column-to-cap beam connection. The bent-to-superstructure joint performed as monolithic. The deck-to-girder slippage was negligible indicating full composite action between the deck and the girders. Minor in-plane rotations starting from run 4, were attributed to the fundamental mode being the in-plane rotation and the un-symmetric damages in the columns that relocated the pier center of stiffness.

4.4. Analytical Investigation

The analytical portion of the research study comprised two broad phases: (1) Pretest analytical studies helped in determining the design forces and the loading protocol; (2) post-test studies aimed to validate the analytical model based on the correlation between the analytical results and measured response of the bridge, and conduct parametric studies. The former was discussed in Shoushtari et al. 2019 [23], and the latter is presented in this section.

4.4.1. Analytical Modelling

A three-dimensional analytical model of the bridge was developed using the open source structural analysis software, OpenSees [24]. Schematic views of the OpenSees model for the whole bridge and the bent are shown in Fig. 4. The OpenSees model comprised frame, two-node link, and zero-length elements.

Columns elements from column-footing interface (Nodes 1 and 2) to the column-cap beam interface (Nodes 7 and 8) were modeled using forceBeamColumn elements, which allow for the spread of plasticity along the length of the element. Gauss-Lobato method was used for defining integration points. Column bases (Nodes 1 and 2) were assumed to be fixed. The hinge fiber section was assigned to the column element from Nodes 1 and 2 to 38.1 mm (1.5 in.) above the footing where Nodes 3 and 4 were placed. Hinge core concrete was defined using confined pressure resulting from the hinge and column spirals as proposed by Saiidi et a. 2010. Using Pauly and Priestly [25] equation for plastic hinge length, yielding of the hinge longitudinal bars were expected to develop to 152.4 mm (6 in.) above hinge elements, where Nodes 5 and 6 were defined. In this length, column section comprising hinge longitudinal bars in addition to those of the column was assigned. Column fiber section was assigned for elements connecting Nodes 5 and 6 to Nodes 7 and 8. *Concrete02* and *ReinforcingSteel* materials were used to model concrete and longitudinal bars in the nonlinear elements. Confined properties of the concrete in the columns were calculated using Mander's model [26]. Figures 00 and 00 show the stress-strain

behavior for cover and core concrete as well as the reinforcing steel. The defined "aggregator" option in OpenSees was used to add cracked section shear and torsional properties to the column fiber element sections. Nodes 9 to 16 were placed at the centerline of the cap beam. Rigid links were used to connect columns and girders to the cap beam elements.

The superstructure was modeled using a grillage in which *elasticBeamColumn* was used to model deck and girder elements and *twoNodeLink* to model clusters of four studs connecting girders to deck elements. Force-deformation relationships obtained by Shrestha et al. 2016 [27] pull-out and shear tests were assigned to the link elements. The axial stiffness of the link element was defined using elastic bilinear uniaxial material object and shear stiffness was defined using multi-linear elastic uniaxial material object. A modification factor of 0.5 for torsional constant was assigned to the longitudinal beam elements representing deck, and the elastic transverse beams that connected longitudinal deck elements together. Poisson's ratio of grillage beams was set equal to zero as there is no interaction between axial force and bending moment in two perpendicular directions in the grillage [28,29]. The deck elements were assumed to be cracked with 40% of the gross sectional rigidity [30]. Girders were supported on rollers at the abutments.

The deck panels mass was lumped at the nodes defined at the center of each deck pocket along the length of each girder. The superimposed masses were lumped at the nodes defined at the center of mass for each concrete block or lead pallet. Mass per length was assigned to the columns, cap beam, and girders. The actual material properties that were used in the analysis are listed in Table 2. The P-delta effects were included in the analysis. 2% damping ratio was assigned to the model using "Rayleigh" command. The measured shake-table accelerations in the transverse and longitudinal directions were used as the input ground motions using "UniformExcitationPattern" command. At both ends of the columns zero length elements were defined. The bond slip properties in terms of moment-rotation curves were incorporated in zero length elements. The bondslip model proposed by Wehbe et al. [31] was used in the analysis. To achieve the moment-rotation curve for bond slip modeling, section moment-curvature analysis was performed. The resulting curve was then modified based on the steel strain at the extreme section fiber at two points; yield, and the ultimate. The modified bilinear moment-rotation curve was specified as a property of a hysteretic material in the positive and negative directions. Due to the overturning effect, in the transverse direction of the bent, moment-rotation curves were obtained for both compressive and tensile force, and were assigned interchangeably to the positive and negative directions of the south and north columns.

4.4.2. Analytical Results

Figure 5 compares the measured and calculated bent displacement response for the transverse and longitudinal directions, respectively. Figure 6 presents the resultant measured and calculated displacements. Results are shown for three representative earthquake runs including Run 3 (the design earthquake), Run 8 (the last run), and Run 5 (as a moderate amplitude run). It can be seen that the calculated displacement histories matched the measured displacements with a good accuracy. The analytical model was able to successfully capture peak points as well as the waveforms. The maximum measured resultant drift ratios were 3.58%, 5.78%, 6.87%, and the maximum calculated drift ratios were 3.19%, 6.24%, and 8.82% for the three representative runs, respectively. The analytical model was able to simulate the maximum drift ratios within 11%, 8%, and 29% of the measured drift ratios for these runs. The higher error for the last run is

attributed to the fact that during this run failure happened and the model did not aim at capturing the post-failure behavior of the bridge. It is concluded that the analytical model led to the results that matched the measured data with reasonable accuracy.

Figure 7 shows measured versus calculated force histories for the same runs. The analytical model was able to simulate the maximum base shear for these run with less than 10% error in the longitudinal direction and with less than 40% in the transverse direction.

The measured and calculated force-displacement curves and the associated envelopes are shown in Figures 8 and 9, respectively. Results indicate that in the longitudinal direction, the initial stiffness, yield point, and envelope of the model were in a very good agreement with the measured data. However, the correlation is weaker in the transverse direction. This is attributed to the uncertainties in the developed friction force at the abutments and the minor in-plane rotations. Another reason is that despite the axial load variations in the column during the earthquake runs, a constant axial force is assumed for the development of the moment-rotation curves for modeling bondslip in the transverse direction. It was concluded that the analytical model was sufficiently accurate in simulating the most important response parameters of the bent model in the longitudinal direction. More refinements to the model may better the accuracy of the model in capturing the bridge response in the transverse direction.

4.4.3. Parametric Studies

After the analytical model was in a sufficiently good agreement with the measured results, it was utilized to investigate the effects of vertical seismic excitations. Response parameters of interest were the peak responses of the bent, the columns, the cap beam, and the deck-to-girder and girder-to-cap connections. The studies focused on the bridge response under the design earthquake (1xDE) and the last run (2.25xDE).

The set of ground motions for this study included seven ground motion records selected from PEER database. The average of the peak responses for each earthquake, was used to investigate the effects of the parametric variations in the model. Table 3 lists the selected ground motions. Included in the table are the V/H ratios for both horizontal components of each motion. Also shown in the table are the time interval between PGA_V and PGA_H ($t_{PGA_V} - t_{PGA_H}$), hereafter referred to as t_{V-H}, for each horizontal component. The average of the two t_{V-H}, is also included in the table. As seen, motions 1, 2 and 7 are examples of early arrivals of PGA_V, while the peak acceleration of the VGM for motions 3 and 6 tend to coincide with those of horizontal motions. The time axis of the measured records was compressed by a factor of 0.592 to account for similitude requirements. The elastic response spectra for all DE motions and for each direction are shown in Figures 10 to 12. The longitudinal and transverse periods of the bridge are also marked in the plots. The bridge was subjected to each of the seven motions with (w/) and without (w/o) including the vertical component. Results are presented in Table 4 through 7.

As seen in the Table 4, the vertical excitation generated significant amplification of the axial forces, with the change being larger for the tensile forces. There was only slight changes (not a specific trend) in the column moments and as a result in column shears. The differences for the column moments were below 9%, and under 3% for the column shears. Overall, the results show that the VGM does not significantly affect the plastic hinge moments and shears of

the columns. The comparison of the average peak moments and shear of the cap beam with and without the VGM is presented in Table 5. The vertical ground motion increased the cap beam moments slightly, 13% at most. The change in average peak shear in the cap beam was below 5%. The relatively large differences in the shear are associated with the higher fluctuations in the column axial forces. Cap-to-girder moments were the most sensitive response parameters to the inclusion of the VGM with demands in case of including VGM being more than 10 times the case without it. Finally, deck to girder connecters changes about 20% in the DE level and about 56% in the 2.25xDE level.

4.5. Design Implications

This section lists design implications of the shake table test and the analytical studies. Based on these implications, design guidelines are provided for the column-footing and column-cap beam connections.

4.5.1. Rebar Hinge Pocket Connection

- The embedment length of the rebar hinge element in the footing was sufficient to develop the full moment capacity of the hinge section while the pocket connection and the footing remained undamaged.
- The hinge throat was adequate to allow for the rotation of the hinge element.
- Shear design of the rebar hinge based on the modified shear friction method that accounts for the effect of the cyclic loads (Saiidi et al. (2010) [20]), successfully exceeded the shear demands even under biaxial motions representing 2.25xDE.
- The shear capacity of the rebar hinge depends on the column axial loads which can be significantly affected by vertical ground motions. In regions near to the faults, the vertical component of the ground motions have to be considered in the hinge shear design.

4.5.2. Column-To-Hybrid Cap Beam Grouted Duct Connection

- Design and detailing of the grouted duct connection combined with hybrid cap beam, ensured the successful transfer of the column plastic moment. No ducts or bar pullout was noticed.
- Peak strain in column bars occurred just below the cap beam and some yielding penetrated into the precast cap beam. No intentional debonding of the column bars at the column-footing interface was required to allow for the spread of yielding beyond the interface. In fact, spalling of the grout in the duct just above the interface acted as the intentional debonding.

4.5.3. Steel Plate Girder-to-Cap Beam SDCL Connection

- The slippage and rotation of the girders relative to the cap beam were almost zero indicating that the joint exhibited rigid behavior.
- Deck longitudinal bars remained well below yielding while transferring the superstructure negative moment. Furthermore, no extensive cracking in the panels parallel to the joint above cap beam or debonding in concrete/UHPC interface was observed.

- Cap beam stirrups remained in the elastic range, which indicates that the SDCL connection successfully transferred the cap beam-to-superstructure positive moment superstructure

4.5.4. Deck Connection

- No debonding or cracking was observed in the UHPC/concrete interface indicating sufficient bond.
- Only hairline cracks were observed at the UHPC/concrete interface over the pier, which implies that the lap-spliced UHPC joint over the pier successfully provided the continuity over the pier.
- Deck-to-girder connectors remained undamaged with only negligible slippage between deck and girder which shows a nearly composite action.

4.6. Conclusions

1) Relatively routine analytical modeling methods using nonlinear force-based elements and fiber sections for column and rebar hinge sections, elastic elements for capacity protected components, and rigid joints and link or zero-length elements with simple force-deformation relationships to model the ABC connections led to results that reasonably matched the measured response of the bridge model.
2) Among all response parameters of the bridge, cap beam-to-girder moment and column tensile forces were the most sensitive to the inclusion of vertical ground motions. This effect is more stressed in case of nearly coincident horizontal and vertical peak accelerations.
3) When vertical component of the motions was also applied to the analytical model, hinge shear demand under the ground motions with shorter interval between horizontal and vertical peak accelerations exceeded the calculated shear capacity.
4) The effect of vertical excitations has to be taken into account in the design and analysis of bridges in regions near active faults. Of particular concern are cap beam-to-girder moment and column axial forces that could be sensitive to vertical component effect.
5) The design of rebar hinge connections should include the effect of vertical earthquake component in near-fault zones.

4.7. References

1. Matsumoto, E. E., M. C. Waggoner, G. Sumen, and M. E. Kreger, (2001). “Development of a precast bent cap system”. FHWA Rep. No. FHWA/ TX-0-1748-2. Austin, TX: Center for Transportation Research, Univ. of Texas.
2. Restrepo, J. I., M. J. Tobolski, and E. E. Matsumoto, (2011). “Development of a precast bent cap system for seismic regions.” NCHRP Rep. 681. Washington, DC: National Cooperative Highway Research Program.
3. Tazarv, M., and Saiidi, M. S., (2014). “Next generation of bridge columns for accelerated bridge construction in high seismic zones”. Rep. No. CCEER-14-06. Reno, NV: Dept. of Civil and Environmental Engineering, Univ. of Nevada.
4. Mehraein, M., and M. S. Saiidi. (2016). “Seismic performance of bridge column-pile-shaft pin connections for application in accelerated bridge construction”. Rep. No. CCEER-16-01. Reno, NV: Univ. of Nevada.

5. Mehrsoroush, A., and M. S. Saiidi. (2016). “Cyclic response of precast bridge piers with novel column-base pipe pins and pocket cap beam connections”. J. Bridge Eng. 04015080.
6. Sadeghnejad, A., Azizinamini, A., (2017), “Extending the Application of Simple for Dead and Continuous for Live Load Steel Bridge System to ABC Applications in Seismic Regions. Phase II-Experimental” Web-based quarterly Research Seminar, ABC-UTC research center, Florida International University.
7. Shrestha, G. (2018). Seismic Studies of Superstructure and Substructure Connections for Accelerated Bridge Construction (Doctoral dissertation).
8. Lee, H., and K. Mosalam. 2014. “Seismic Evaluation of the Shear Behavior in Reinforced Concrete Bridge Columns Including Effect of Vertical Accelerations.” Earthquake Engineering & Structural Dynamics 43 (3): 317–37.
9. Kim, S., C. Holub, and A. Elnashai. 2011. “Analytical Assessment of the Effect of Vertical Earthquake Motion on RC Bridge Piers.” Journal of Structural Engineering 137 (2): 252–60.
10. Kunnath, S., E. Erduran, Y. Chai, and M. Yashinsky. 2008. “Effect of Near-Fault Vertical Ground Motions on Seismic Response of Highway Overcrossings.” Journal of Bridge Engineering 13 (3): 282–90.
11. Wang, Z., L. Dueñas-Osorio, and J. Padgett. 2013. “Seismic Response of a Bridge-Soil-Foundation System under the Combined Effect of Vertical and Horizontal Ground Motions.” Earthquake Engineering & Structural Dynamics 42 (4): 545–64.
12. Shoushtari, E., Saiidi, M., and Itani, A., Moustafa, M. (2019a) “Design, construction, and Shake Table Testing of a Steel Girder Bridge System with ABC Connections”, ASCE Journal of Bridge Engineering, Manuscript submitted for publication
13. American Association of State Highway and Transportation Officials (AASHTO), (2012). AASHTO LRFD Bridge Design Specifications, 6th edition.
14. American Association of State Highway and Transportation Officials (AASHTO). (2014). “Guide Specifications for LRFD Seismic Bridge Design”, Washington, D.C
15. Amirihormozaki, Ebrahim, Gokhan Pekcan, and Ahmad Itani. "Analytical modeling of horizontally curved steel girder highway bridges for seismic analysis." Journal of Earthquake Engineering 19.2 (2015): 220-248.
16. Hambly, E. C. [1990] Bridge Deck Behaviour, 2nd ed.
17. Carden, L. P., Itani, A., and Buckle, I. G. (2005) “Seismic load path in steel girder bridge superstructures,” Center for Civil Engineering Earthquake Research, Dept. of Civil Engineering, University of Nevada, Reno, Nevada, Report No. CCEER-05-03.
18. American Association of State Highway and Transportation Officials (AASHTO). (2014). “Guide Specifications for LRFD Seismic Bridge Design”, Washington, D.C.
19. American Association of State Highway and Transportation Officials (AASHTO), (2012). AASHTO LRFD Bridge Design Specifications, 6th edition.

4.8. Tables

Table 1 Design properties of bridge components

Scale factor	0.35
Span length	10.6 m (34 ft-8 in.)
Width of the bridge	3.4 m (11 ft)
Number of girders in each span	4
Column diameter	406 mm (16 in.)
Column height	2.1 m (84 in.)
Axial load index (dead load)	5.7%
Column longitudinal bar	12#5 [dia.= 16 mm (0.625 in.)]
Column longitudinal steel ratio	1.83%
Column transverse steel	#3 [dia.= 9.5 mm (0.375 in.)] @ 63 mm (2.5 in.)
Column transverse steel ratio	1.25%
Rebar hinge longitudinal bar	6#5 [dia.= 16 mm (0.625 in.)]
Rebar hinge longitudinal steel ratio	2.40%
Rebar hinge transverse steel	#3 [dia.= 9.5 mm (0.375 in.)] @ 38 mm (1.5 in.)

Table 2. Measured compressive strength of conventional concrete, grout, and UHPC

Material	Element	Test-day compressive strength, MPa (ksi)
Conventional concrete	Precast bent	64.0 (9.3)
	CIP cap beam	52.6 (7.6)
	Deck - east span	58.9 (8.6)
	Deck - west span	43.5 (6.3)
Grout	Deck pocket - east Span	80.8 (11.7)
	Deck pocket - west Span	75.3 (10.9)
	Column-to-footing	64.8 (9.4)
	Column-to-cap beam	85.2 (12.3)
UHPC	Deck joints	126.3 (18.3)
	Deck joint over the pier	151.1 (21.9)

Table 3 Ground motions for parametric studies

GM #	Earthquake Event	PGA H_1	PGA H_2	PGA V	V/H	Shortest $t_{(V-H)}$	Average $t_{(V-H)}$
1	Northridge-94 [Sylmar]	0.62	0.93	0.61	0.66	-3.01	-4.15
2	Northridge-94 [Arleta]	0.35	0.31	0.55	1.57	-1.28	-2.03
3	Northridge-94 [Canoga Park]	0.37	0.39	0.51	1.28	-0.03	-1.12
4	Northridge-94 [Newhall]	0.58	0.6	0.57	0.95	0.04	0.55
5	Loma Prieta-89 [Corralitos]	0.65	0.48	0.46	0.71	-0.07	-0.79
6	Kobe-95 [Takarazuka]	0.71	0.62	0.43	0.61	0.1	0.17
7	Imperial Valley-06 [Agrarias]	0.29	0.19	0.48	1.66	-4.49	-4.51

Table 4 Average peak column forces without (w/o) and with (w/) VGM.

			w/o		w/		Change,%
Tensile Force [kip (kN)]	N-Col	1xDE	18.69	83.1	41.32	183.8	121.1%
		2.25xDE	16.97	75.5	73.31	326.1	332.0%
	S-Col	1xDE	10.77	47.9	35.99	160.1	234.1%
		2.25xDE	11.14	49.6	68.97	306.8	519.0%
Compressive Force [kip (kN)]	N-Col	1xDE	109.03	485.0	146.14	650.1	34.0%
		2.25xDE	115.35	513.1	180.76	804.1	56.7%
	S-Col	1xDE	117.95	524.7	142.56	634.1	20.9%
		2.25xDE	117.99	524.9	182.18	810.4	54.4%
Transverse Moment [kip-in (kN-m)]	N-Col	1xDE	1,943.22	219.6	2,021.22	228.4	4.0%
		2.25xDE	2,115.15	239.0	2,208.38	249.5	4.4%
	S-Col	1xDE	2,238.75	252.9	2,209.37	249.6	-1.3%
		2.25xDE	2,222.80	251.1	2,313.50	261.4	4.1%
Longitudinal Moment [kip-in (kN-m)]	N-Col	1xDE	1,968.83	222.4	2,013.79	227.5	2.3%
		2.25xDE	2,157.16	243.7	2,348.60	265.4	8.9%
	S-Col	1xDE	2,037.89	230.3	2,116.96	239.2	3.9%
		2.25xDE	2,187.22	247.1	2,346.61	265.1	7.3%
Transverse Shear [kip (kN)]	N-Col	1xDE	28.84	128.3	29.35	130.6	1.7%
		2.25xDE	29.73	132.2	29.79	132.5	0.2%
	S-Col	1xDE	32.16	143.1	31.60	140.6	-1.8%
		2.25xDE	30.72	136.7	31.58	140.5	2.8%
Longitudinal Shear [kip (kN)]	N-Col	1xDE	28.42	126.4	28.54	127.0	0.4%
		2.25xDE	30.05	133.7	30.06	133.7	0.0%

	S-Col	1xDE	29.11	129.5	29.37	130.6	0.9%
		2.25xDE	30.05	133.7	29.95	133.2	-0.4%

Table 5 Average peak cap beam responses without (w/o) and with (w/) VGM.

		w/o		w/		change,%
Positive Moment [kip-in (kN-m)]	1xDE	3,118.92	352.4	3,203.22	361.9	2.7%
	2.25xDE	3,041.00	343.6	3,427.16	387.2	12.7%
Negative Moment [kip-in (kN-m)]	1xDE	-2,786.17	-314.8	-3,092.01	-349.4	11.0%
	2.25xDE	-2,839.63	-320.8	-3,120.39	-352.6	9.9%
Shear [kip (kN)]	1xDE	66.17	294.3	65.24	290.2	-1.4%
	2.25xDE	62.99	280.2	66.13	294.2	5.0%

Table 6 Average moment demands in girder-to-cap beam connection without (w/o) and with (w/) VGM.

			w/o		w/		change,%
Positive Moment [kip-in (kN-m)]	Interior girders	1xDE	37.81	4.3	327.13	37.0	765.2%
		2.25xDE	60.69	6.9	752.38	85.0	1139.8%
	Exterior girders	1xDE	65.17	7.4	322.52	36.4	394.9%
		2.25xDE	147.98	16.7	698.54	78.9	372.1%
Negative Moment [kip-in (kN-m)]	Interior girders	1xDE	-958.39	-108.3	-1,256.13	-141.9	31.1%
		2.25xDE	-1063.06	-120.1	-1,885.84	-213.1	77.4%
	Exterior girders	1xDE	4.93	0.6	219.54	24.8	4349.2%
		2.25xDE	-33.20	-3.8	605.25	68.4	-1922.9%

Table 7 Average shear demands in deck-to-girder connectors without (w/o) and with (w/) VGM.

		w/o		w/		
Interior Girder [kip (kN)]	1xDE	13.33	59.3	15.96	71.0	19.7%
	2.25xDE	14.13	62.9	22.10	98.3	56.4%
Exterior Girder [kip (kN)]	1xDE	12.38	55.1	14.92	66.4	20.5%
	2.25xDE	13.28	59.1	20.47	91.1	54.1%

4.9. Figures

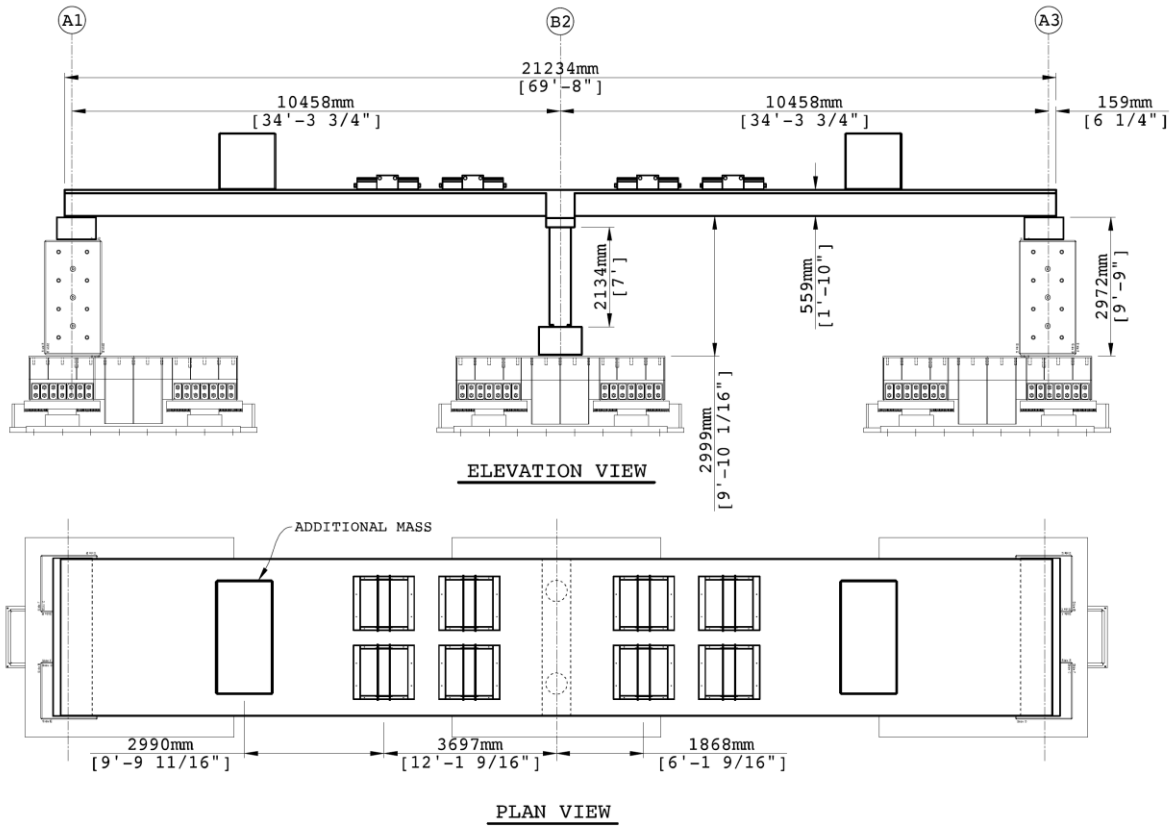

Fig. 1 Elevation and plan view of the bridge model

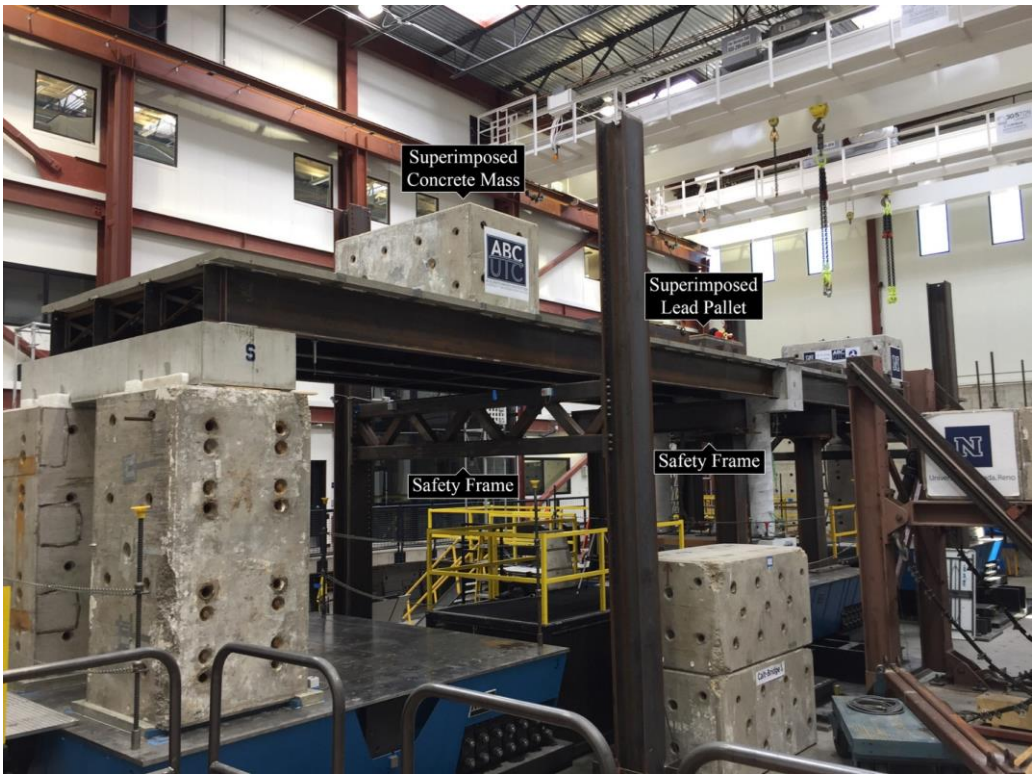

Fig. 2 Test setup

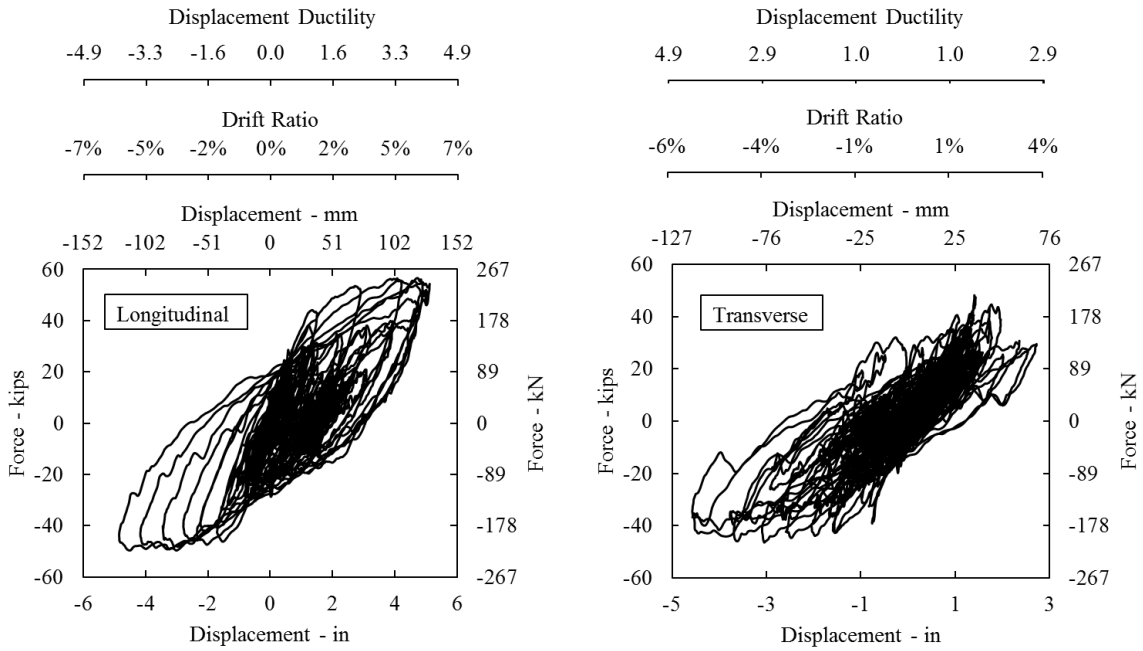

Fig. 3 Force displacement hysteresis curves

a)

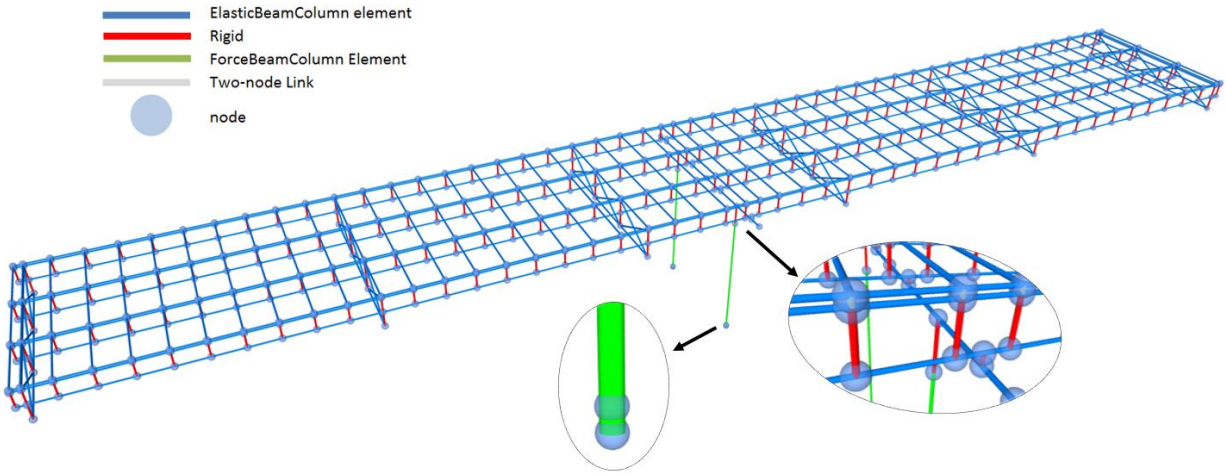

Fig. 4 Sketch of the OpenSees model for a) the whole bridge, b) bent

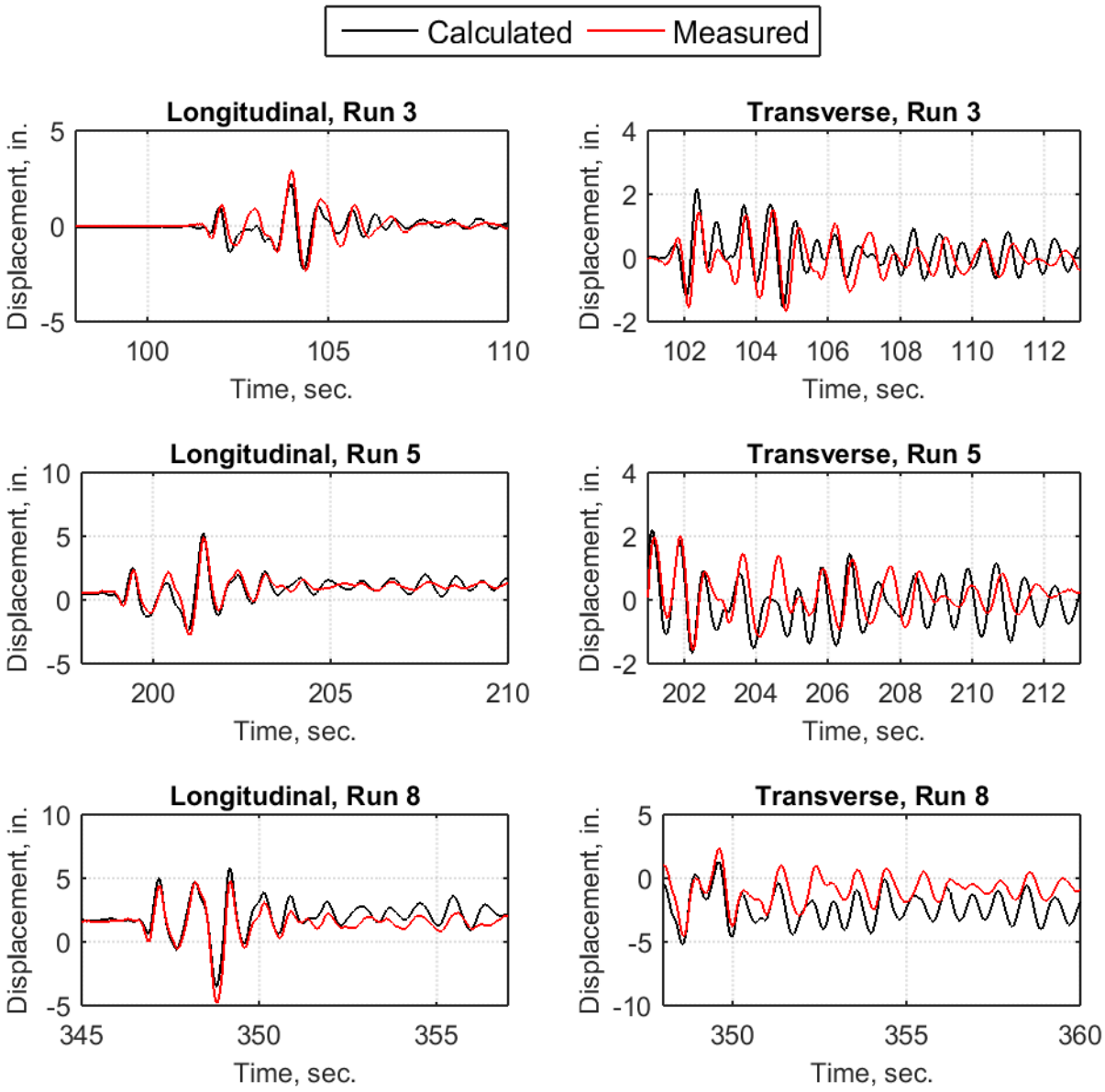

Fig. 5 Measured versus calculated displacement histories in the longitudinal and transverse directions for Run 3 (DE), Run 5 (1.5xDE), and Run 8 (2.25xDE).

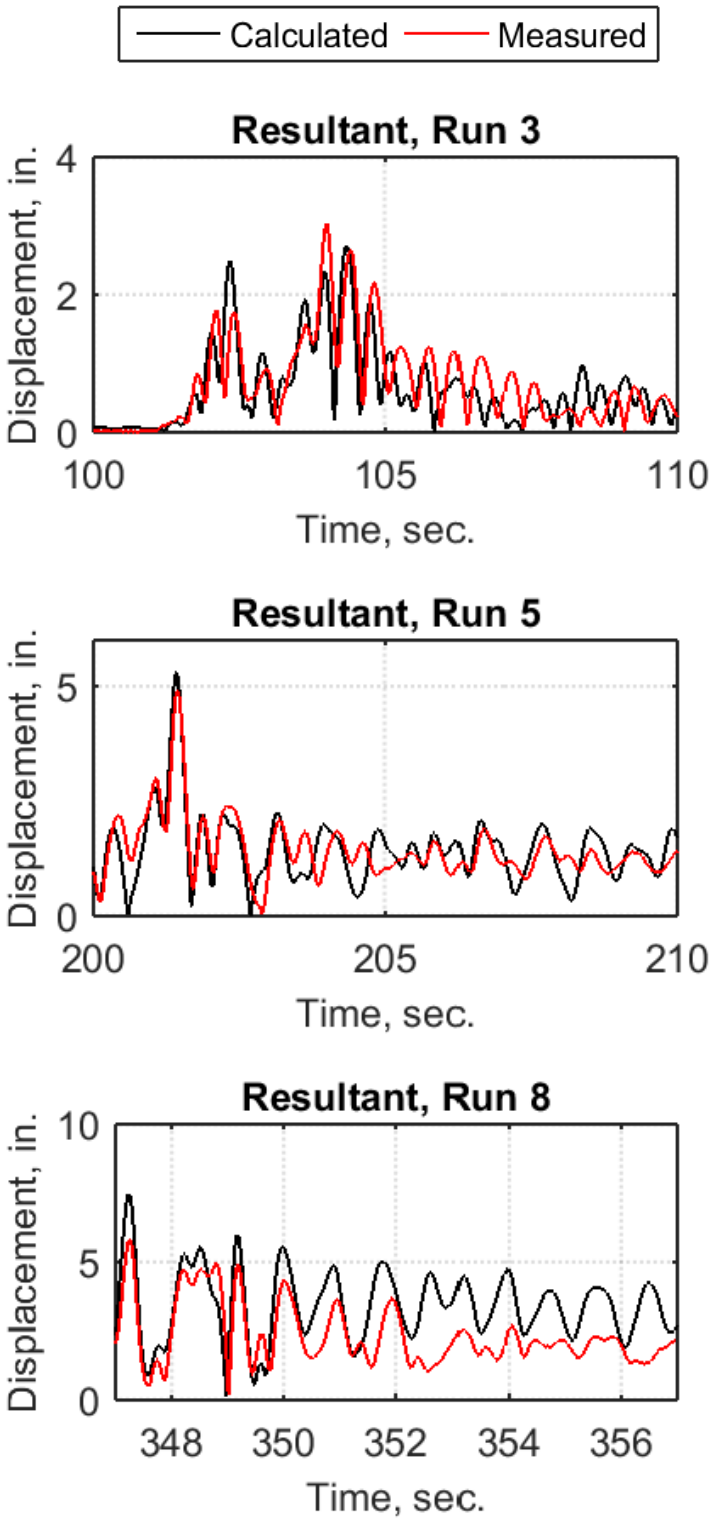

Fig. 6 Measured versus calculated resultant displacement histories for Run 3 (DE), Run 5 (1.5xDE), and Run 8 (2.25xDE).

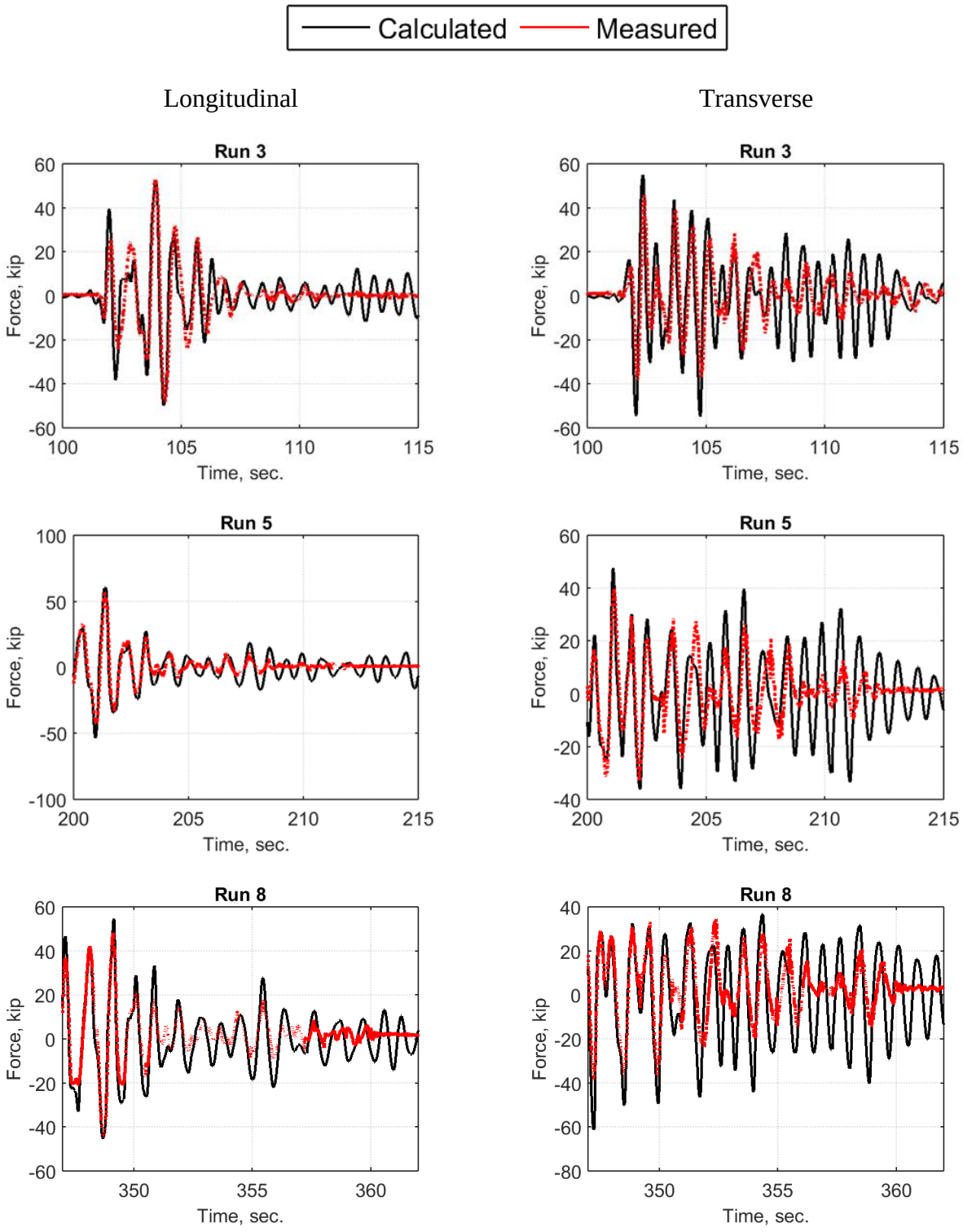

Fig. 7 Measured versus calculated force histories in the longitudinal and transverse directions for Run 3 (DE), Run 5 (1.5xDE), and Run 8 (2.25xDE).

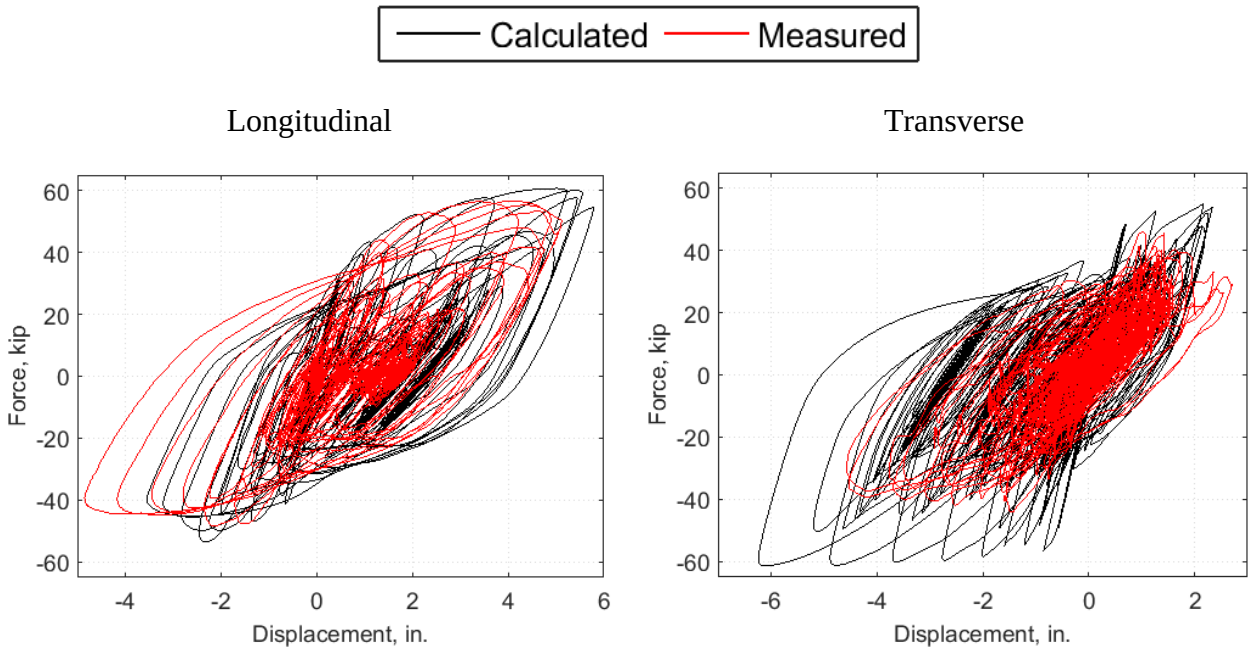

Fig. 8 Measured versus calculated cumulative hysteresis curves in the longitudinal and transverse directions (runs 1 to 8)

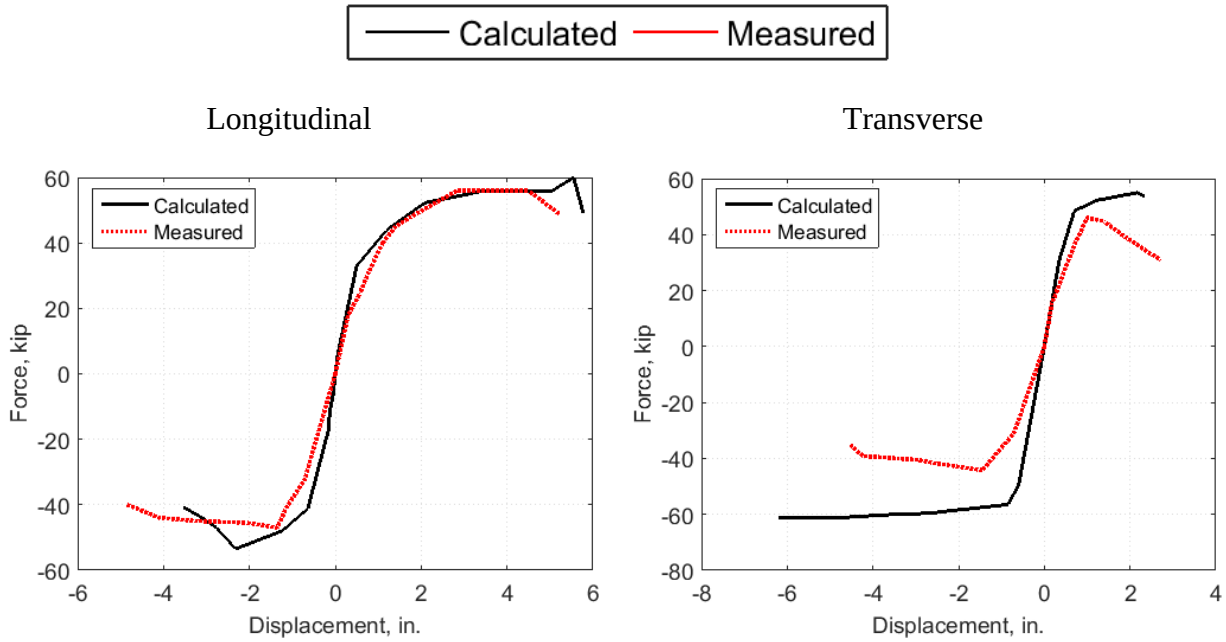

Figure 9. Measured versus calculated force-displacement envelopes in the longitudinal and transverse directions (runs 1 to 8)

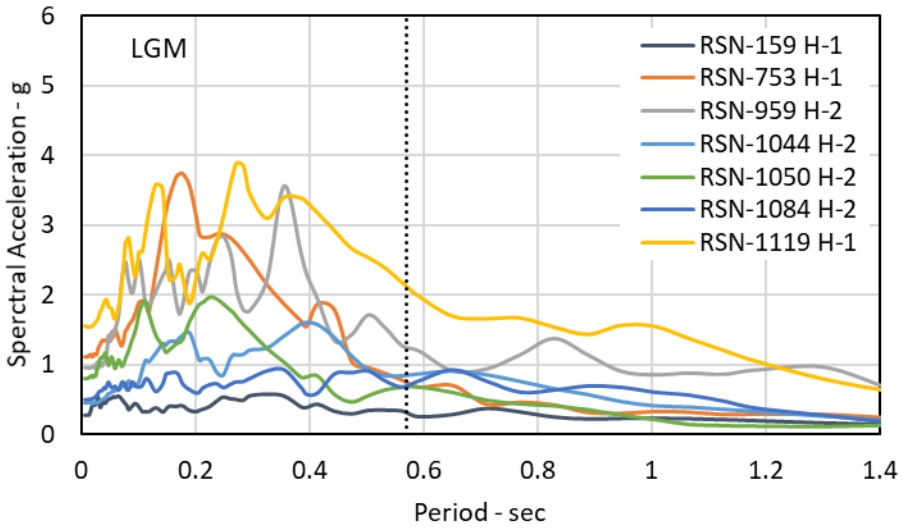

Figure 10 Spectral accelerations for DE motions - Longitudinal component

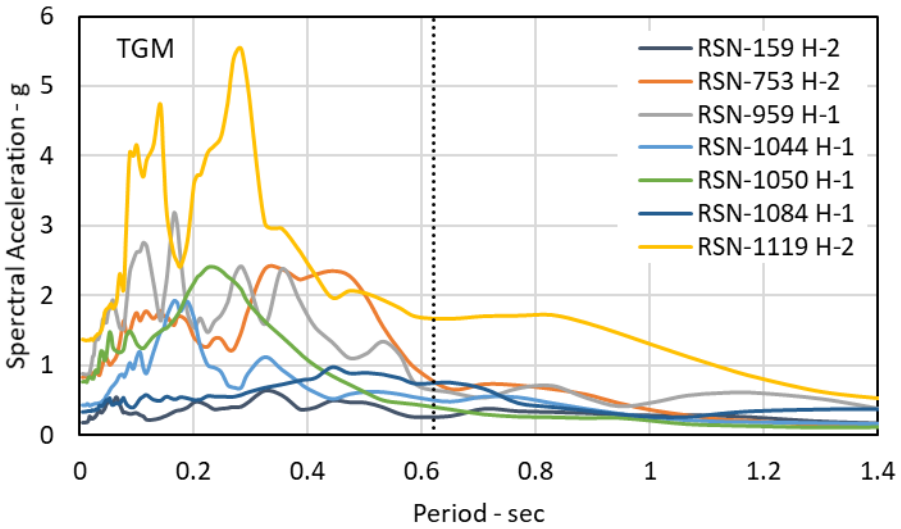

Figure 11 Spectral accelerations for DE motions - Transverse component

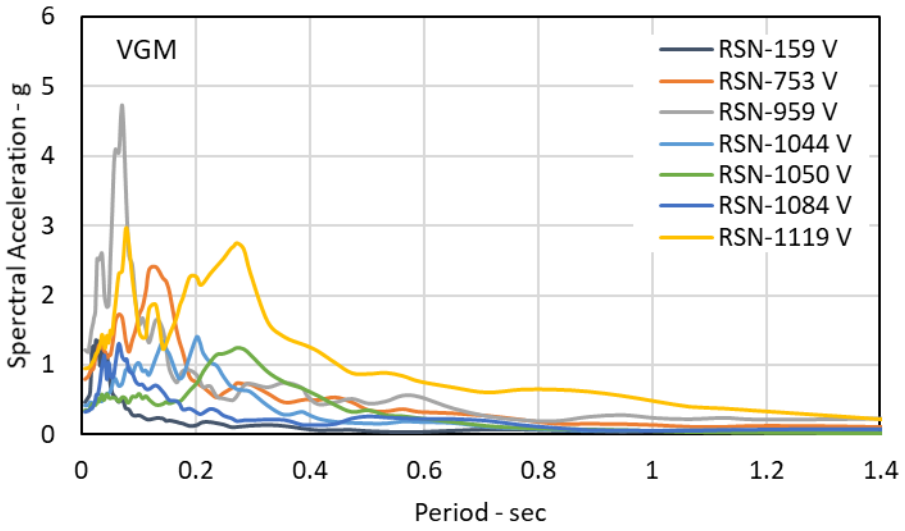

Figure 12 Spectral accelerations for DE motions - Vertical component

CHAPTER 5: SUMMARY AND CONCLUSIONS

5.1. Summary

Many connections intended for use in accelerated bridge construction (ABC) have been developed and investigated in terms of their local behavior in the past few years. However, to facilitate the use of ABC in routine bridge design and construction in moderate and high seismic zones, information on the holistic seismic performance of the bridge systems integrating various ABC column and superstructure connections is of great interest and highly desired. The lack of sufficient experimental facilities has been, in part, the reason for the scarcity of bridge system seismic testing. The study presented in this document was aimed to address this knowledge gap.

This report presents the design, construction, experimental studies, and analytical investigation of a 0.35 scale, two-span steel girder bridge model incorporating prefabricated elements and six ABC connection types under different levels of earthquake intensity. The ABC connections incorporated in the bridge model were: 1) rebar hinge pocket connection (connecting columns to the footing); (2) column to hybrid cap beam grouted duct connection; (3) SDCL (simple for dead, continuous for live) seismic detail for superstructure to bent cap connection; (4) panel-to-girder grouted pocket connection; (5) short-spliced deck panel rebars in the transverse panel-to-panel joints filled with ultra-high performance concrete (UHPC); and (6) spliced deck panel rebars in UHPC-filled panel-to-panel joint over the pier. The bridge model was subjected to eight biaxial earthquake motions with increasing amplitudes simulating a modified version of the 1994 Northridge-Sylmar earthquake record.

The main objective of the study was to evaluate the performance of ABC bridges combining multiple connection types under various levels of bi-directional earthquakes including motions that simulated 225% of the design level earthquake. Other objectives were to assess the adequacy of some of the emerging design methods for critical ABC connections, the constructability of the prefabricated elements and ABC constructions, the applicability of the current analytical modeling methods for ABC bridges, and the effect of key parameters that were not included in the experimental phase of the study.

A comprehensive state-of-the-art literature review was conducted on the ABC connections that were selected for incorporation in the test model and was presented in Ch. 2. Chapter 3 presented the pre-test analytical investigation conducted to determine the design forces for the preliminary design of the components, the input ground motion, and the loading protocol. Another objective was to predict the test model performance based on the damage states developed for the conventional bridges. Chapter 4 and Appendices A and B, presented the results of the shake table test that were utilized to evaluate the three-dimensional finite element model developed in OpenSees software package as part of the pre-test analytical studies. The model was further used for selected parametric studies such as exploring the effect of vertical excitations and bi-axial motions. Design guidelines for column-to-cap beam and column-to-footing connections were subsequently developed based on the test results and parametric studies.

5.2. Observations of Analytical Studies

The key observations from the analytical studies were:

1) Pretest analytical studies investigating the seismic performance of the bridge test model under a large number of input earthquake motions that included near-fault and far-field

records showed that near-fault motions were more demanding in terms of the maximum and residual drift ratios compared to far-field motions. The effect of near-fault ground motion tended to be more severe under higher-amplitude motions (for instance the 200% the design earthquake compared to 150% and 100% design level).

2) Relatively routine analytical modeling methods using nonlinear force-based elements and fiber sections for column and rebar hinge sections and elastic elements for capacity protected components led to results that reasonably matched the measured response of the bridge model.

3) Among all response parameters of the bridge, cap beam-to-girder moment and column tensile forces were the most sensitive to the inclusion of vertical ground motions. This effect is more stressed in case of nearly coincident horizontal and vertical peak accelerations.

4) When vertical component of the motions was applied to the analytical model, hinge shear demand underground motions with shorter interval between horizontal and vertical peak accelerations exceeded the calculated shear capacity.

5) When only the transverse component of the input motion was applied to the bridge model, the peak bent resultant displacement and peak transverse displacement were approximately 80% and 100% of those under biaxial motions, respectively. Demands associated with longitudinal loading direction such as longitudinal shear and moment in the columns and longitudinal displacement were almost zero.

6) For the bridge model under longitudinal component of the input motion, almost the same peak bent resultant displacement as that under biaxial motions was obtained. Despite no transverse motion was applied to the bridge, approximately 15% to 20% of column transverse shear and moment demands and displacement in case of bi-axial motion were developed in the bridge.

5.3. Conclusions

The key conclusions drawn from the experimental and analytical studies conducted in this investigation are highlighted as follows.

1) The seismic response of the ABC bridge systems can be predicted reasonably well with relatively routine modeling methods that incorporate fiber elements for nonlinear zones and linear elements elsewhere.

2) The effect of vertical excitations has to be taken into account in the design and analysis of bridges in regions near active faults. Of particular concern are cap beam-to-girder moment and column axial forces that could be sensitive to vertical component effect.

3) The design of rebar hinge connections should include the effect of vertical earthquake component in bridges located in near-fault zones.

APPENDIX A: ANALYTICAL RESULTS

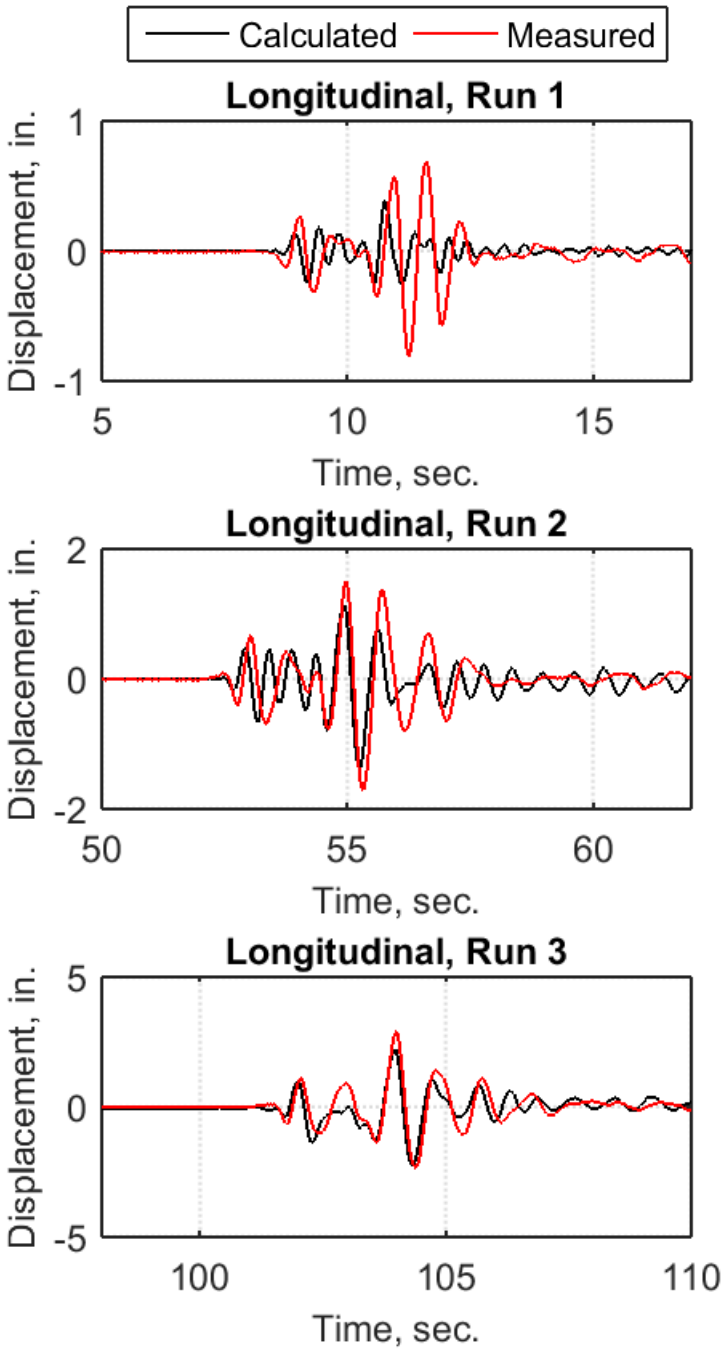

Figure A.1 Measured and calculated displacement histories in the longitudinal direction, Runs 1 to 3

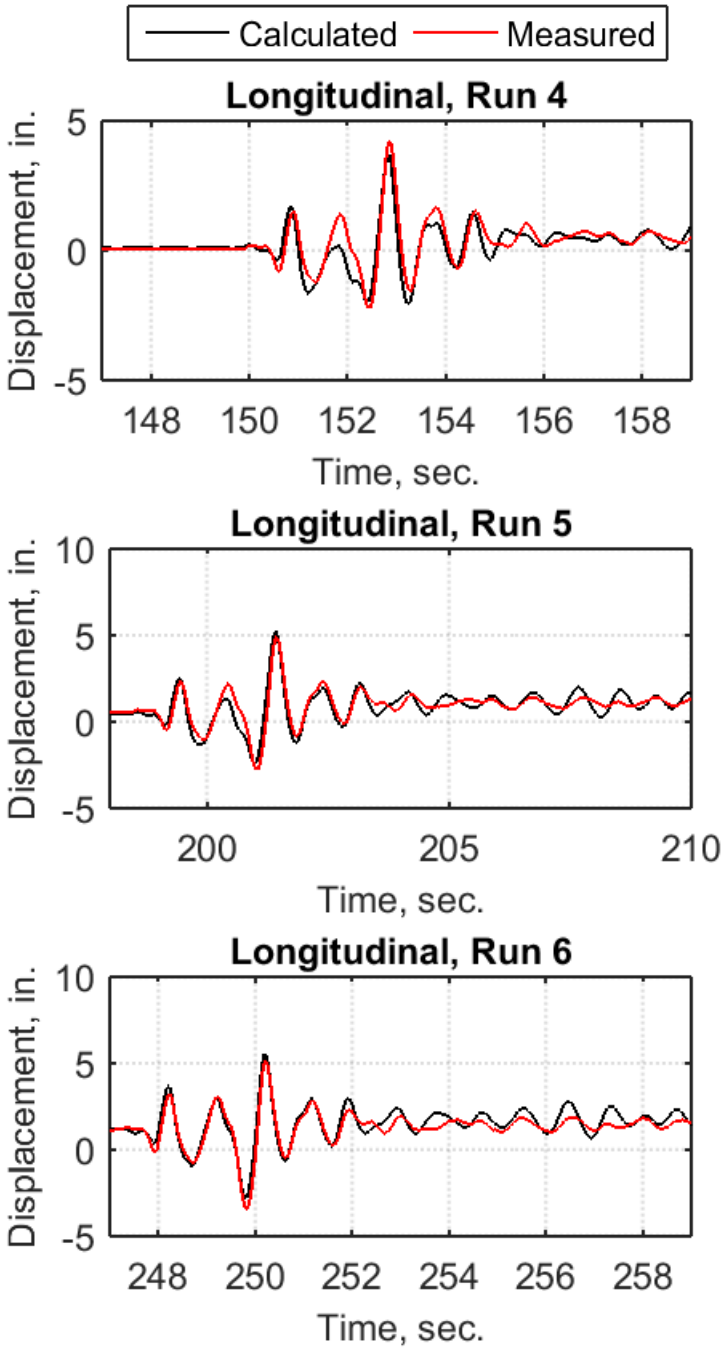

Figure A.2 Measured and calculated displacement histories in the longitudinal direction, Runs 4 to 6

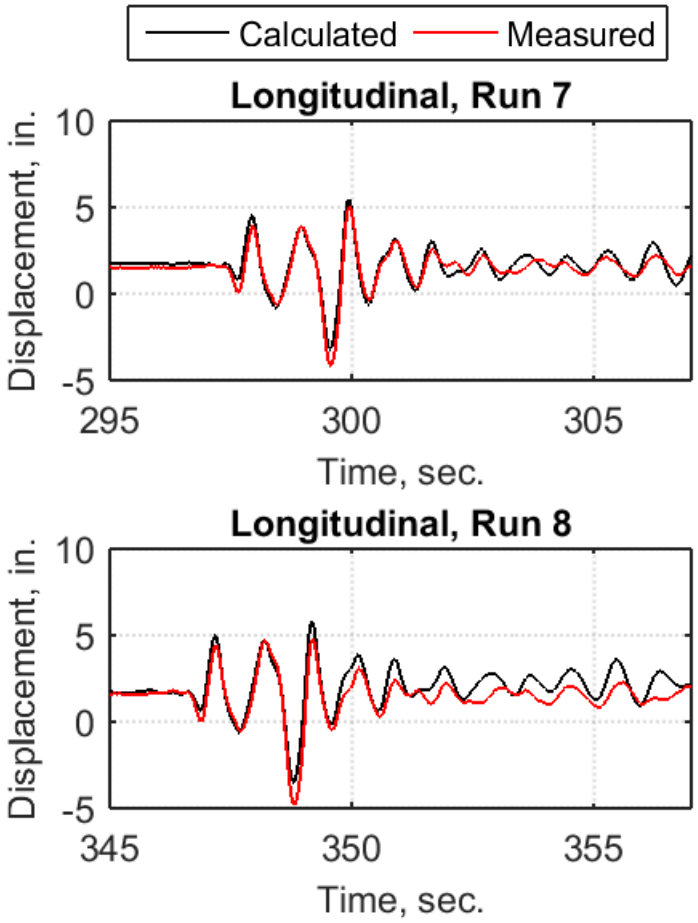

Figure A.3 Measured and calculated displacement histories in the longitudinal direction, Runs 7 and 8

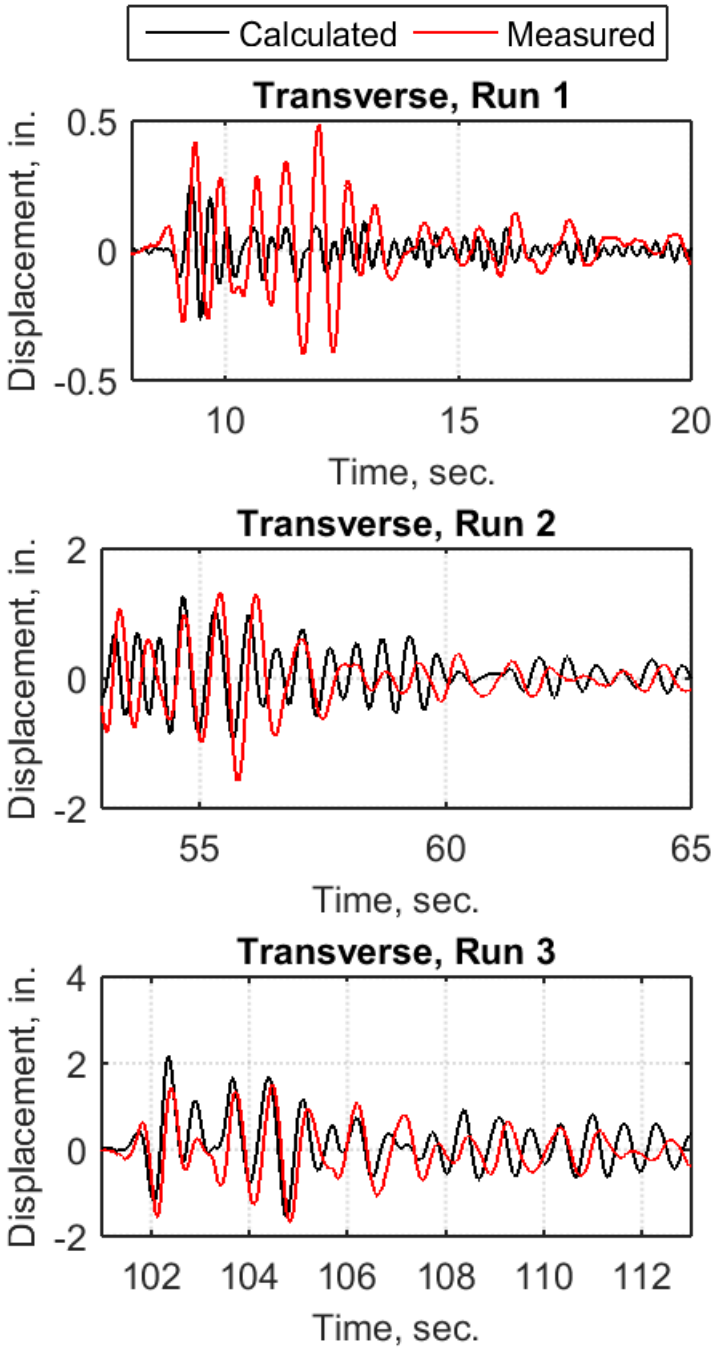

Figure A.4 Measured and calculated displacement histories in the transverse direction, Runs 1 to 3

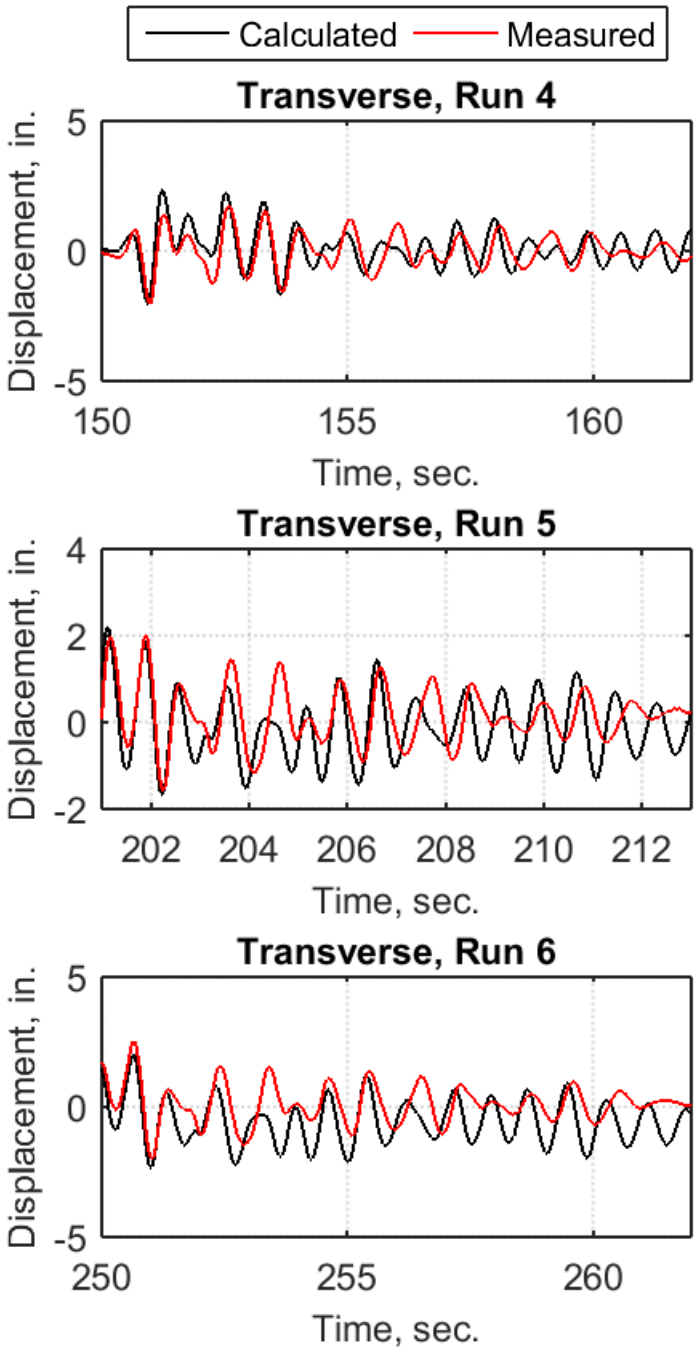

Figure A.5 Measured and calculated displacement histories in the transverse direction, Runs 4 to 6

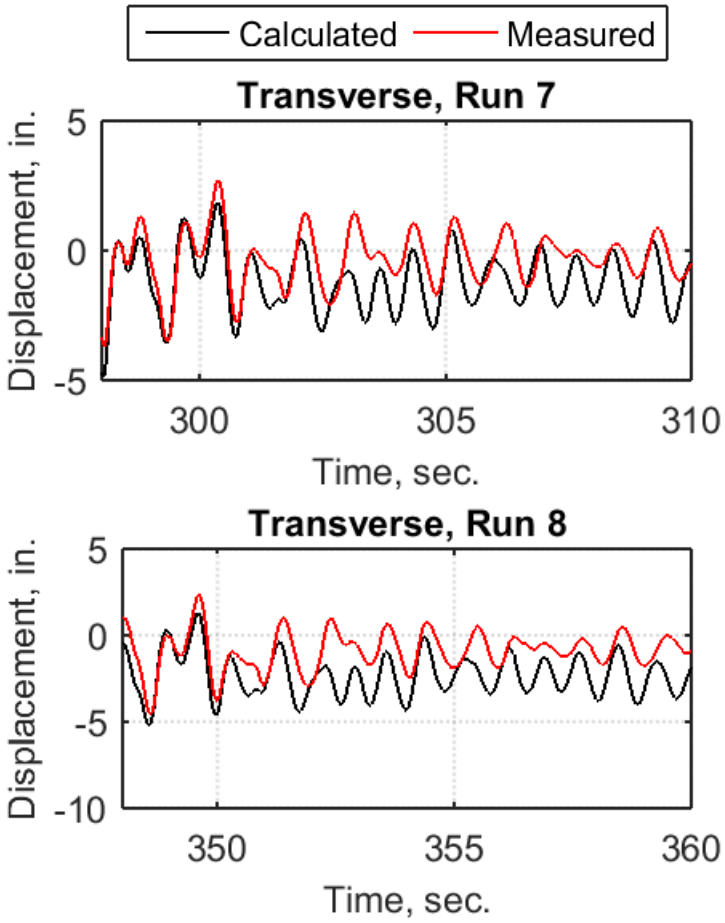

Figure A.6 Measured and calculated displacement histories in the transverse direction, Runs 7 and 8

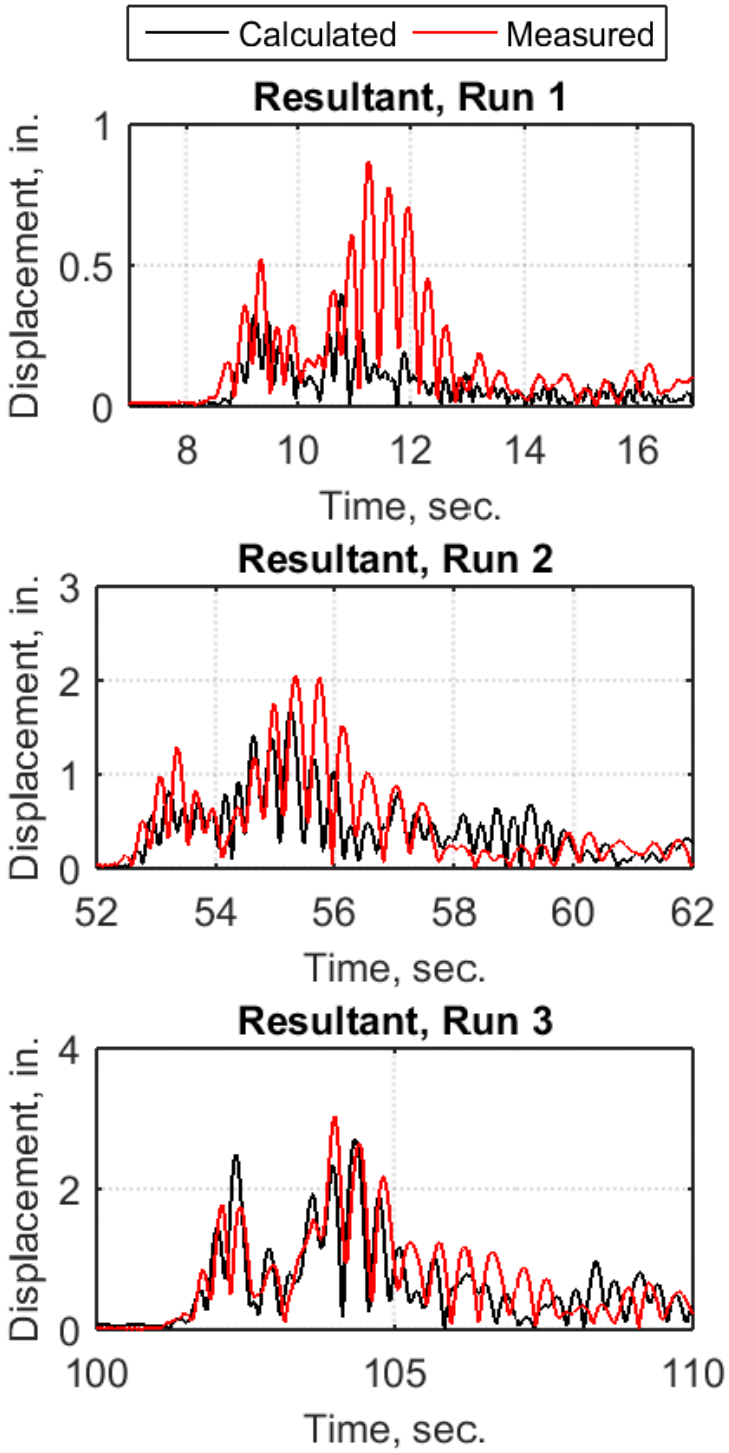

Figure A.7 Measured and calculated resultant displacement histories, Runs 1 to 3

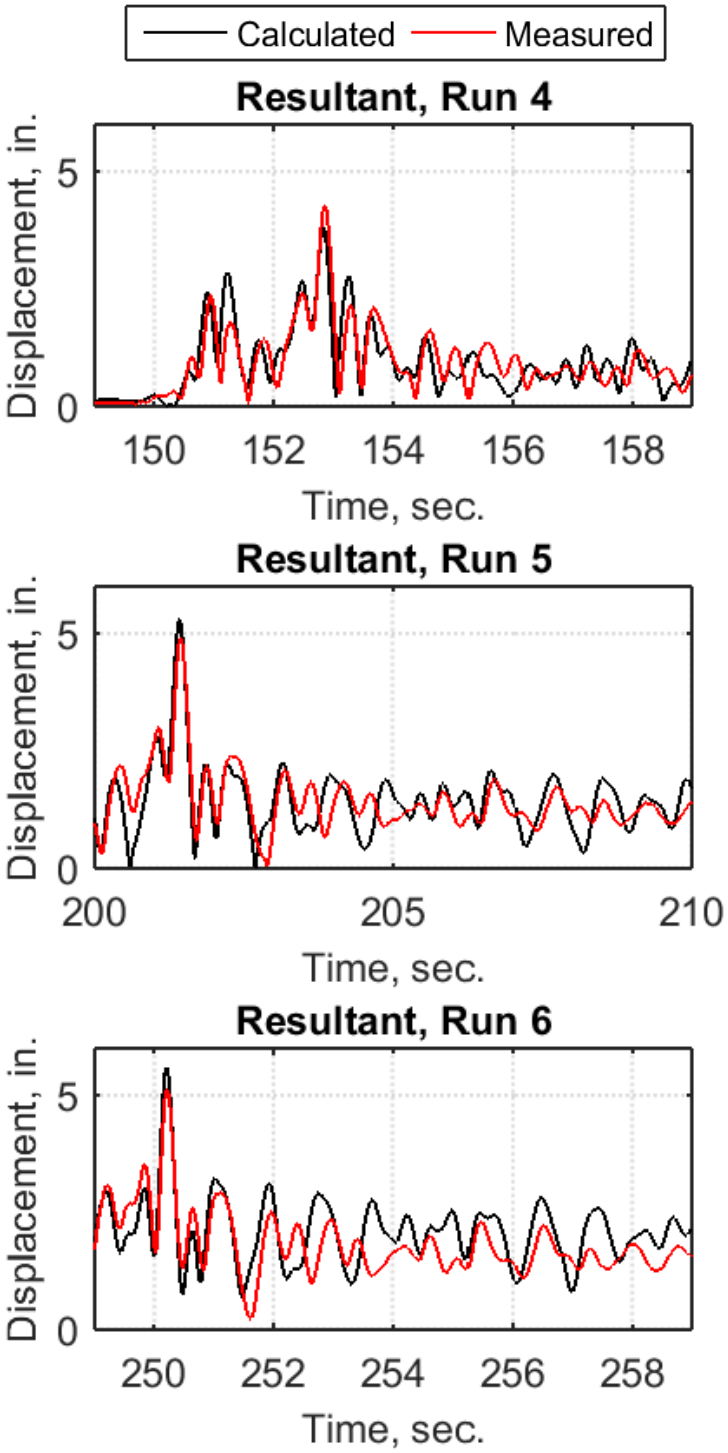

Figure A.8 Measured and calculated resultant displacement histories, Runs 4 to 6

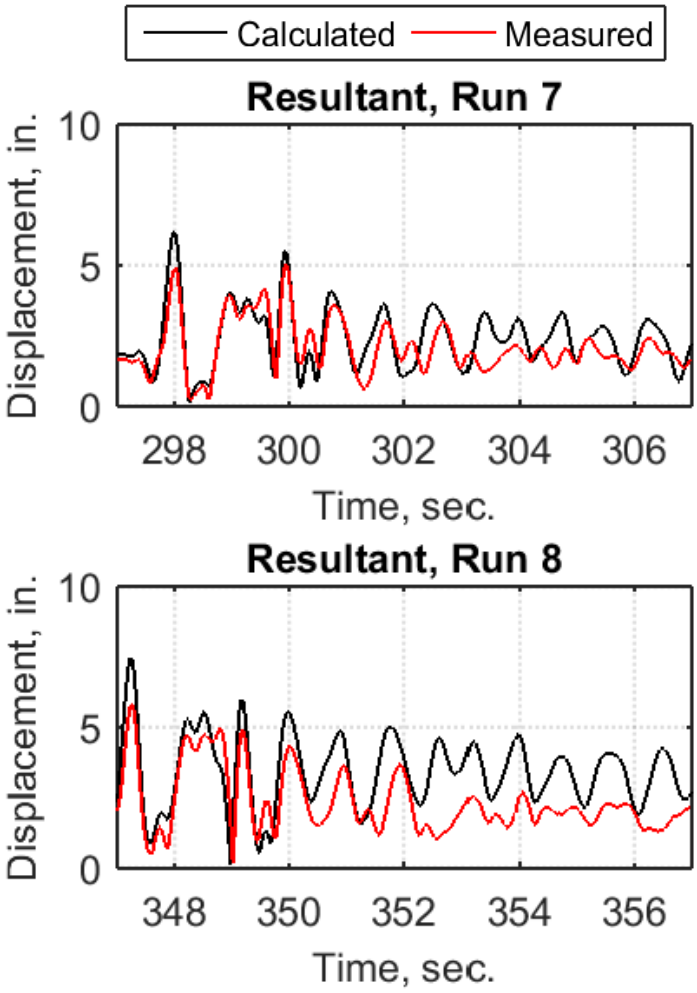

Figure A.9 Measured and calculated resultant displacement histories, Runs 7 and 8

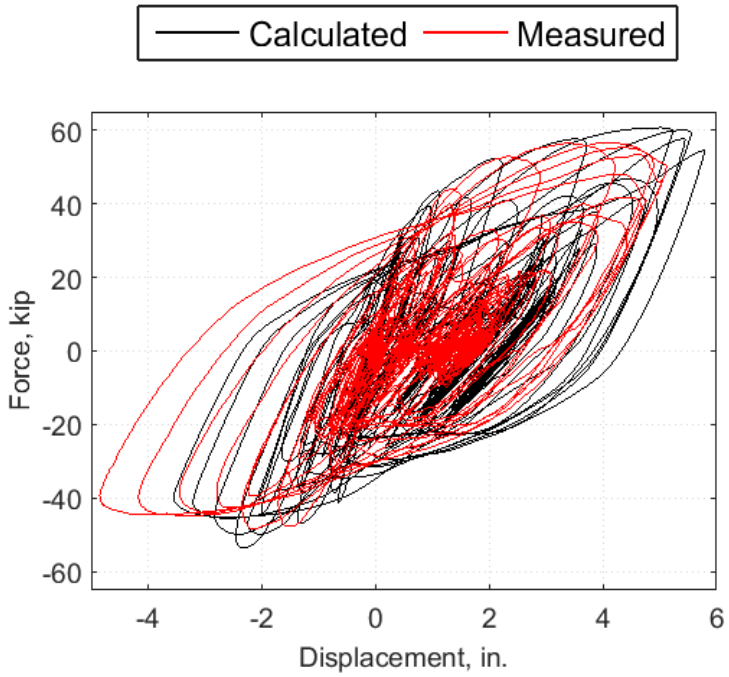

Figure A.10 Cumulative measured and calculated hysteresis curve in the longitudinal direction

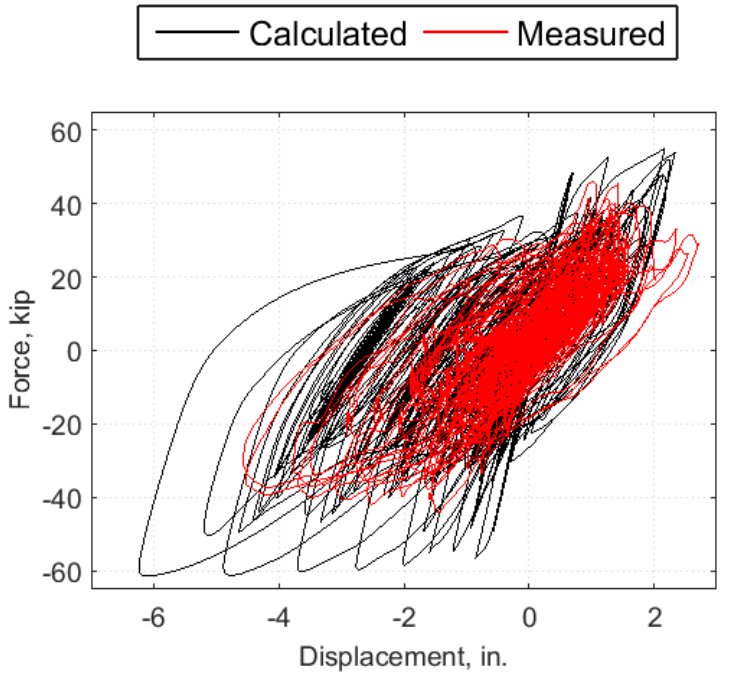

Figure A.11 Cumulative measured and calculated hysteresis curve in the transverse direction

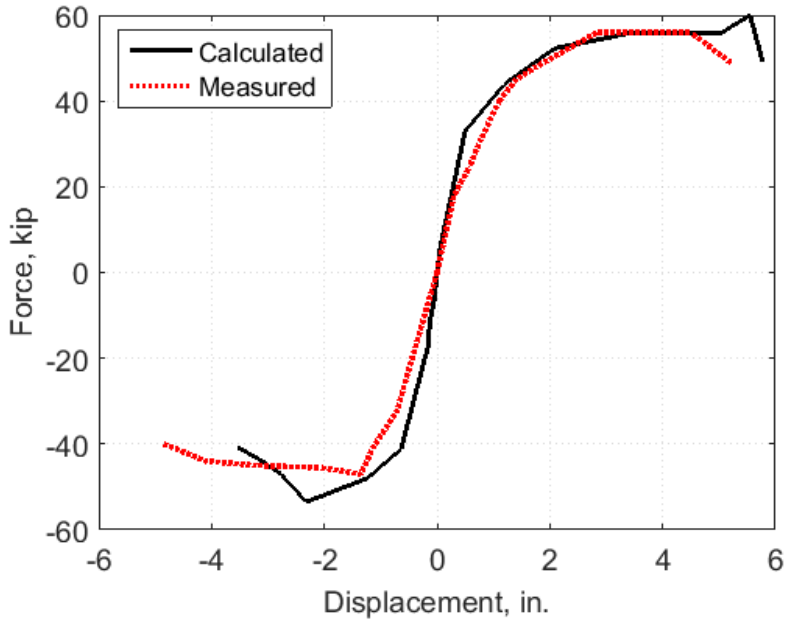

Figure A.12 Measured and calculated envelopes in the longitudinal direction

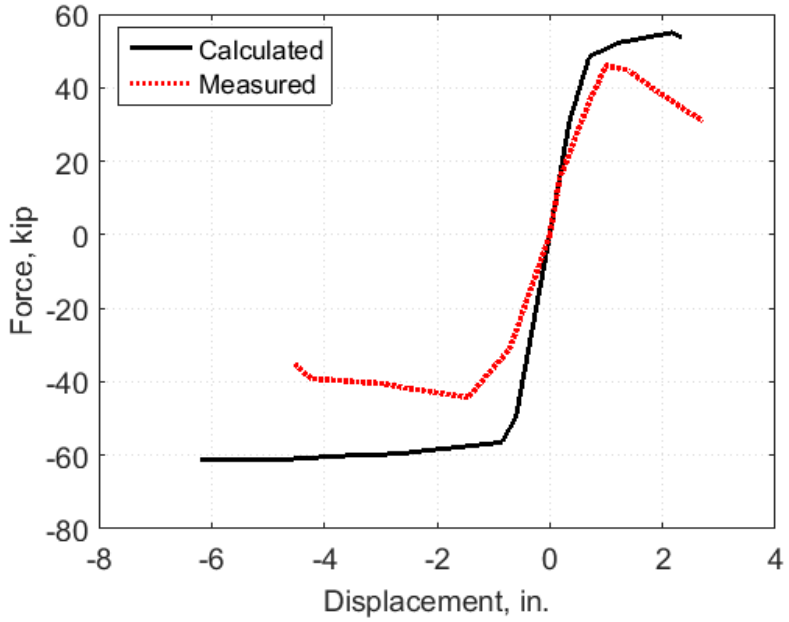

Figure A.13 Measured and calculated envelopes in the transverse direction

APPENDIX B: ABC-UTC DESIGN GUIDELINES FOR REBAR HINGE POCKET CONNECTIONS AND COLUMN TO HYBRID CAP BEAM GROUTED DUCT CONNECTIONS

NOTATIONS

A_{sp} = Area of one hinge hoop or spiral (in.^{2})

B_c = Column largest cross-sectional dimension (in.)

c = Cohesion factor

d_{bl} = Diameter of longitudinal column reinforcement (in.)

D_{s1} = Depth of the precast cap beam (in.)

f_c' = Concrete compressive strength (ksi)

f_{cg}' = Nominal compressive strength of grout (cube strength) (ksi)

f_y = Hinge bar yield strength (ksi)

f_{ye} = Expected yield stress of longitudinal column reinforcement (ksi)

f_{yh} = Nominal yield stress of the hinge reinforcement (ksi)

f_{yp} = Steel pipe yield stress (ksi)

$K1$ = Fraction of concrete strength available to resist interface shear (ksi)

$K2$ = Limiting interface shear resistance (ksi)

l_{ac} = Anchored length of column longitudinal bars beyond the ducts (in.)

l_d = Tension development length of the rebar hinge longitudinal bars (in.)

L_p = Plastic hinge length (in.)

t = Height of the hinge throat (in.)

P = Applied axial load, under the combined action of the vertical load and the maximum lateral load (kips)

P_u = Design axial load (kips)

S_h = Spacing of transverse hoops or spirals in equivalent CIP joint

t_p = Pipe thickness (in.)

T_s = Total tension force in rebar hinge longitudinal bars (kips)

V_n = Nominal shear capacity of the rebar hinge section (k

V_u = Shear demand at the hinge (kips)

μ = Shear friction factor

θ = Angle between the horizontal axis of the bent cap and the pipe helical corrugation or lock seam (deg)

ϕ_y = Hinge section effective yield curvature

ϕ_u = Hinge section ultimate curvature

d_b = Hinge bar diameter (in.)

θ_n = Hinge ultimate rotation

θ_e = Hinge elastic rotation

θ_p = Hinge plastic rotation

θ_{close} = Hinge rotation corresponding to the hinge throat closure

ϕ = Shear strength reduction factor

1.0—REBAR HINGE POCKET CONNECTIONS

C1.0

Rebar hinge is the most commonly used column hinge in the United States that can be used either at the top or bottom of reinforced concrete columns. Design of the rebar hinges has not been codified; however, Cheng et al. (2010) developed a step by step design guideline for rebar hinges based on extensive experimental and analytical studies.

Rebar hinge pocket or socket (in which the hinge element is precast or consists of a rebar cage alone, respectively) connection is a viable alternative connection for accelerated bridge construction (ABC), which combines rebar hinge details with those of the pocket connection. A hinge element integrated with a precast column is extended into a pocket left in the footing. The hinge element may be precast or consist of a reinforcing cage that extends from the column into a footing opening. The former is shown in Figure 1.1-1. The latter would consist of only the hinge reinforcement cage as shown in Figure 1.1-2 (Culmo et al. 2017). Only a few experimental studies have incorporated rebar hinge pocket connections as part of a precast bent or bridge system (Mehrsoroush et al. 2017, Mohebbi et al. 2017, Shoushtari et al. 2019).

	Design and detailing guidelines for rebar hinge pocket and socket connections are presented herein based on previous research.

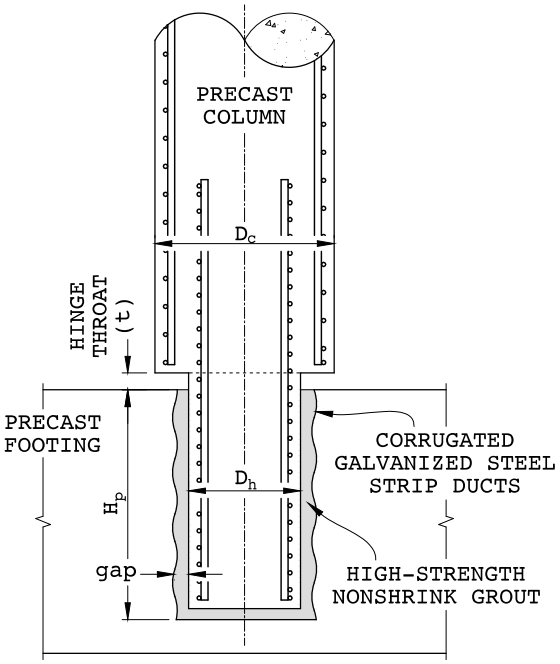

Figure 1.1-1—Column to Footing Rebar Hinge Pocket Connection

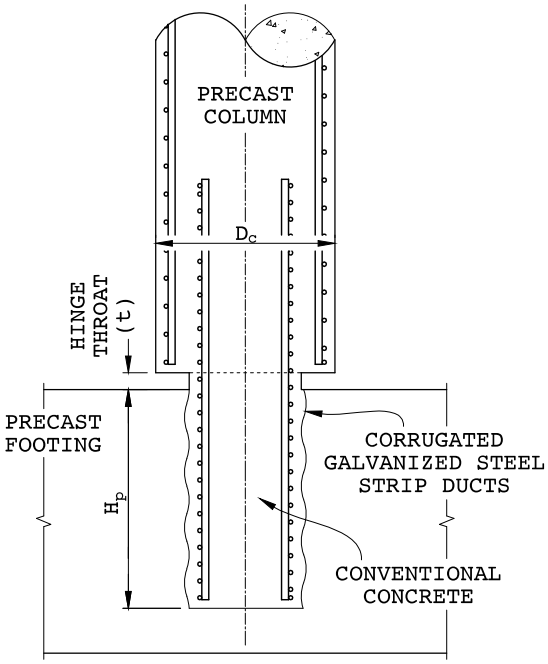

Figure 1.1-2—Column to Footing Rebar Hinge Socket Connection

1.1—Minimum Area of Rebar Hinge Section The gross area of the rebar hinge section shall be at least: $A_g \geq \frac{P_u}{0.2 f_c'}$ (1.1-1) P_u = Design axial load (kips) f_c' = Concrete compressive strength (ksi)	**C1.1** Eq. 1.1-1 was recommended by Cheng et al. (2010). It is intended to avoid compressive failure at the hinge.
1.2—Minimum Transverse Steel	**C1.2**

The volumetric ratio of the transverse reinforcement in a rebar hinge section shall be determined based on moment-curvature analysis of the hinge for a minimum curvature ductility of 10. Transverse steel can be in the form of spiral or hoops and shall be extended l_d into the column and adjoining member, where: l_d = Tension development length of the rebar hinge longitudinal bars in accordance to Article 5-11-2-1 (AASHTO, 2012).	Experimental studies by Cheng et al. (2010) showed that using a target curvature ductility of 10 ensures ductile behavior of the hinge specimen. The Mortensen-Saiidi method (Mortensen and Saiidi 2002) is a non-iterative performance-based method that was developed to design confinement reinforcement in concrete columns for a specified performance level. For hinge section, the core concrete is essentially confined by the transverse reinforcement in both the hinge and the column because of the relatively small depth of the hinge throat. The hinge cover concrete is confined by the column transverse steel for the same reason. Therefore, an effective confined lateral pressure, and transverse steel ratio should be used in determining the confined concrete properties in the moment-curvature analysis of the hinge section (Cheng et al. 2010).
1.3—Shear Design The plastic shear demand at the hinge shall satisfy Eq. 1.3-1. $V_u \leq \varphi_s V_n$ (1.3-1) Where: V_u = Shear demand at the hinge (kips), determined based on Article 8.6.1 AASHTO (2014) V_n = Nominal shear capacity of rebar hinge section (kips) φ_s = 0.9 for shear in reinforced concrete Nominal shear capacity of a two-way hinge section shall be taken as:	**C1.3** The amount of longitudinal steel is determined from shear design procedure. The design procedure is iterative and may require revision of the hinge area or longitudinal steel. Under lateral loading, the flexural moment at the hinge section causes flexural crack. Therefore, conventional shear friction theory (ACI 318 2008; AASHTO 2012) that assumes a clamping force at the entire interface is not applicable (Cheng et al. 2010). Experimental studies have shown that cyclic loads reduce roughness in the hinge and the aggregate interlock in the compression zone of the hinge (Cheng et al. 2010). Therefore, a reduced shear friction factor is recommended in Eq. 1.3-2, compared to the corresponding factor in AASHTO (2012), which is μ=0.6, for concrete cast against

$V_n = \mu(P + T_s)$ (1.3-2) where: P = Applied axial load, under the combined action of the vertical load and the maximum lateral load (kips) T_s = Total tension force in rebar hinge longitudinal bars (kips) μ = 0.45, shear friction factor	hardened concrete which is not intentionally roughened.
1.4—Hinge Throat Thickness The height of the hinge throat, *t*, as shown in Figures 1.1-1 and 1.1-2, shall satisfy the following criteria: $\theta_n < \theta_{close}$ (1.4-1) where: $\theta_n = \theta_e + \theta_p$ (1.4-2) $\theta_e = t\,\phi_y$ (1.4-3) $\theta_p = L_p\,(\phi_y - \phi_y)$ (1.4-4) $L_p = t + 0.15\,f_y\,d_b$ (1.4-5) $\theta_{close} = sin^{-1}\,(t / 0.5\,B_c)$ (1.4-6) Where: L_p = Plastic hinge length (in.) t = Height of the hinge throat (in.) f_y = Hinge bar yield strength (ksi) ϕ_y = Hinge section effective yield curvature ϕ_u = Hinge section ultimate curvature d_b = Hinge bar diameter (in.) θ_n = Hinge ultimate rotation	**C1.4** The purpose of hinge throat is to allow for hinge rotation and avoid closure of the gap that could damage the edge of the column and increase the hinge moment. Sufficient height of the hinge throat ensures that hinge closure is prevented (Cheng et al. 2010).

θ_e = Hinge elastic rotation θ_p = Hinge plastic rotation θ_{close} = Hinge rotation corresponding to the hinge throat closure B_c = Column largest cross-sectional dimension (in.)		
1.5—Pocket Minimum Depth When the hinge element is precast, the depth of a rebar hinge pocket, H_p, as shown in Figures 1.1-1 , shall be at least: $H_p \geq l_d + cc + gap$ (1.5-2) where: H_p = Rebar hinge pocket or socket depth (in.) l_d = Required tension development length of the hinge longitudinal bars into the adjoining members in accordance to Article 5-11-2-1 (AASHTO, 2012) (in.) cc = Concrete cover over hinge reinforcement (Article 5-12-3 ,AASHTO 2012) (in.) gap = The gap between the precast hinge element and pocket base (Article 1.7, Figure 1.1-1) (in.) When the hinge element consists of only extended hinge rebar cage (Figure 1.1-2), *gap* shall be taken as zero.		**C1.5** Providing concrete cover over the reinforcement at the end of the hinge specimen is not necessary, as filler material between the specimen and pocket provides adequate protection against corrosion. However, concrete cover, when provided, shall be considered in Eq. 1.5-2.

1.6—Pocket and Socket Details	**C1.6**
Pockets and sockets shall be constructed with helical, lock-seam, corrugated steel pipes, conforming to ASTM A706. The pipe thickness (t_p) shall be greater than 0.06 in.	The 0.06 in., which was proposed by Restrepo et al. (2011), ensures the constructability of the pipe. Further information about corrugated steel pipe material and thickness can be found in Tazarv and Saiidi (2015), and Restrepo et al. (2011).
When precast hinge elements are used, high-strength, non-shrink grout shall be used as the pocket filler. The grout shall be sufficiently fluid when rebar hinge specimen is embedded into the pocket. The compressive strength of the filler material sampled and tested according to an appropriate ASTM standard shall be at least 15 percent higher than concrete compressive strength of the footing.	The requirement for grout compressive strength exceeding that of the concrete in the footing ensures that no weak link is formed in the connection. The 15-percent overstrength factor is due to the fact that compressive strength of 2.0-in cubes (as recommended by ASTM for grout sampling) are typically more than those obtained from cylinder testing. Further information can be found in Tazarv and Saiidi (2015).
The gap between the pocket and rebar hinge specimen shall be at least 2.0 in. but no more than 4.0 in.	Sufficient gap between the hinge specimen and pocket not only provides adequate construction tolerance, but also ensures that filler material easily flows through the pocket.
When the hinge element consists of hinge rebar cage alone, concrete with a compressive strength of at least equal to that of the footing shall be used as the socket filler.	

2.0—COLUMN TO HYBRID CAP BEAM GROUTED DUCT CONNECTIONS	**C2.0** A grouted duct connection includes corrugated metal ducts embedded in the adjoining precast members to anchor individual projected column longitudinal reinforcing bars. The ducts are then filled with high-strength non-shrink grout. Several researchers have studied bond behavior and performance of the grouted duct connections (Matsumoto et al. 2001, Pang et al. 2008, Steuck et al. 2009, Restrepo et al. 2011). Experimental studies have shown that grouted duct connections are emulative of cast-in-place construction. Hybrid cap beams consist of a precast and a cast-in-place segment with the former incorporating grouted ducts. A column to hybrid cap beam grouted duct connection consists of a lower precast cap beam (stage I cap beam or precast dropped cap beam) to support the girders and a cast-in-place portion (stage II cap beam) to integrate the pier and superstructure. Column bars are extended into the corrugated metal ducts that are grouted afterward, but extend beyond the ducts into the CIP segment of the cap beam (Fig.2.1-1).

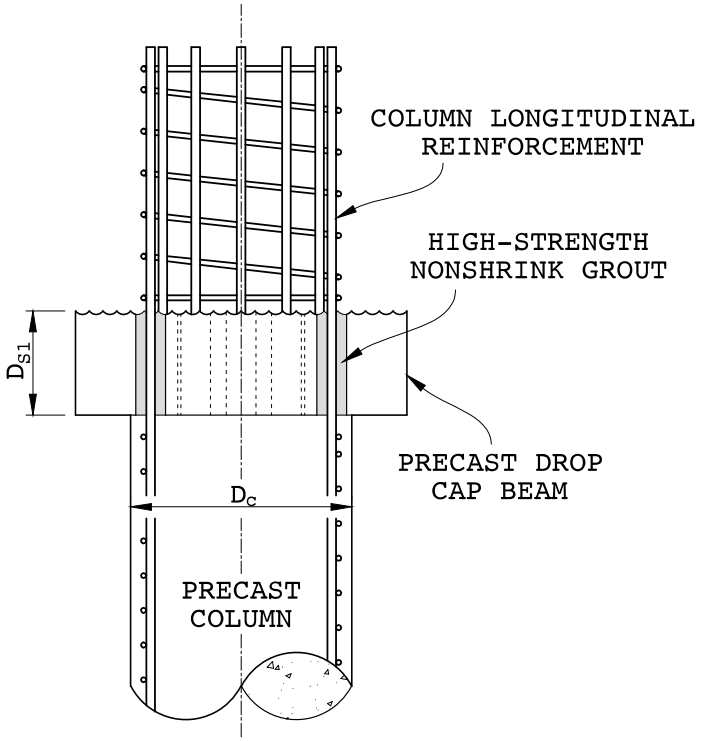

Figure 2.1-1—Column To Hybrid Cap Beam Grouted Duct Connection

2.1—Joint Design

Joint proportioning and joint shear design shall satisfy AASHTO (2014) 8-13.

The full depth of the combined lower and upper parts of the cap beam participates in resisting the joint forces in both the longitudinal and transverse directions.

In the precast part of the cap beam, joint transverse reinforcement shall be placed around the ducts that anchor the column bars.

2.2—Minimum Anchorage Length for Column Longitudinal Bars

Anchorage of the column longitudinal bars is provided through bond in a combination of grouted

C2.2

Eq. 2.2-1 is based on research by Matsumoto et al. 2008.

ducts and CIP concrete. The stress that is transferred through bond in the ducts is:

$$f_s = \frac{D_{s1} f'_{cg}}{2 d_{bl}} \quad (2.2\text{-}1)$$

Where:

f_s = Steel stress transferred through bond in the ducts (ksi)

D_{s1} = Depth of the precast cap beam (in.)

f'_{cg} = Nominal compressive strength of grout (cube strength) to be taken no greater than 7 ksi (ksi)

d_{bl} = Diameter of longitudinal column reinforcement (in.)

The extension of the bars beyond the ducts shall Satisfy the following equation:

$$l_{ac} \geq \frac{2 d_{bl} (f_{ye} - f_s)}{f'_{cg}} \quad (2.2\text{-}2)$$

l_{ac} = Anchored length of column longitudinal beyond the ducts (in.)

f_{ye} = Expected yield stress of longitudinal column reinforcement (ksi)

f'_c = Concrete compressive strength (ksi)

Grout compressive strength in Eq. 2.2-1 shall be limited to 7000 psi.

2.3—Precast Cap Beam Design Precast cap beam shall be designed for its self-weight and the superstructure. Depth of the precast cap beam shall be sufficient to develop the required strength in column bars for construction loading. Torsional moments due to sequential placement of girders shall be taken into consideration in design of the precast cap beam.	
2.4—Details of Grouted Ducts Semi-rigid corrugated metal (steel) ducts specified per ASTM A653 shall be used to anchor column bars.	**C2.4** Semi-rigid corrugated metal ducts provide sufficient anchorage between the column bar, grout, and surrounding concrete (Restrepo et al. 2011). Matsumato et al. (2001) provides background and details on grouting of duct connections in terms of grout testing, grout placement, and other grouting issues.
2.5—Interface Load Transfer Strength The load transfer strength at the column-cap beam interface shall be calculated in accordance to AASHTO 5.8.4.1-3 equation, using the following parameters: c = 0 μ = 0.6 K1 = 0.2 ksi K2 = 0.8 ksi	**C2.5** Specified values for c, μ, K1 and K2 in equation 5.8.4.1-3 were proposed by Marsh et al. (2011). It was shown that, to account for cyclic loading effects and the potential for significant cracking, the cohesion factor, c, should be ignored.

3.0—REFERENCES

ACI Committee, & International Organization for Standardization. (2008). Building code requirements for structural concrete (ACI 318-08) and commentary. American Concrete Institute.

American Association of State Highway and Transportation Officials (AASHTO), (2012). "AASHTO LRFD Bridge Design Specifications", 6th edition.

American Association of State Highway and Transportation Officials (AASHTO). (2014). "Guide Specifications for LRFD Seismic Bridge Design", Washington, D.C.

Cheng, Z. Y., Saiidi, M. S., & Sanders, D. (2010). "Seismic Design Method for Reinforced Concrete Two-Way Column Hinges". ACI Structural Journal, 107(5).

Culmo, M. P., Marsh, L., Stanton, J., & Mertz, D. (2017). "Recommended AASHTO Guide Specifications for ABC Design and Construction" (No. NCHRP Project 12-102).

Marsh, L.M., Wernli, M., B.E.Garrett, J.F.Stanton, M.O.Eberhard, and M.D.Weinert. (2011). NCHRP Report 698 "Application of Accelerated Bridge Construction Connections in Moderate-to-High Seismic Regions". Washington, D.C.: National Cooperative Highway Research Program, Transportation Research Board.

Matsumoto, E. E., Mark, C., Waggoner, M. E. K., Vogel, J., & Wolf, L. (2008). "Development of a precast concrete bent-cap system". PCI journal.

Matsumoto, E. E., Waggoner, M. C., Sumen, G., Kreger, M. E., Wood, S. L., & Breen, J. E. (2001). "Development of a Precast Bent Cap System" (No. Report no. RR-1748-2). University of Texas at Austin. Center for Transportation Research.

Mehrsoroush, A., Saiidi, M., & Ryan, K. (2017). "Development of Earthquake-Resistant Precast Pier Systems for Accelerated Bridge Construction in Nevada". (No. 555-14-803).

Mohebbi, A., Saiidi, M. S., & Itani, A. M. (2018). "Shake Table Studies and Analysis of a Precast Two-Column Bent with Advanced Materials and Pocket Connections". Journal of Bridge Engineering, 23(7), 04018046.

Mortensen, J., and M. Saiidi, "A Performance-Based Design Method for Confinement in Circular Columns," Civil Engineering Department, University of Nevada, Reno, Report No. CCEER 02-07, November 2002.

Pang, J., K.P.Steuck, L.Cohagen, Stanton, J., and Eberhard, M. (2008). "Rapidly Constructible Large-Bar Precast Bridge-Bent Seismic Connection'. Olympia, WA: Washington State Department of Transportation. WA-RD 684.2

Restrepo, J. I., M. J. Tobolski, and E. E. Matsumoto, (2011). "Development of a precast bent cap system for seismic regions." NCHRP Rep. 681. Washington, DC: National Cooperative Highway Research Program.

Shoushtari, E., Saiidi, M., and Itani, A., Moustafa, M. (2019) "Design, Construction, and Shake Table Testing of a Two-Span Steel Girder Bridge System with ABC Connections". ASCE Journal of Bridge Engineering

Steuck, K., Stanton, J., and Eberhard, M. (2009). “Anchorage of Large-Diameter Reinforcing Bars in Ducts”. ACI Structural Journal, Volume 106, No. 4, pp. 506-513.

Tazarv, M., & Saiidi, M. S. (2015). “Design and Construction of Precast Bent Caps with Pocket Connections for High Seismic Regions”. Report No. CCEER 15-06, August 2015